ISSN 0021-3438 (Print)
ISSN 2412-8783 (Online)

IZVESTIYA
NON-FERROUS METALLURGY

Vol. 30, No. 4, 2024

Scientific and Technical Journal
Founded in 1958
4 Issues per year

ИЗВЕСТИЯ ВУЗОВ
ЦВЕТНАЯ МЕТАЛЛУРГИЯ

Том 30, № 4, 2024

Научно-технический журнал
Основан в 1958 г.
Выходит 4 раза в год

ISSN 0021-3438 (Print)
ISSN 2412-8783 (Online)

IZVESTIYA NON-FERROUS METALLURGY

Vol. 30, No. 4
2024

Scientific and Technical Journal Founded in 1958 4 Issues per year http://cvmet.misis.ru

Journal is included into the List of the peer-reviewed scientific publications recommended by the Highest Attestation Commission of the Ministry of Education and Science of the Russian Federation for publishing the results of doctoral and candidate dissertations

Abstracting/Indexing: Russian Science Citation Index (RSCI), Chemical Abstracts (Online), INIS, OCLC ArticleFirst, Ulrich's Periodicals Directory, VINITI Database (Abstract Journal)

Founder

National University of Science and Technology "MISIS"
Address: 1 Bld, 4 Leninskiy Prosp., Moscow 119049, Russia
http://www.misis.ru

Editor-in-Chief

Evgeny A. Levashov
Prof., Dr. Sci. (Eng.), Acad. of the RANS, NUST MISIS, Moscow, Russia

Deputy Editor

Vladislava A. Ignatkina
Prof., Dr. Sci., NUST MISIS, Moscow, Russia

Editorial Board

Abhilash – Dr., Ph.D., CSIR – National Metallurgical Laboratory, Jamshedpur, India
E.V. Ageev – Prof., Dr. Sci. (Eng.), SouthWest State University, Kursk, Russia
M.V. Ananyev – Prof., Dr. Sci. (Chem.), Federal State Research and Development Institute of Rare Metal Industry (JSC "Giredmet"), Moscow, Russia
N.A. Belov – Prof., Dr. Sci. (Eng.), NUST MISIS, Moscow, Russia
E.V. Bogatyreva – Prof., Dr. Sci. (Eng.), NUST MISIS, Moscow, Russia
V.B. Deev – Prof., Dr. Sci. (Eng.), NUST MISIS, Moscow, Russia
V.M. Denisov – Prof., Dr. Sci. (Chem.), Siberian Federal University, Krasnoyarsk, Russia
D.V. Drobot – Prof., Dr. Sci. (Chem.), Russian Technological University (MITHT), Moscow, Russia
F.V. Grechnikov – Prof., Dr. Sci. (Eng.), Acad. of RAS, Samara National Research University n.a. S.P. Korolev (Samara University), Samara, Russia
D.V. Gunderov – Dr. Sci. (Phys.-Math.), Institute of Molecule and Crystal Physics Ufa Research Center of the RAS, Ufa, Russia
B.B. Khina – Dr. Sci. (Phys.-Math.), The Physical-Techical Institute of NAS of Belarus, Minsk, Belarus
D.V. Louzguine – Prof., Dr. Sci., Tohoku University, Sendai, Japan
S.V. Mamyachenkov – Prof., Dr. Sci. (Eng.), Ural Federal University, Yekaterinburg, Russia
Z.A. Mansurov – Dr. Sci. (Chem.), Prof., Institute of Combustion Problems, Almaty, Kazakhstan
N.V. Nemchinova – Prof., Dr. Sci. (Eng.), Irkutsk National Research Technical University, Irkutsk, Russia
K.V. Nikitin – Prof., Dr. Sci. (Eng.), Samara State Technical University, Samara, Russia
H.A. Oye – Prof., Dr., Norwegian University of Science and Technology, Trondheim, Norway
P.V. Polyakov – Prof., Dr. Sci. (Chem.), Siberian Federal University, Krasnoyarsk, Russia
E.S. Prusov – Cand. Sci. (Eng.), Vladimir State University, Vladimir, Russia
V.N. Rychkov – Prof., Dr. Sci. (Chem.), Ural Federal University, Ekaterinburg, Russia
D. Sadoway – Prof., Dr., Massachusetts Institute of Technology, Boston, USA
G.A. Salishchev – Prof., Dr. Sci. (Eng.), Belgorod National Research University, Belgorod, Russia
D.V. Shtansky – Prof., Dr. Sci. (Phys.-Math.), NUST MISIS, Moscow, Russia
V.M. Sizyakov – Prof., Dr. Sci. (Eng.), Saint-Petersburg Mining University, St. Petersburg, Russia
Stopic Srecko – Dr.-Ing. habil., RWTH Aachen University, Aachen, Germany
B.B. Straumal – Prof., Dr. Sci. (Phys.-Math.), Institute of Solid State Physics of the RAS, Chernogolovka, Moscow region
O.Yu. Tkacheva – Dr. Sci. (Chem.), Institute of High Temperature Electrochemistry of the Ural Branch of the RAS, Yekaterinburg, Russia
M. Verhaege – Prof., Dr., University of Gent, Belgium
G.M. Vol'dman – Prof., Dr. Sci. (Chem.), Russian Technological University (MITHT), Moscow, Russia
G. Xanthopoulou – Dr., National Center for Scientific Research "Demokritos", Agia Paraskevi, Attica, Greece
A.L. Yerokhin – Prof., Dr., University of Manchester, United Kingdom
Onuralp Yücel – Prof., Dr., Istanbul Technical University, Maslak, Istanbul, Turkey
Yu.P. Zaikov – Prof., Dr. Sci. (Chem.), Institute of High Temperature Electrochemistry of the Ural Branch of the RAS, Yekaterinburg, Russia
R.Kh. Zalavutdinov – Cand. Sci. (Phys.-Math.), A.N. Frumkin Institute of Physical Chemistry and Electrochemistry of the RAS, Moscow, Russia
M. Zinigrad – Prof., Dr., Ariel University, Ariel, Israel
A.I. Zouboulis – Prof., Dr., Aristotle University of Thessaloniki, Greece

Editorial Staff

Address: NUST MISIS, 1 Bld, 4 Leninskiy Prosp.,
Moscow 119049, Russia
Phone: +7 (495) 638-45-35
E-mail: izv.vuz@misis.ru

Certificate of registration No. 015842 (13.03.1997)
Re-registration PI No. ФС77-79229 (25.09.2020)

Subscription: Ural-Press Agency

© NUST MISIS, Moscow, 2024
© Izvestiya. Non-Ferrous Metallurgy, 2024

Leading Editor – A.A. Kudinova
Executive Editor – O.V. Sosnina
Layout Designer – E.A. Legkaya

Signed print 16.12.2024. Format 60×90 1/8.
Offset paper No. 1. Digital printing. Quires 9,75
Order 21217. Free price

Printed in the printing house of the MISIS Publish House
1 Bld, 4 Leninskiy Prosp., Moscow 119049, Russia. Phone/fax: +7 (499) 236-76-17

Articles are available under Creative Commons Attribution Non-Commercial No Derivatives

ISSN 0021-3438 (Print)
ISSN 2412-8783 (Online)

ИЗВЕСТИЯ ВУЗОВ
ЦВЕТНАЯ МЕТАЛЛУРГИЯ

Том 30, № 4
2024

Научно-технический журнал Основан в 1958 г. Выходит 4 раза в год http://cvmet.misis.ru

Журнал включен в Перечень рецензируемых научных изданий, рекомендованных ВАК Минобрнауки РФ
для публикации результатов диссертаций на соискание ученых степеней

Журнал включен в базы данных: Russian Science Citation Index (RSCI), Chemical Abstracts (Online), INIS, OCLC ArticleFirst,
Ulrich's Periodicals Directory, РИНЦ, БД/РЖ ВИНИТИ

Учредитель

ФГАОУ ВО Национальный исследовательский технологический университет «МИСИС»
Адрес: 119049, г. Москва, Ленинский пр-т, 4, стр. 1
http://www.misis.ru

Главный редактор

Евгений Александрович Левашов
д.т.н., академик РАЕН, профессор, НИТУ МИСИС, г. Москва

Заместитель главного редактора

Владислава Анатольевна Игнаткина
д.т.н., профессор, НИТУ МИСИС, г. Москва

Редакционная коллегия

Е.В. Агеев – д.т.н., ЮЗГУ, г. Курск
М.В. Ананьев – д.х.н., АО «Гиредмет», г. Москва
Н.А. Белов – д.т.н., проф., НИТУ МИСИС, г. Москва
Е.В. Богатырева – д.т.н., НИТУ МИСИС, г. Москва
Г.М. Вольдман – д.х.н., проф., РТУ (МИТХТ), г. Москва
Ф.В. Гречников – д.т.н., акад. РАН, проф., СНИУ, г. Самара
Д.В. Гундеров – д.ф.-м.н., ИФМК УНЦ РАН, г. Уфа
В.Б. Деев – д.т.н., проф., НИТУ МИСИС, г. Москва
В.М. Денисов – д.х.н., проф., СФУ, г. Красноярск
Д.В. Дробот – д.х.н., проф., РТУ (МИТХТ), г. Москва
Ю.П. Зайков – д.х.н., проф., ИВТЭ УрО РАН, г. Екатеринбург
Р.Х. Залавутдинов – к.ф.-м.н., ИФХЭ РАН, г. Москва
С.В. Мамяченков – д.т.н., проф., УрФУ, г. Екатеринбург
З.А. Мансуров – д.х.н., проф., Институт проблем горения, г. Алматы, Казахстан
Н.В. Немчинова – д.т.н., проф., ИРНИТУ, г. Иркутск
К.В. Никитин – д.т.н., проф., СамГТУ, г. Самара
П.В. Поляков – д.х.н., проф., СФУ, г. Красноярск
Е.С. Прусов – к.т.н., доцент, ВлГУ, г. Владимир
В.Н. Рычков – д.х.н., проф., УрФУ, г. Екатеринбург
Г.А. Салищев – д.т.н., проф., НИУ «БелГУ», г. Белгород
В.М. Сизяков – д.т.н., проф., СПГУ, г. Санкт-Петербург
Б.Б. Страумал – д.ф.-м.н., проф., ИФТТ РАН, г. Черноголовка
О.Ю. Ткачева – д.х.н., ИВТЭ УрО РАН, г. Екатеринбург
Б.Б. Хина – д.ф.-м.н., доц., ФТИ НАН Беларуси, г. Минск, Беларусь
Д.В. Штанский – д.ф.-м.н., проф., НИТУ МИСИС, г. Москва
Abhilash – Dr., Ph.D., CSIR – National Metallurgical Laboratory, Jamshedpur, India
D.V. Louzguine – Prof., Dr., Tohoku University, Sendai, Japan
H.A. Oye – Prof., Dr., Norwegian University of Science and Technology, Trondheim, Norway
D. Sadoway – Prof., Dr., Massachusetts Institute of Technology, Boston, USA
Stopic Srecko – Dr.-Ing. habil., RWTH Aachen University, Aachen, Germany
M. Verhaege – Prof., Dr., University of Gent, Belgium
G. Xanthopoulou – Dr., National Center for Scientific Research «Demokritos», Agia Paraskevi, Attica, Greece
A.L. Yerokhin – Prof., Dr., University of Manchester, United Kingdom
Yücel Onuralp – Prof., Dr., Istanbul Technical University, Maslak, Istanbul, Turkey
M. Zinigrad – Prof., Dr., Ariel University, Ariel, Israel
A.I. Zouboulis – Prof., Dr., Aristotle University of Thessaloniki, Greece

Редакция журнала

Адрес: 119049, г. Москва, Ленинский пр-т, 4, стр. 1,
НИТУ МИСИС

Тел.: +7 (495) 638-45-35

E-mail: izv.vuz@misis.ru

Свидетельство о регистрации № 015842 от 13.03.1997 г.
Перерегистрация ПИ № ФС77-79229 от 25.09.2020 г.

Подписка: Агентство «Урал-пресс»

Ведущий редактор – А.А. Кудинова

Выпускающий редактор – О.В. Соснина

Дизайн и верстка – Е.А. Легкая

Подписано в печать 16.12.2024. Формат 60×90 1/8.
Бум. офсетная № 1. Печать цифровая. Усл. печ. л. 9,75
Заказ 21217. Цена свободная

Отпечатано в типографии Издательского Дома МИСИС
119049, г. Москва, Ленинский пр-т, 4, стр. 1. Тел./факс: +7 (499) 236-76-17

© НИТУ МИСИС, Москва, 2024
© «Известия вузов. Цветная металлургия», 2024

Статьи доступны под лицензией Creative Commons
Attribution Non-Commercial No Derivatives

CONTENTS

Metallurgy of Non-Ferrous Metals

Pressure Treatment of Metals

Physical Metallurgy and Heat Treatment

СОДЕРЖАНИЕ

Металлургия цветных металлов

Обработка металлов давлением

Металловедение и термическая обработка

UDC 66.01
https://doi.org/10.17073/0021-3438-2024-4-5-10

Research article
Научная статья

Investigation of the conditions (nature) of pentacoordinated aluminum oxide formation

P.A. Solodovnikova[1], **M.A. Mashkovtsev**[1,2], **V.N. Rychkov**[1], **G.V. Ginko**[1], **T.E. Telegin**[1], **M.V. Ugryumova**[1]

[1] **Ural Federal University n.a. the First President of Russia B.N. Eltsin**
19 Mira Str., Ekaterinburg 620002, Russia

[2] **Institute of High Temperature Electrochemistry of the Ural Branch of the Russian Academy of Sciences**
20 Akademicheskaya Str., Ekaterinburg 620137, Russia

✉ Polina A. Solodovnikova (solly.polly@yandex.ru)

Abstract: Aluminum oxide is widely used as a catalyst carrier, including in internal combustion engine systems, where operating temperatures exceed 1000 °C. As such, aluminum oxide must exhibit enhanced thermal stability. This property is linked to the presence of pentacoordinated centers on the surface of the γ-phase of Al_2O_3. This paper examines the effect of the pH during aluminum hydroxide precipitation on the formation of pentacoordinated centers on the surface of aluminum oxide. The samples of aluminum hydroxide were synthesized via controlled double-jet precipitation, followed by thermal decomposition into oxides. Precipitation was carried out at constant pH levels, and for comparison, parallel samples were synthesized at pH values of 5, 6, 7, 8, and 9. The precursors for precipitation were a 1 M aluminum nitrate solution (Al^{3+}) and a 10 wt. % ammonia solution (NH_4OH). The solutions were introduced into the reactor in a dropwise mode with continuous stirring. The resulting aluminum oxide samples were analyzed using *X*-ray diffraction and nuclear magnetic resonance techniques. The data show a direct correlation between the pH of aluminum hydroxide precipitation and the presence of pentacoordinated centers on the aluminum oxide surface: the higher the pH, the lower the content of pentacoordinated atoms. Additionally, a relationship was observed between the pH value and the size of the coherent scattering region, with an increase in coherent scattering observed at higher pH levels.

Keywords: pentacoordinated aluminum oxide, thermostability, controlled double-jet precipitation.

For citation: Solodovnikova P.A., Mashkovtsev M.A., Rychkov V.N., Ginko G.V., Telegin T.E., Ugryumova M.V. Investigation of the conditions (nature) of pentacoordinated aluminum oxide formation. *Izvestiya. Non-Ferrous Metallurgy*. 2024;30(4):5–10.
https://doi.org/10.17073/0021-3438-2024-4-5-10

Исследование условий (природы) образования пентакоординированного оксида алюминия

П.А. Солодовникова[1], **М.А. Машковцев**[1,2], **В.Н. Рычков**[1], **Г.В. Гинько**[1], **Т.Е. Телегин**[1], **М.В. Угрюмова**[1]

[1] **Уральский федеральный университет им. первого Президента России Б.Н. Ельцина**
Россия, 620002, г. Екатеринбург, ул. Мира, 19

[2] **Институт высокотемпературной электрохимии УрО РАН**
Россия, 620137, г. Екатеринбург, ул. Академическая, 20

✉ Полина Александровна Солодовникова (solly.polly@yandex.ru)

Аннотация: Оксид алюминия находит широкое применение в качестве носителя катализаторов, в том числе в системах двигателей внутреннего сгорания автомобилей, где рабочие температуры достигают свыше 1000 °C, в связи с чем он должен обладать повышенной термической устойчивостью, или термостабильностью. Данный параметр связывают с наличием пентакоординированных центров на поверхности γ-фазы Al_2O_3. В настоящей работе описано влияние pH осаждения гидроксида алюминия на присутствие пентакоординированных центров на поверхности оксида алюминия. Методом контролируемого двухструйного осаждения синтезировали образцы гидроксида алюминия с его последующим термическим разложением до оксидов. Осаждение проводили при поддержании постоянного значения pH, и для сравнения были синтезированы параллели при постоянных значениях pH = 5, 6, 7, 8 и 9. Исходные реагенты для осаждения представляли собой раствор нитрата алюминия (Al^{3+} = 1 M) и раствор аммиака (10 мас. % NH_4OH). Растворы подавали в реактор в капельном режиме при постоянном перемешивании. Полученные образцы оксида алюминия исследовали методами рентгенофазового анализа и ядерного магнитного резонанса. Полученные данные свидетельствуют о прямой зависимости между значением pH осаждения гидроксидов алюминия и образованием пентакоординированых центров на поверхности получаемых оксидов алюминия: чем выше значение pH осаждения, тем меньше содержание пентакоординированных атомов. Кроме того, была обнаружена зависимость между значением pH осаждения и размерами области когерентного рассеяния – наблюдался ее рост с увеличением pH.

Ключевые слова: пентакоординированный оксид алюминия, термостабильность, контролируемое двухструйное осаждение.

Для цитирования: Солодовникова П.А., Машковцев М.А., Рычков В.Н., Гинько Г.В., Телегин Т.Е., Угрюмова М.В. Исследование условий (природы) образования пентакоординированного оксида алюминия. *Известия вузов. Цветная металлургия*. 2024;30(4):5–10. https://doi.org/10.17073/0021-3438-2024-4-5-10

Introduction

Aluminum oxide is widely used in industry due to its highly developed specific surface area, which is significantly influenced by the synthesis method and conditions [1—13]. Aluminum oxide powder is a key component of automotive catalysts, serving as a carrier for precious metal particles on its surface [7—9; 11]. For automotive catalysts, aluminum oxide powders must exhibit a stable structure, high specific surface area, and developed porosity, while being resistant to extreme operating temperatures up to 1100 °C. These properties largely depend on the presence of pentacoordinated aluminum oxide atoms (Al^V), also known as penta-centers [13—17].

Precipitation is the most common method for synthesizing pentacoordinated aluminum oxide due to the process's simplicity from a technological perspective. Aluminum salt solutions are often used as the precursor, with the choice of precipitant solution depending on the pH. A specific case is the controlled double-jet precipitation (CDJP) method, where the process is conducted at a constant pH with discrete dropwise addition of solutions into the reactor. After precipitation, the resulting suspension undergoes various processing steps, including filtration, drying, and calcination, producing aluminum oxide [18; 19].

The calcination temperature significantly affects the structure of the resulting oxide [18]. For instance, low-temperature phases of aluminum oxide form at temperatures up to 700 °C, while high-temperature phases form at temperatures above 700 °C [20].

Particular attention is given to the γ-phase of aluminum oxide, which is a metastable, transitional, structurally polymorphic form [21—26]. The bulk and surface structures of γ-aluminum oxide, along with its formation and thermal stability, have been the subject of numerous studies [21—26]. However, due to the low crystallinity and corresponding small particle size of γ-aluminum oxide, traditional analytical methods for determining its surface structure are significantly limited.

Several authors have reported that pentacoordinated Al^{3+} atoms are present on the surface of the γ-phase of aluminum oxide [13—17], which affect the material's thermal stability by interacting with the catalytically active phase. The detection of coordination centers (tetra-, penta-, or octa-) is possible using nuclear magnetic resonance (NMR).

It should be noted that the literature lacks data on the influence of the synthesis pH on the formation of pentacoordinated centers, as well as on the relationship between the presence of pentacoordinated centers and the crystallite characteristics of aluminum oxide obtained at various pH levels.

The aim of this study is to investigate the effect of the synthesis pH of aluminum hydroxide on the formation of pentacoordinated Al^{3+} atoms in its oxide.

Materials and method

Controlled double-jet precipitation of aluminum hydroxides at constant pH in batch mode was selected as the synthesis method for the samples. After precipitation, the samples were dried and calcined, resulting in aluminum oxide.

The synthesis of the samples was conducted as follows: aluminum nitrate and ammonia solutions were added dropwise while maintaining a constant pH throughout the precipitation process. The selected pH values were 5, 6, 7, 8, and 9.

The concentrations of the precipitation solutions were as follows: $C(Al^{3+})$ = 1 M and 10 wt. % NH_4OH. To produce 100 g of aluminum oxide, 2 L of aluminum nitrate solution was used. The process was carried out at room temperature, with the stirrer set at 500 rpm, and aluminum nitrate solution was fed at a rate of 10 mL/min. Drying was conducted in an oven for

4 h at 130 °C. The thermal treatment involved heating at a rate of 500 °C/h to 500 °C, holding at 500 °C for 4 h, followed by cooling in the furnace to room temperature.

After synthesis, the content of pentacoordinated aluminum oxide atoms was determined by nuclear magnetic resonance (NMR), and the values of the coherent scattering region (CSR) were calculated after conducting *X*-ray phase analysis.

^{27}Al NMR spectra were recorded at room temperature using an “Agilent VNMR 400” pulsed spectrometer (USA) at a frequency of 104.23 MHz with magic angle spinning (MAS). The rotor spinning frequency was 10 kHz. The spectra were processed using the “Dmfit” program.

The phase composition of the samples was determined using *X*-ray diffraction analysis. Measurements were performed over angles ranging from 10° to 80°. The *X*-ray patterns were processed using the “OriginPro” software, with baseline subtraction and smoothing of the peaks.

Results and discussion

The obtained nuclear magnetic resonance (NMR) results are presented in Fig. 1. Data are shown for the two samples that differ most significantly in terms of penta-center content, synthesized at pH = 5 and pH = = 9. The samples were labeled accordingly. NMR spectrum analysis revealed that the sample labeled pH = 9 does not have pentacoordinated aluminum atoms on its surface, as indicated by the absence of the corresponding peak. In contrast, the sample labeled pH = 5 is characterized by the presence of a peak, which corresponds to the presence of pentacoordinated centers.

Figure 2 presents the *X*-ray diffraction patterns for the same samples. The *X*-ray diffractograms show that the degree of crystallization of the samples varies depending on the pH of the precipitation, and all samples consist of γ-Al_2O_3 (JCPDS, 10-0425). No impurities of aluminum hydroxide or high-temperature phases of aluminum oxide were detected. As the precipitation pH increases, a decrease in peak width at half maximum is observed, indicating an increase in crystallite size. The *X*-ray diffractograms of the sample at pH = 9 are characterized by sharp peaks, with the pH = 9 sample exhibiting higher crystallinity than the pH = 5 sample. Additionally, the pH = 5 sample shows the highest number of defects.

The crystallite sizes of the aluminum oxide samples were calculated using the Scherrer method. It was found that the crystallite size increases with the rise in the pH of the precipitation process. The data obtained are presented below:

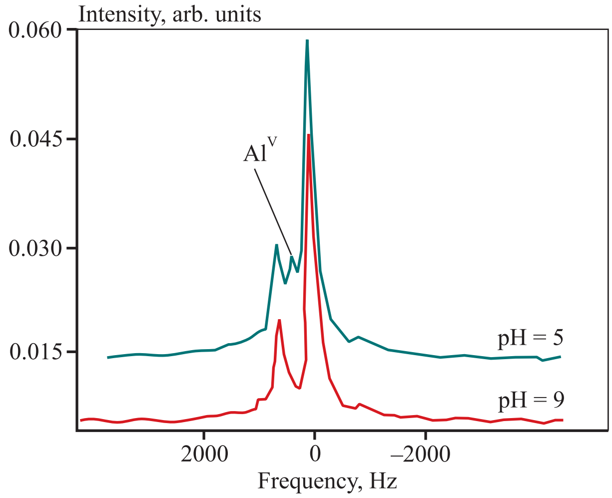

Fig. 1. NMR spectra of aluminum oxide samples

Рис. 1. ЯМР-спектры образцов оксида алюминия

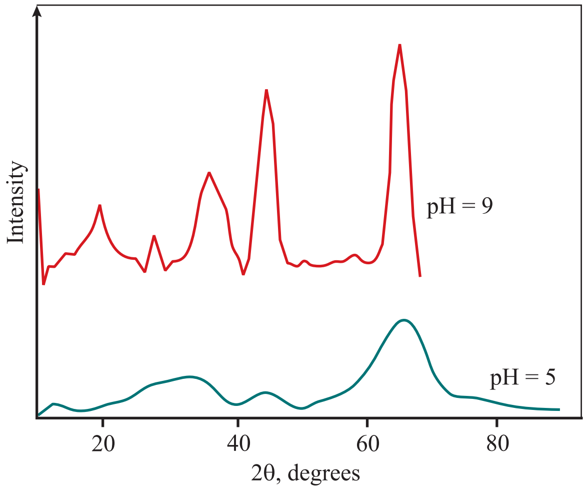

Fig. 2. XRD diffractograms of aluminum oxide samples

Рис. 2. Рентгенограммы образцов оксида алюминия

Sample	Al-5	Al-6	Al-7	Al-8	Al-9
Size, nm	1,17	1,71	2,52	3,31	3,67

Based on the research results, correlations were established between the pH values of the precipitation and the proportion of pentacoordinated Al^{3+} atoms, as well as the size of the coherent scattering region (CSR). A dependence of the studied parameters on the pH of precipitation was demonstrated: the proportion of pentacoordinated Al^{3+} atoms decreases with increasing synthesis pH (Fig. 3), while the crystallite size, on the other hand, increases (Fig. 4).

The sample labeled pH = 5 exhibits the highest number of defects and the greatest proportion of pentacoordinated aluminum atoms, while the sample labeled pH = 9 is characterized by the fewest defects and a significantly lower content of pentacoordinated atoms. Overall, as the pH of precipitation and the size of the CSR increase, the content of penta-centers in aluminum oxides decreases significantly.

Conclusion

The study demonstrated that the pH of aluminum hydroxide precipitation has a substantial effect on the content of pentacoordinated atoms in the resulting oxides. As the pH of precipitation and the size of the CSR increase, the proportion of pentacoordinated atoms on the surface of aluminum oxide decreases. These findings can be applied in further research into the mechanism of pentacoordinated atom formation on the surface of aluminum oxide, which holds practical value in the production of catalyst supports and adsorbents.

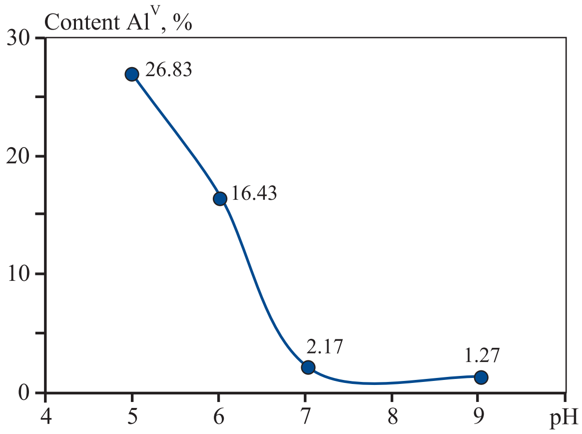

Fig. 3. Correlation between pH value and Al^V content

Рис. 3. Корреляция между значением pH
и содержанием Al^V

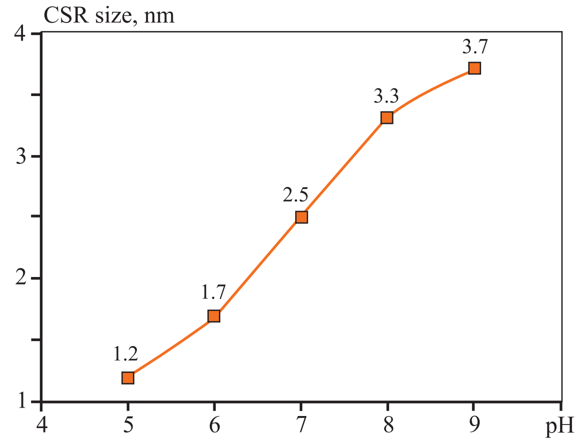

Fig. 4. Correlation between pH value and CSR size

Рис. 4. Корреляция между значением pH
и размерами ОКР

References

1. Industrial alumina chemicals. *Analytical Chemistry*. 1987;59:706A—706A.
https://doi.org/10.1021/ac00137a744
2. Ratnasamy P., Knözinger H. Infrared and optical spectroscopic study of Co—Mo—Al_2O_3 catalysts. *Journal of Catalysis*. 1978;54(2):155—165.
https://doi.org/10.1016/0021-9517(78)90038-6
3. Rahimpour M.R., Jafari M., Iranshahi D. Progress in catalytic naphtha reforming process: A review. *Applied Energy*. 2013;109:79—93.
https://doi.org/10.1016/j.apenergy.2013.03.080
4. Datsko T.Y., Zelentsov V.I. Dependence of the surface charge and the fluorine adsorption by γ-aluminum oxide on the solution temperature. *Surface Engeneering and Applied Electrochemistry*. 2009;45:404—410.
https://doi.org/10.3103/S1068375509050111
5. Sattler J.J.H.B., Ruiz-Martinez J., Santillan-Jimenez E., Weckhuysen B.M. Catalytic dehydrogenation of light alkanes on metals and metal oxides. *Chemical Reviews*. 2014;114:10613—10653.
https://doi.org/10.1021/cr5002436
6. Yashnik S.A., Kuznetsov V.V., Ismagilov Z.R. Effect of χ-alumina addition on H_2S oxidation properties of pure and modified γ-alumina. *Chinese Journal of Catalysis*. 2018;39:258—274.
https://doi.org/10.1016/S1872-2067(18)63016-5
7. Morales-Perez A.A., Martínez-Hernandez A., Fuentes G.A. NO adsorption during lean-rich cycles on Pt—Ba/γ-Al_2O_3 traps in a gas stream simulating the exhaust of gasoline engines. *Adsorption*. 2015;21:677—686.
https://doi.org/10.1007/s10450-015-9718-0
8. Wang J., Wen J., Shen M. Effect of interaction between $Ce_{0.7}Zr_{0.3}O_2$ and Al_2O_3 on structural characteristics, thermal stability, and oxygen storage capacity. *Journal of Physical Chemistry*. 2008;112(13):5113—5122.
https://doi.org/10.1021/jp711331g
9. Li S., Li X., Dan Y., Jiao Y., Deng J., Xiong L., Wang J., Chen Y. Designed synthesis of nanostructured Al_2O_3 stabilized homogeneous CeO_2—ZrO_2 solid solution as highly active support for Pd-only three-way catalyst. *Molecular Catalysis*. 2019;477:110513.
https://doi.org/10.1016/j.mcat.2019.110513
10. Kang D., Yu X., Ge M., Lin M., Yang X., Jing Y. Insights into adsorption mechanism for fluoride on cactus-like

amorphous alumina oxide microspheres. *Chemical Engineering Journal*. 2018;345:252—259.
https://doi.org/10.1016/j.cej.2018.03.174

11. Yang X., Li Q., Wang Z., Gong X., Yu Z., Guo Y., Wang L., Guo Y., Zhan W., Zhang J., Dai S. Taming the stability of Pd active phases through a compartmentalizing strategy toward nanostructured catalyst supports. *Nature Communications*. 2019;10:1611.
https://doi.org/10.1038/s41467-019-09662-4
12. Jang E.J., Lee J., Jeong H.Y., Kwak J.H. Controlling the acid-base properties of alumina for stable PtSn-based propane dehydrogenation catalysts. *Applied Catalysis, A: General*. 2019;572:1—8.
https://doi.org/10.1016/j.apcata.2018.12.024
13. Kwak J.H., Hu J.Z., Kim D.H., Szanyi J., Peden C.H.F. Penta-coordinated Al^{3+} ions as preferential nucleation sites for BaO on γ-Al_2O_3: An ultra-high-magnetic field ^{27}Al MAS NMR study. *Journal of Catalysis*. 2007;251(1):189—194.
https://doi.org/10.1016/j.jcat.2007.06.029
14. Kwak J.H., Hu J., Mei D., Yi C., Kim D.H., Peden C.H.F., Allard L., Szanyi J. Coordinatively unsaturated Al^{3+} centers as binding sites for active catalyst phases of platinum on γ-Al_2O_3. *Science*. 2009;325:1670—1673.
https://doi.org/10.1126/science.1176745
15. Lee J., Jang E.J., Kwak J.H. Effect of number and properties of specific sites on alumina surfaces for Pt—Al_2O_3 catalysts. *Applied Catalysis, A: General*. 2018;569:16833.
https://doi.org/10.1016/j.apcata.2018.10.004
16. Wang Ya., Pei C., Wang X., Sun G., Zhao Z., Gong J. The role of pentacoordinate Al^{3+} sites of Pt/Al_2O_3 catalysts in propane dehydrogenation. *Fundamental Research*. 2022;388:4—13.
https://doi.org/10.1016/j.fmre.2022.08.020
17. Wang Z., Jiang Y., Jin F., Stampfl C., Hunger M., Baiker A., Huang J. Strongly enhanced acidity and activity of amorphous silica—alumina by formation of pentacoordinated Al^{V} species. *Journal of Catalysis*. 2019;372:1—7.
https://doi.org/10.1016/j.jcat.2019.02.007
18. Ivanova A.S., Melgunov M.S. Aluminum oxide: application, methods of preparation, structure and acid-base properties. Moscow: Kalvis, 2009. 105 p. (In Russ.).
Иванова А.С., Мелгунов М.С. Оксид алюминия: применение, способы получения, структура и кислотно-основные свойства. М.: Калвис, 2009. 105 с.
19. Pakhomov N.A. Scientific bases of preparation of catalysts: introduction to theory and practice. Novosibirsk: SB RAS, 2011. 261 p. (In Russ.).
Пахомов Н.А. Научные основы приготовления катализаторов: введение в теорию и практику. Новосибирск: СБ РАС, 2011. 261 с.
20. Levin I., Bendersky L.A., Brandon D.G., Rühle M. Cubic to monoclinic phase transformations in alumina. *Acta Materialia*. 1997;45:3659—3669.
https://doi.org/10.1016/S1359-6454(97)00040-2
21. Ivanova A.S., Litvak G.S., Kryukova G.N., Tsybulya S.V., Paukshtis E.A. Real structure of metastable forms of aluminum oxide. *Kinetics and Catalysis*. 2000;41:137—141.
https://doi.org/10.1007/BF02756150
22. Anna K.K., Bogireddy K.R., Agarwal V., Bon R.R. Synthesis of α and γ phase of aluminium oxide nanoparticles for the photocatalytic degradation of methylene blue under sunlight: A comparative study. *Materials Letters*. 2022;317:132085. https://doi.org/10.1016/j.matlet.2022.132085
23. Kureti S., Weisweiler W. A new route for the synthesis of high surface area γ-aluminium oxide xerogel. *Applied Catalysis, A: General*. 2002;225:251—259.
https://doi.org/10.1016/S0926-860X(01)00870-5
24. Fernandes E.P., Silva T.S., Carvalho C.M., Selvasembian R., Chaukura N., Oliveira L.M.T.M., Meneghetti S.M.P., Meili L. Efficient adsorption of dyes by γ-alumina synthesized from aluminum wastes: Kinetics, isotherms, thermodynamics and toxicity assessment. *Journal of Environmental Chemical Engineering*. 2021;9:106198.
https://doi.org/10.1016/j.jece.2021.106198
25. Mahinroosta M., Allahverdi A. Production of high purity α- and γ-alumina from aluminum dross. *Encyclopedia of Renewable and Sustainable Materials Engeneering*. 2020;2:473—482.
https://doi.org/10.1016/b978-0-12-803581-8.11473-0

Information about the authors

Polina A. Solodovnikova – Postgraduate Student, Engineer, Department of Rare Metals and Nanomaterials, Ural Federal University n.a. the First President of Russia B.N. Eltsin (UrFU).
https://orcid.org/0000-0003-3303-8518
E-mail: solly.polly@yandex.ru

Maxim A. Mashkovtsev – Cand. Sci. (Chem.), Associate Prof., Department of Rare Metals and Nanomaterials, UrFU; Head of the Ceramics Laboratory of the Institute of High Temperature Electrochemistry of the Ural Branch of the Russian Academy of Sciences.
https://orcid.org/0000-0002-4914-262X
E-mail: m.a.mashkovtcev@urfu.ru

Vladimir N. Rychkov – Dr. Sci. (Chem.), Professor, Department of Rare Metals and Nanomaterials, UrFU.
E-mail: v.n.rychkov@urfu.ru

Georgiy V. Ginko – Student, Department of Rare Metals and Nanomaterials, UrFU.
https://orcid.org/0009-0001-0536-292X
E-mail: egorginko@gmail.com

Trofim E. Telegin – Student, Department of Rare Metals and Nanomaterials, UrFU.
https://orcid.org/0009-0004-9180-5281
E-mail: teleginte@gmail.ru

Maria V. Ugrumova – Student, Department of Rare Metals and Nanomaterials, UrFU.
https://orcid.org/0009-0009-2425-2476
E-mail: mari.ugryumova.02@mail.ru

Информация об авторах

Полина Александровна Солодовникова – инженер-исследователь, аспирант Уральского федерального университета им. первого Президента России Б.Н. Ельцина (УрФУ).
https://orcid.org/0000-0003-3303-8518
E-mail: solly.polly@yandex.ru

Максим Алексеевич Машковцев – к.х.н., доцент кафедры редких металлов и наноматериалов УрФУ; заведующий лабораторией керамики Института высокотемпературной электрохимии УрО РАН.
https://orcid.org/0000-0002-4914-262X
E-mail: m.a.mashkovtcev@urfu.ru

Владимир Николаевич Рычков – д.х.н., профессор кафедры редких металлов и наноматериалов УрФУ.
E-mail: v.n.rychkov@urfu.ru

Георгий Васильевич Гинько – студент кафедры редких металлов и наноматериалов УрФУ.
https://orcid.org/0009-0001-0536-292X
E-mail: egorginko@gmail.com

Трофим Егорович Телегин – студент кафедры редких металлов и наноматериалов УрФУ.
https://orcid.org/0009-0004-9180-5281
E-mail: teleginte@gmail.ru

Мария Викторовна Угрюмова – студент кафедры редких металлов и наноматериалов УрФУ.
https://orcid.org/0009-0009-2425-2476
E-mail: mari.ugryumova.02@mail.ru

Contribution of the authors

P.A. Solodovnikova – literature search and analysis, manuscript writing the article, data presentation and interpretation.

M.A. Mashkovtsev – idea, conceptualization, consulting.

V.N. Rychkov – participation in the discussion of results, consulting.

G.V. Ginko – synthesis of samples at a constant pH = 5, 6, 7, and 8.

T.E. Telegin – synthesis of samples at a constant pH = 9.

M.V. Ugrumova – analysis of the synthesized samples.

Вклад авторов

П.А. Солодовникова – поиск и анализ литературы, написание рукописи статьи, оформление и представление экспериментальных данных.

М.А. Машковцев – идея, концептуализация, консультирование.

В.Н. Рычков – участие в обсуждении результатов, консультирование.

Г.В. Гинько – синтез образцов при постоянном pH = 5, 6, 7 и 8.

Т.Е. Телегин – синтез образцов при постоянном pH = 9.

М.В. Угрюмова – анализ синтезированных образцов.

The article was submitted 13.12.2023, revised 13.05.2024, accepted for publication 16.05.2024

Статья поступила в редакцию 13.12.2023, доработана 13.05.2024, подписана в печать 16.05.2024

METALLURGY OF NON-FERROUS METALS / МЕТАЛЛУРГИЯ ЦВЕТНЫХ МЕТАЛЛОВ

UDC 541.138
https://doi.org/10.17073/0021-3438-2024-4-11-21

Research article
Научная статья

On the cementation purification of zinc solutions

A.V. Kolesnikov, E.I. Ageenko

Chelyabinsk State University
129 Bratiya Kashiriny Str., Chelyabinsk 454001, Russia

✉ Egor I. Ageenko (ag-40@mail.ru)

Abstract: The article focuses on researching the technology of cementation purification of zinc sulfate solutions from impurities that adversely affect the electrolysis of zinc. The purpose of this work is to explore new approaches for deep cementation purification of solutions, aimed at reducing the consumption of zinc dust and activating additives (antimony and copper compounds) in the technological process, while improving the quality of the purified solution by decreasing the content of cobalt, nickel, and cadmium in the solution supplied for zinc electrolysis. In this study, a new technology for the cementation purification of industrial solutions was developed, which includes the following stages of impurity removal using zinc dust: preliminary purification stage to remove copper to a concentration of 90–110 mg/L; co-precipitation of copper, cadmium, cobalt, and nickel with the addition of antimony trioxide; deep purification of the solutions from all impurities remaining after the first stage. The purification process was conducted under the following conditions: the preliminary deposition took place at a temperature of 50 °C, with a duration of 30 min and a zinc dust consumption of 0.2–0.4 g/L; the first purification stage occurred at a temperature of 80 °C, for a duration of 1 h, with a zinc dust consumption of 2–3 g/L, and an antimony dosage of 3–6 mg/L; the second purification stage was carried out at a temperature of 75–80 °C, for a duration of 1 h, with a zinc dust consumption of 2–3 g/L, and dosages of copper sulfate and antimony at 50 mg/L and 2–3 mg/L, respectively.

Keywords: cementation, cobalt, cadmium, nickel, copper, zinc dust, antimony trioxide, temperature, solution purified for electrolysis.

For citation: Kolesnikov A.V., Ageenko E.I. On the cementation purification of zinc solutions. *Izvestiya. Non-Ferrous Metallurgy*. 2024;30(4):11–21. https://doi.org/10.17073/0021-3438-2024-4-11-21

К вопросу цементационной очистки цинковых растворов

А.В. Колесников, Е.И. Агеенко

Челябинский государственный университет
Россия, 454001, г. Челябинск, ул. Братьев Кашириных, 129

✉ Егор Игоревич Агеенко (ag-40@mail.ru)

Аннотация: Статья посвящена исследованиям технологии цементационной очистки сульфатных цинковых растворов от примесей, отрицательно влияющих на электролиз цинка. Цель работы – поиск новых вариантов глубокой цементационной очистки растворов, позволяющих сократить расходы цинковой пыли и активирующих добавок (соединений сурьмы и меди) в технологическом процессе и улучшить качество очищенного раствора (снижением в нем содержаний кобальта, никеля, кадмия), подаваемого на электролиз цинка. Разработана новая технология цементационной очистки промышленных растворов, включающая следующие три стадии цементации примесей цинковой пылью: предварительная – очистка растворов от меди до концентрации 90–110 мг/л; первая – совместное осаждение меди, кадмия, кобальта, никеля с добавкой триоксида сурьмы; вторая – глубокая очистка растворов от всех оставшихся после 1-й стадии примесей. Эти стадии осуществлялись при следующих режимах: предварительное осаждение протекало при температуре $t = 50$ °С, продолжительности $\tau = 30$ мин и расходе цинковой пыли $m = 0{,}2\div0{,}4$ г/л; 1-я стадия очистки – $t = 80$ °С, $\tau = 1$ ч, $m = 2\div3$ г/л, дозировка по сурьме – 3–6 мг/л; 2-я стадия очистки – $t = 75\div80$ °С, $\tau = 1$ ч, $m = 2\div3$ г/л, дозировка медного купороса по меди – 50 мг/л, по сурьме – 2–3 мг/л. Разработанный метод позволяет снизить содержание примесей в исходном растворе до необходимых пределов для электролиза высококачественного цинка марки SHG. При этом расход цинковой пыли на первую и вторую стадии цементации должен уменьшиться до 35 кг/т цинка.

Ключевые слова: цементация, кобальт, кадмий, никель, медь, цинковая пыль, триоксид сурьмы, температура, очищенный для электролиза раствор.

Для цитирования: Колесников А.В., Агеенко Е.И. К вопросу цементационной очистки цинковых растворов. *Известия вузов. Цветная металлургия.* 2024;30(4):11–21. https://doi.org/10.17073/0021-3438-2024-4-11-21

Introduction

In recent years, there has been an increasing demand for high-quality zinc of the "Special High Grade" (SHG), in which the zinc content is 0.015 wt. % higher compared to the TsOA grade zinc (Table 1).

One of the main requirements for producing high-quality zinc is obtaining solutions that are deeply purified from cobalt and nickel. This becomes more challenging at facilities with high levels of organic matter, iron, and other impurities in the electrolytes, which are processed for cementation purification. The operational practices of zinc plants show that cobalt is the primary impurity in zinc solutions, and other trace impurities are highly correlated with it. In 95 cases out of 100, it can be assumed that removing cobalt from the solutions to concentrations of less than 1 mg/L reduces the other impurities to levels acceptable for electrolysis [1; 2].

Analysis of studies on the kinetics of cementation with zinc dust

As a rule, the cementation process proceeds quickly compared to corrosion and cannot be characterized by a single mechanism from start to finish. The entire cementation process, from the moment the cementing metal comes into contact with the solution to the final stage of reaction slowdown, can be divided into several distinct periods, each governed by its own laws [3].

A typical kinetic curve of the cementation process rate is presented in Fig. 1. Its form allows for the identification of four periods in the cementation process. As noted in the study [3], period *I* is observed only when passivating films are present on the surface of the metal and is associated with their removal due to dissolution upon interaction with the electrolyte. However, if the metal surface is in an active state (without passivating films) at the moment of contact with the solution, the surface activation period is absent, and cementation begins immediately after the metal is immersed in the electrolyte, i.e., without an induction period.

According to [3], the second period (*II*) is associated with the process of forming the cathodic surface, which cannot be separated from the process of its growth

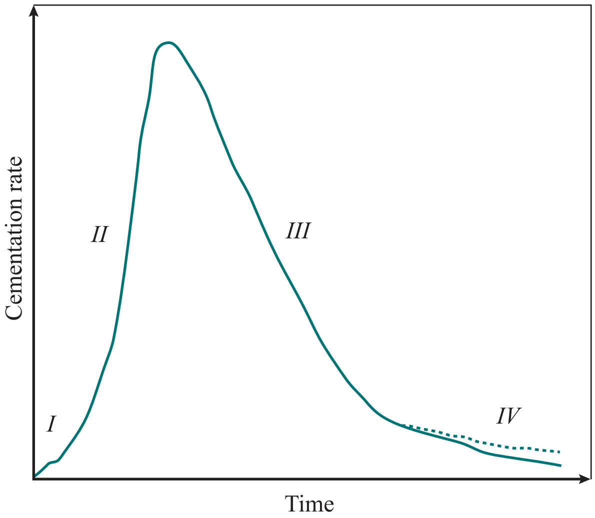

Dependence of cementation rate on time
I, *II*, *III*, *IV* – periods of the cementation process

Зависимость скорости цементации от времени
I, *II*, *III*, *IV* – периоды процесса цементации

Table 1. **Chemical compositions (wt. %) of zinc grades TsOA and SHG**

Таблица 1. Химический состав (мас. %) цинка марок ЦОА и SHG

Zinc grade	Zn, not less than	Impurities, not more than					
		Pb	Cd	Fe	Cu	Sn	Al
TsOA	99.98	0.01	0.003	0.003	0.001	0.001	Not standardized
SHG	99.995	0.003	0.003	0.002	0.001	0.001	0.005

in thickness. As soon as the first crystallization centers of the reduced metal appear, the growth of the existing centers begins simultaneously with the formation of new ones.

The third period (*III*) is the main phase of the process, during which the precepitation of the reduced metal primarily grows, and the concentration of its ions in the solution decreases. The rates of side reactions during the main period can generally be neglected.

The fourth period of cementation (*IV*) is the final phase of the reaction's slowdown, which is typically accompanied by a significant increase in the role of side reactions (see the dashed line in Fig. 1). These side reactions often terminate the reduction process long before thermodynamic equilibrium is reached [3].

In the hydrometallurgical production of zinc, the neutral zinc solution (pH = 5.0÷5.2) obtained after the complete dissolution of roasted zinc concentrate in sulfuric acid undergoes cementation purification to remove copper, cadmium, nickel, cobalt, antimony, thallium, and certain uncontrolled trace impurities.

Cementation precipitation of impurity metals (Me^{Z+}) from the solution is carried out using metallic zinc. This process is based on the fact that zinc does not contaminate the zinc solution and is more electro-negative than the precipitated impurities, which is why it acts as a reducing agent for impurity cations. The impurities precipitated on the zinc during cementation form the following decreasing series in terms of cementation rate at temperatures ≤ 70 °C: Cu > Cd > Ni > Co, while Fe^{2+} does not precipitate. At temperatures above 80 °C, as noted in the literature, cadmium precipitates less than nickel and cobalt. This order is typical for the impurity concentrations encountered in zinc production.

The tasks of cementation purification of zinc solutions from impurities include the following:

— improving the degree of solution purification;

— increasing the cadmium content in the cementation precipitates (a raw material for cadmium production);

— reducing the specific consumption of the cementing agent (zinc dust).

The factors influencing the cementation process include temperature, pH level, the quantity and ratio of precipitated impurities, the mass of solid suspended particles in the initial solution, the duration of the operations, and the methods for separating the cementation precipitates from the solution [1].

The degree of cementation purification of the neutral solution effectively increases only during a limited contact time between the zinc dust and the solution (20—30 min). After that, the oxidation of the reduced cadmium begins to dominate over the precipitation of impurities, and the purification performance no longer improves, and may even worsen if "fresh" cementing agent is not added [1].

Thus, the intensification of cementation, as shown in the aforementioned studies, is achieved by the following methods:

— increasing the specific consumption and dispersity of the zinc dust;

— using activators for zinc dust;

— increasing the temperature to the optimal level;

— increasing the stirring rate of the solution;

— avoiding prolonged contact between the solution and the cementing agent.

In the initial stages of cementation purification, copper and cadmium are usually removed. Copper is relatively easily removed from the solution with a stoichiometric consumption of zinc, while complete removal of cadmium is more challenging, as its cementation precipitate can redissolve. The presence of arsenic, antimony, germanium, and oxidizers like Fe^{3+} in the zinc solution promotes the dissolution of cadmium precipitates [2].

An understanding of which metals can be precipitated from a solution via cementation with zinc can be gained by comparing the standard electrode potentials of the metals. Electrochemical theory suggests that all metals with a standard potential more positive than –0.763 V can be cemented with zinc.

Practical approaches to purifying zinc solutions from impurities that negatively impact zinc electrolysis

Based on data from the information-analytical database [1], we analyzed the technologies and purification parameters used by 32 plants worldwide for cobalt removal, considering both periodic and continuous schemes, the number of purification stages, activators, purification temperatures, and the cobalt content in the purified solutions. The majority of plants use continuous impurity removal processes, typically with two or three stages. In 22 % of the cases, α—β-naphthol is used as an alternative to zinc dust for cobalt removal. The most common temperature range for cobalt purification is 60—70 °C. The level of cobalt removal is relatively consistent, with final concentrations ranging between 0.1 and 2.0 mg/L. Common zinc dust activators include Sb_2O_3, As_2O_3, $CuSO_4$, with Schlippe's salt and potassium tartrate used less frequently.

One zinc plant implemented a two-stage purification process using zinc dust with different particle sizes: +0.063—0.25 mm in the first stage and –0.063 mm in the second. In the second stage, copper sulfate and antimony compounds were added as activators. This stage operated at a temperature of 70—90 °C. The first stage was designed to reduce copper and cadmium concentrations in the solution to less than 1 mg/L (Cu) and 7—10 mg/L (Cd), resulting in a copper-cadmium cake that could be used for cadmium production. The second stage focused on purifying the solution from nickel, cobalt, cadmium, and other impurities to meet the specifications required for SHG zinc electrolysis [1]. However, when the new scheme was introduced, challenges emerged in preparing the solutions for zinc electrolysis. The situation became more complex when the plant processed zinc concentrates and oxidized ores with high cobalt and nickel content, leading to increased levels of these metals in the zinc solutions undergoing cementation purification. This situation necessitated a more thorough investigation of the cementation process for cobalt and nickel.

It is well established [1; 2] that the most common method for purifying zinc solutions from cobalt is cementation with zinc dust, along with the addition of activators, most frequently arsenic and antimony in the form of salts, oxides, or elemental substances. Zinc dust activation is typically enhanced when antimony and arsenic are introduced into the solution along with copper ions. Some studies have demonstrated the advantages of using pentavalent antimony as an activator for the removal of Co^{2+} and Ni^{2+} at concentrations of 0.25—0.4 mg/L [4].

Zinc dust containing inclusions of lead, aluminum, copper, and antimony is also employed for the cementation of Co^{2+} and Ni^{2+} [5—7]. In one study [5], it was proposed to purify zinc sulfate solutions from impurities using zinc dust with the following composition, in %: 0.001—0.03 Al, 0.05—1.0 Pb, and occasionally 0.02—0.1 Cu. The alloy for producing zinc dust is prepared by adding lead and zinc to a zinc-aluminum alloy [5—7]. The purification process with zinc dust is conducted in two stages, following a counter-current principle. Zinc dust containing these impurities is added in excess during the second stage of cementation, where cobalt and nickel are removed from the solution. At least part of the cementation precipitate, along with excess zinc dust, is directed back to the first stage of cementation to precipitate cadmium and copper from the solution.

The authors of study [8] examined the effect of PbO and oxides formed during the first stage of the Harris process, which represents a mixture of lead and antimony oxides. Their findings showed that lead oxides in the solution promote more complete precipitation of cobalt and nickel during cementation with zinc dust. To enhance nickel precipitation efficiency, it was suggested to introduce zinc cakes, as well as lead and zinc sulfides [1]. Another study [9] proposed that in addition to antimony, the purification process could benefit from the addition of lead salts (20—100 mg/L), sulfur (100—5000 mg/L), activated carbon, bentonite, and limestone.

The Debari zinc-electrolyte plant in India was commissioned in 1967 [10], and its production capacity was expanded to 45000 tons in 1976. During this expansion, an electrolyte purification process was introduced, which involved the addition of K—Sb-tartrate to zinc dust for cementation of impurities. Initially, the zinc dust consumption was 62 kg per ton of zinc, but starting in 1977, the specific consumption steadily increased, reaching 80 kg per ton due to the declining quality of zinc sulfide raw materials. Based on studies aimed at reducing zinc dust consumption, a two-stage purification scheme was developed. The first stage involved a reduced amount of zinc dust, and the resulting copper-cadmium cake was removed from the process. In the second stage, additional zinc dust was introduced, and the cake separated by a hydrocyclone was returned to the first purification stage. The implementation of this two-stage method reduced zinc dust consumption to 35—40 kg per ton.

In study [11], a three-stage purification process is described. In the first stage, recycled zinc dust from the second and third stages is introduced, and at a temperature of 70—75 °C, copper and cadmium are completely precipitated, along with a significant portion of cobalt. The precipitate is separated in two thickeners, each 9 meters in diameter. The overflow is heated to 95 °C and sent to the second stage (a cascade of four tanks). Here, the remaining cobalt is removed by adding Sb_2O_3 powder to the first tank and zinc dust to the first, third, and fourth tanks. The excess zinc dust, together with the cobalt precipitate, is separated from the solution in hydrocyclones and returned to the first purification stage. The hydrocyclone overflow is sent to the third stage, which serves as the final purification and acts as a buffer before the solution is sent for filtration. A small amount of zinc dust is added in the third stage to prevent cobalt, cadmium, and copper from re-dissolving into the solution. The pH of the solution is maintained at 3.6—3.8 for better filterability. Filtration is carried out using filter presses with polypropylene fabric and kraft paper. The filtered solution is then sent to electrolysis.

Several studies have demonstrated the effectiveness of removing cobalt from solutions using butyl xanthate and other organic substances such as hydroxylamine, ethylenediamine, urea, and water-soluble nitroso compounds, water-soluble salts of nitroso compounds [12; 13], as well as salts of tartaric acid [14]. At the same time, it has been noted [1] that the presence of organic substances significantly slows down the cementation of cobalt due to their adsorption on the cathodic areas of the zinc metal. Therefore, the methods developed for impurity removal [15] are of practical importance not only for wastewater treatment but also for obtaining high-quality solutions for electrolysis.

It has been established [16] that the addition of nonylphenol polyethylene glycol and polyethylene glycol negatively affects the cementation of cobalt, while the addition of dinaphthylmethane-4,4-disulfonic acid does not influence the cementation process. It was shown that copper has a positive effect on cobalt cementation, whereas antimony has a negative effect. It was also noted that at a temperature of 65—85 °C, the cementation reaction of Co^{2+} proceeds in a kinetic regime and follows first-order reaction kinetics. The studied process includes two periods: an initial period (up to 4 min) and a main period (up to 10 min), which is associated with intensive hydrogen evolution.

Publications [17; 18] xplore the effect of surfactants (SAA) on the cementation of nickel using zinc powder with a particle size of 54—74 μm from solutions containing 180 mg/L of nickel and 200 mg/L of copper, respectively. Surfactant additions ranged from 15—30 mg/L. It was found that the presence of surfactants inhibits the nickel cementation process, resulting in smaller grain sizes and lower porosity of the cementation precipitates. As the temperature increases, nickel crystal size and precipitate porosity also increase.

Study [18] also investigated the effect of adding nonylphenol polyethylene glycol on cadmium cementation using zinc powder with a particle size of 54—74 μm from solutions containing 202 mg/L Cd^{2+} and 200 mg/L Cu^{2+} at a pH of 4.5. It was found that, unlike the negative effects on nickel cementation observed with all tested surfactants, the cadmium cementation process was accelerated. The rate constant for cadmium cementation in the presence of copper ($K{\cdot}10^3$, cm/s) decreased in the following order: from 4.2 in the presence of nonylphenol polyethylene glycol, to 3.7 (without additives), to 3.3 with the addition of polyethylene glycol, and to 2.6 in the presence of dinaphthylmethane-4,4-disulfonic acid.

The authors of study [19] noted that in organizing a continuous process for purifying solutions to permissible levels of impurities that negatively affect zinc electrolysis, the presence of surfactants in the initial solution would require an increased consumption of zinc dust to achieve the desired level of purification.

In study [20], Sb_2O_3 powder was used as an activator for cobalt cementation. Optimal conditions were determined for cobalt cementation from zinc sulfate solutions containing 150 000 mg/L $ZnSO_4$ and 24 mg/L cobalt. The Co^{2+} concentration in the solution was reduced to 1 mg/L under the following cementation conditions: zinc dust with a particle size of 120—150 μm was used at a dosage of 5 g/L; Sb_2O_3 was added at 4 mg/L; the pH of the solution was 4.5; and the temperature was 85 °C. The optimal conditions for cobalt removal with antimony (*III*) oxide were established as follows [20]: temperature of 80—85°C, Cu^{2+} concentration of 200—300 mg/L, and Sb to Co ratio of (0.5—2) : 1.

In study [21], a modified method for deep purification of zinc sulfate solutions from cobalt was described. The initial solution contained (in mg/L): 80—180 Cu, 300—450 Cd, 4—8 Co, 4—8 Ni, 5—12 Ti, and 0.1—0.15 As. Under optimal conditions—zinc powder dosage of 3.0—3.5 g/L, potassium antimony tartrate ($K(SbO)C_4H_4O_6$) at 1 mg/L, $CuSO_4$ at a minimum of 25 mg/L, pH = 4.5÷4.8, temperature of 80—85 °C, and a contact time of 3.0—3.5 h a purified solution was obtained, containing 0.1 mg/L Co, less than 0.3 mg/L Ni, and increased levels of copper (0.13—0.15 mg/L), cadmium (1.0 mg/L), and thallium (2.0 mg/L).

Study [22] investigated the conditions for purifying zinc sulfate solutions from cobalt, with zinc concentrations of 154 000 mg/L and impurities (in mg/L) as follows: Cu — 290, Cd — 610, Co — 22, Fe — 3, Ni — 6, Sb — 2. Cementation was carried out in two stages at a temperature of 70 °C, pH = 4.5, with the addition of 20 mg/L Cu^{2+}, 100 mg/L As, and 2 g/L zinc powder. In the first stage, the degree of cobalt purification reached 50 %. After the second stage, cobalt concentrations in the solution were reduced to less than 0.75 mg/L.

Research [23] investigated the impact of metal salt additives (Cu, Cd, Pb, Sb, Sn) on the kinetics of cobalt cementation using zinc powder with particle sizes ranging from 50 to 750 μm and a specific surface area of 1.74 m^2/g. The optimal conditions for cementation were identified as follows: temperature of 85 °C, and additive concentrations (in mg/L) of Cu — 15, Cd — 10, and Sb — 2. The cobalt cementation process was found to follow a first-order kinetic model, with an activation energy of 51 kJ/mol. Significant differences were noted between the cementation behavior of cobalt in industrial and synthetic solutions.

Research conducted in study [24] demonstrated that when Sb_2O_3 is added during cobalt cementation, antimony co-precipitates with cobalt, resulting in a cementation product containing a metallic CoSb compound.

Study [25] explored the cementation of cobalt using zinc powder from a solution containing (in mg/L): 13—28 Co, 3.0 Sb_2O_3, and 150 000 Zn at a pH of 5.0. The optimal cementation conditions, which reduced the cobalt concentration to less than 0.5 mg/L, were determined to be: temperature 85 °C, contact time 90 min, stirring speed of the pulp 300 rpm, and zinc powder consumption (particle size <55 μm) of 1.6 g/L.

Optimal conditions for cobalt and nickel cementation in the presence of $CuSO_4$ and $K(SbO)C_4H_2O_6$ as activators were identified in study [26]: temperature 80 °C, contact time 75 min, and zinc powder consumption of 1500 % of the stoichiometric amount, with an Sb : Co = 1. It was noted that extending the purification time beyond 75 min resulted in partial dissolution of the cementation precipitates. The absence of copper in the solution significantly affected nickel cementation, while the absence of arsenic had a lesser impact.

Study [27] highlighted the negative effect of high zinc concentrations on cobalt cementation. It was noted that at zinc concentrations greater than 50000 mg/L, only a few percent of cobalt was removed from the solution after 3 h. The cementation process was carried out on a rotating zinc disk at 90 °C, with an initial cobalt concentration of 10 mg/L, pH = 3.3, and no activators.

Study [28] examined the mechanism of cobalt removal using zinc dust with the addition of As_2O_3 and Cu in a galvanic cell with a membrane, a zinc anode, and a copper cathode. The cell design was described, and the following cathodic reactions were presented: $2H^+ + 2e^- = H_2\,(г)$, $2Co^{2+} + 2HAsO_2 + 6H^+ + 10e^- = 2CoAs + 4H_2O$. The anodic reaction was: $Zn = Zn^{2+} + 2e$. It was shown that the degree of cobalt removal increased with higher temperatures and the amount of added As_2O_3. The addition of Cu^{2+} accelerated cobalt precipitation, explained by the formation of a galvanic couple between zinc and copper. The pattern of cobalt cementation changed significantly with the addition of activators. Comparative data on cobalt cementation rates (relative units) were provided in studies [28, 29]: 1 (no additives), 1.1 (copper added), 3.0 (antimony added), 18.0 (copper + antimony added) at a temperature of 73 °C, with initial solution concentrations (in mg/L): Co — 30, Cu — 30, Sb — 1.5, and zinc dust consumption of 4 g/L, pH = 3.6.

Studies [2; 9; 30] have noted that the effect of surfactants (SAA) on cementation processes lies in their adsorption on the surface of cementation elements, creating additional resistance in the electrical circuit, which reduces the current. In macroelectrolysis, the desired current can be easily maintained by adjusting the voltage supplied to the bath, but in low-power cementation systems, overcoming this additional resistance would require selecting a galvanic couple with a high electromotive force (EMF). Ultimately, the presence of surfactants in solutions undergoing cementation leads to an increase in the time required to achieve the target residual concentration of the precipitated metal in the solutions [30—34].

An analysis of the literature shows that nearly all plants have implemented a three-stage purification scheme, which includes an intermediate stage for partially removing copper from the process. It is known that for deep purification of solutions from cobalt and nickel, increased consumption of zinc dust with a particle size of less than 55 μm is necessary, along with the mandatory addition of antimony compounds and the presence of copper in the solution. A significant reduction in zinc dust consumption was achieved at the “Zinkgruvan” plant (Kokkola, Finland) by using arsenic trioxide during the cementation stage [1]. Additionally, this plant differs from other known purification schemes in the sequence of operations: after the intermediate stage of partial copper precipitation, the first stage involves deep purification from cobalt and nickel (while at most other plants, the first stage targets copper and cadmium), and the final stage focuses on deep cadmium purification (while other facilities prioritize cobalt and nickel at this stage).

In light of the above, the present study investigated a purification scheme involving deep precipitation of cobalt and nickel in the first stage.

The aim of the study is to explore new approaches for deep cementation purification that would reduce the consumption of zinc dust and activating additives (antimony and copper compounds) in the technological process, while improving the quality of the purified solution lowering the concentrations of cobalt, nickel, and cadmium supplied in the solution used for zinc electrolysis.

Experimental

The following technology for cementation purification of industrial solutions is proposed:

Preliminary stage — cementation purification of the solutions from copper to a concentration of 90—110 mg/L ($t = 50$ °C, $\tau = 30$ min, zinc dust consumption $m = 0.2 \div 0.4$ g/L);

Stage 1 — co-precipitation of copper, cadmium, cobalt, and nickel with the addition of antimony trioxide (t = 80 °C, τ = 1 h, m = 2÷3 g/L, antimony dosage — 3—6 mg/L);

Stage 2 — deep purification of the solutions from all impurities remaining after the first stage (t = 75÷80 °C, τ = 1 h, m = 2÷3 g/L, copper sulfate dosage — 0—50 mg/L, antimony dosage — 2—3 mg/L).

The overall consumption of reagents was as follows: zinc dust — 4.2—6.4 g/L, copper sulfate dosage — 50 mg/L, antimony dosage — 5—9 mg/L. The variation in reagent consumption is due to the differing impurity content in the neutral industrial zinc solution used in the experiments.

The following starting materials were used:

— neutral industrial zinc solutions with the following average composition (in mg/L): Zn — 136 800, Co — 4.09, Cd — 562, Cu — 306, Ni — 3.85, Sb — 0.41, As — 0.35, total Fe — 91.1, Fe^{2+} — 22.9;

— antimony trioxide solution — a suspension with a solid concentration of 800 mg/L;

— copper sulfate solution;

— fine zinc dust.

During the preliminary precipitation stage, copper was cemented from zinc solutions obtained during the leaching of roasted zinc concentrate, using zinc dust (40—60 % fraction size —0.063 mm).

As a result of the preliminary precipitation, filtrates with varying copper concentrations were obtained and used in the first stage of cementation purification:

Filtrate number	1	2	3	4	5	6	7
Cu, mg/L	65	93	100	115	124	200	300

In the first stage of cementation, the starting filtrate with different residual copper concentrations (from 65 to 300 mg/L) after the preliminary precipitation was treated with antimony as a Sb_2O_3 pulp (with an Sb: (Co + Ni) ratio of 1 : 1), and zinc dust with a particle size of –0.063 mm was added for impurity precipitation (Cu, Cd, Co, and Ni) at a dosage of 2.5 g/L. Cementation at this stage was carried out at 80 °C for 1 h. The parameters (zinc dust consumption, temperature, and duration of the process) were determined through additional experiments using filtrates obtained after preliminary copper precipitation to concentrations of 90—110 mg/L. The effect of copper content in the filtrates after preliminary precipitation on the residual cadmium and cobalt content in the solution after the first stage of cementation was established:

Cu, mg/L	65	93	100	111	124	200	300
Cd, mg/L	0,12	0,13	0,15	0,25	2,6	4,8	104,5
Co, mg/L	0,26	0,21	0,22	0,27	0,30	0,35	2,62

It is clear that the cadmium and cobalt concentrations in the solution after the first stage of purification decrease as the copper content in the solution following the preliminary cementation is reduced. Thus, a preliminary conclusion can be made that to achieve acceptable levels of cadmium and cobalt for zinc electrolysis, the copper concentration in the solution after the preliminary cementation should be between 90 and 110 mg/L.

As mentioned earlier, additional experiments were conducted to establish more accurate purification conditions, determining the temperature, duration, zinc dust dosage, and activating additives. It was also proven that the preliminary stage of copper precipitation to the indicated concentrations (90—110 mg/L) is necessary. The results of the experiments are presented in Table 2.

The data in Table 2 show that increasing the temperature reduces the concentration of certain impurities in the filtrate. However, at 85 °C, after 1 h, cobalt undergoes reverse dissolution, leading to a rise in its concentration. Therefore, a temperature of 80 °C is considered optimal, as the concentrations of other impurities remain within acceptable limits at this level.

Experiments were also conducted on the cementation of impurities at the first and second stages of purification with varying zinc dust dosages (Table 3), with copper and antimony concentrations of 50 and 2 mg/L, respectively.

As seen from the data (Table 3), acceptable purification results were obtained at the first stage with zinc dust dosages ranging from 2.5 to 4.0 g/L. At the second stage, with high-quality solutions after the first stage, consistently high purification levels for cobalt and cadmium

Table 2. **Chemical analysis of solutions (mg/L) after the first stage of purification from impurities that negatively affect zinc electrolysis**

Таблица 2. Химический анализ растворов (мг/л) после 1-й стадии очистки от примесей, отрицательно влияющих на электролиз цинка

t, °C	Cd	Co	Ni
75	0.15	0.39	0.31
80	0.11	0.22	0.31
85	0.07	0.41	0.21

Table 3. **Concentration of impurities (mg/L) in the solution after purification at different zinc dust dosages (g/L)**

Таблица 3. Концентрация примесей в растворе (мг/л) после очистки при разных дозировках цинковой пыли (г/л)

Stage I				Stage II			
Zinc dust	Cd	Co	Ni	Zinc dust	Cd	Co	Ni
2.5	0.24	0.20	0.29	1.5	0.105	0.233	0.218
3.0	0.23	0.19	0.23	2.0	0.103	0.209	0.162
4.0	0.22	0.13	0.19				

Table 4. **Impurity content in the solution after purification with zinc dust when varying the dosage of activating additives at the second stage of cementation (τ = 1 h, t = 80 °C, zinc dust consumption 2.5 g/L)**

Таблица 4. Содержание примесей в растворе после очистки цинковой пылью при изменении дозировки активирующих добавок на 2-й стадии цементации (τ = 1 ч, t = 80 °C, расход цинковой пыли 2,5 г/л)

Dosage of reagents at the second stage of cementation (mg/L)		Cd, mg/L		Co, mg/L	
Cu	Sb	Solution after the first stage of cementation	Purified solution after the second stage	Solution after the first stage of cementation	Purified solution after the second stage
0	2	0.32	0.11	0.37	0.33
50	2	0.20	0.10	0.35	0.14
50	0	0.15	0.10	0.26	0.28
50	4	0.35	2.59	0.45	0.43

were achieved (at 0.2 and 0.1 mg/L, respectively) with a zinc dust dosage of 1.5 g/L.

Experiments were conducted using different reagent additives as cementation catalysts, specifically with a copper sulfate solution (50 mg/L Cu) and antimony in the form of Sb_2O_3 pulp (6—7 mg/L Sb) at the second stage of purification. The results are shown in Table 4.

The data in Table 4 show that at the second stage of cementation, the introduction of 50 mg/L copper and 2 mg/L antimony minimizes the impurity content in the purified solution. However, increasing the antimony dosage to 4 mg/L, along with the additional introduction of 50 mg/L copper ions during the second stage of purification, worsens the solution quality. In the purified solution, the cadmium content increases to 2.59 mg/L, and cobalt to 0.43 mg/L.

Table 5 provides data on the effect of cementation duration during the first stage on the quality of the obtained solution. The zinc dust consumption was 2.5 g/L. During the first stage of cementation, the solution used came from the leaching of roasted zinc concentrates without the preliminary copper precipitation stage, and its copper content was 300 mg/L.

Table 5. Cobalt and cadmium content (mg/L) at the first stage of purification with increasing process duration

Таблица 5. **Содержание кобальта и кадмия (мг/л) на 1-й стадии очистки при увеличении продолжительности процесса**

τ, min	Cd	Co
0	516	3.54
30	15.5	1.41
60	15.8	0.73
90	59.3	1.64
120	104.5	2.62

According to Table 5, the lowest impurity content is observed after 60 minutes of the first stage, while increasing the duration results in higher cadmium and cobalt concentrations, indicating their reverse dissolution. The data in Table 5 further confirm the necessity of preliminary copper cementation in the solution to a concentration of 90—110 mg/L.

Table 6 presents comparative data on cementation purification of solutions according to the known [1] and developed technologies.

Table 6. **Comparative data of the known and developed technologies**

Таблица 6. Сравнительные данные известной и разработанной технологий

№	Known technology	Developed technology
1	Partial cementation purification from copper	Preliminary stage of cementation purification from copper to a concentration of 90–110 mg/L in the solution
2	First stage of cementation – copper-cadmium purification	First stage of cementation – purification from impurities: Co, Ni, Cd, Cu, etc.
3	Second stage of cementation – purification from Co, Ni, and other cementation impurities	Second stage of cementation – deep purification from cementation impurities remaining in the filtrate after the first stage
4	Total consumption of zinc dust (particle size –0.63 mm) for the 1^{st} and 2^{nd} stages – 75 kg/ton	Total consumption of zinc dust (particle size –0.63 mm) for the 1^{st} and 2^{nd} stages – 35 kg/ton
5	Purified solution content (mg/L): Co – 0.28; Cd – 0.53; Ni – 0.31; Sb – 0.12; Cu – 0.18	Purified solution content (mg/L): Co – 0.1; Cd – 0.1; Ni – 0.2; Sb – 0.015; Cu – 0.069

Conclusions

1. A new scheme for cementation purification of zinc solutions has been proposed, which includes:

— preliminary cementation of impurities using zinc dust in solutions after the leaching stage of roasted products, reducing copper concentrations to 90—110 mg/L;

— conducting the first stage of cementation for cobalt, nickel, and other impurities using zinc dust with a particle size of –0.063 mm at 80 °C, with the addition of antimony compounds;

— carrying out the second stage of cementation for cadmium and other impurities using zinc dust with a particle size of –0.063 mm at 80 °C, with the addition of copper and antimony compounds.

2. The necessity of preliminary copper precipitation from leaching solutions to concentrations of 90—110 mg/L before the first purification stage has been experimentally proven, which significantly improves the performance of cementation purification.

3. The developed method allows for reducing the impurity content in the initial solution to the levels required for the electrolysis of high-quality SHG zinc. At the same time, the zinc dust consumption for the first and second stages can be reduced to 35 kg per ton of zinc.

References

1. Kolesnikov A.V. Research and development of processes for producing high-quality zinc from raw materials with a high content of cobalt and nickel: Diss. ... Dr. Sci. (Eng.). Ekaterinburg: UGTU–UPI, 2007. (In Russ.).
   Колесников А.В. Исследование и разработка процессов получения высококачественного цинка из сырья с повышенным содержанием кобальта и никеля: Дис. ... докт. техн. наук. Екатеринбург: УГТУ—УПИ, 2007.
2. Alkatsev M.I. Cementation processes in non-ferrous metallurgy. Moskow: Metallurgiya, 1981. 113 p. (In Russ.).
   Алкацев М.И. Процессы цементации в цветной металлургии. М.: Метал-лургия, 1981. 113 с.
3. Rotinyan A.L., Tikhonov K.I., Shoshina I.A. Theoretical electrochemistry. Leningrad: Khimiya, 1981. 424 p. (In Russ.).
   Ротинян А.Л., Тихонов К.И., Шошина И.А. Теоретическая электрохимия. Л.: Химия, 1981. 424 с.
4. Voldman G.M., Zelikman A.N. Theory of hydrometallurgical processes. Moskow: Intermet Inzhiniring, 2003. 462 p. (In Russ.).
   Вольдман Г.М., Зеликман А.Н. Теория гидрометаллургических процессов. М.: Интермет Инжиниринг, 2003. 462 с.
5. Ageenko E.I., Kolesnikov A.V., Pavlovsky D.A. Study of the kinetics of cadmium cementation in the presence of a flocculant. *Journal of the Siberian Federal University. Chemistry*. 2023;16(2):287—299. (In Russ.).
   Агеенко Е.И., Колесников А.В., Павловский Д.А. Исследование кинетики цементации кадмия в присутствии флокулянта. *Журнал Сибирского федерального университета. Химия*. 2023;16(2):287—299.
6. Danuta K. Cementation purification of industrial solutions of zinc sulfate. *Rud Imetaleniezel*.1979;24(2):65—75.
7. Quathers R. The method of purification of the electrolyte in hydrometallurgy of zinc. *Metallurgie*. 1976;16(3): 164—166.

8. Abrasheva B., Karoleva V. The influence of lead oxide on the deposition of cobalt and nickel from zinc sulfate solutions by zinc dust. Study of the conditions for using oxides of the first stage according to Harris as an activating additive. *Godishn. Institute of Nonferrous Metallurgy.* 1977;15:19—39.
9. Alkatsev V.M., Alkatseva M.I. The influence of PAA glue on the processes of cementation of copper, cadmium and cobalt. *Izvestiya. Non-Ferrous Metallurgy.* 1991;(2):119—120. (In Russ.).

   Алкацев В.М., Алкацева М.И. Влияние ПАА клея на процессы цементации меди, кадмия и кобальта. *Известия вузов. Цветная металлургия*. 1991;(2):119—120.
10. Ageenko E.I., Kolesnikov A.V., Pavlovsky D.A. Investigation of cadmium cementation kinetics in the presence of surfactants. *Bulletin of the South Ural State University. Ser. Chemistry.* 2023;15(2):107—115. (In Russ.). https://doi.org/10.14529/chem230210

    Агеенко Е.И., Колесников А.В., Павловский Д.А. Исследование кинетики цементации кадмия в присутствии ПАВ. *Вестник ЮУрГУ. Сер. Химия.* 2023;15(2):107—115.
11. Kolesnikov A.V. On the issue of cleaning solutions from cobalt with zinc dust. *Non-Ferrous Metallurgy.* 2012;(1):42—47. (In Russ.).

    Колесников А.В. К вопросу очистки растворов от кобальта цинковой пылью. *Цветная металлургия.* 2012;(1):42—47.
12. Polyakov M.L., Polyakova E.M., Polyakova O.M. Method for purifying zinc sulfate solutions from nickel and cobalt. Author's certificate 358271 (USSR). 1985. (In Russ.).

    Поляков М.Л., Полякова Е.М., Полякова О.М. Способ очистки сульфатных цинковых растворов от никеля и кобальта. Авт. св-во 358271 (СССР). 1985.
13. Kolesnikov A.V. Reduction of copper by metallic zinc in aqueous solutions in the presence of high molecular weight surfactants. *Condensed Matter and Interphases.* 2016;18(1):46—55. (In Russ.).

    Колесников А.В. Восстановление меди металлическим цинком в водных растворах в присутствии высокомолекулярных ПАВ. *Конденсированные среды и межфазные границы.* 2016;18(1):46—55.
14. Bockman O., Ostvold T. The effect of tartaric acid salts on the cementation of cobalt from a solution of zinc sulfate on a rotating zinc disk. *Hydrometallurgy.* 2000;55(1):107—112. https://doi.org/10.1016/S0304-386X(99)00079-1
15. Palant A.A., Bryukvin V.A. Purification of hydrometallurgical solutions from organic impurities. *Non-Ferrous Metals.* 2001;(1):87—89 (In Russ.).

    Палант А.А., Брюквин В.А. Очистка гидрометаллургических растворов от органических примесей. *Цветные металлы.* 2001;(1):87—89.
16. Karavasteva M. The effect of certain surfactants on the cementation of cobalt from zinc sulphate solutions by suspended zinc particles in the presence of copper or antimony. *Canadian Metallurgical Quarterly.* 2001;40(2):179—184. https://doi.org/10.1179/000844301794388416
17. Karavasteva M. Effect of surfactants on the cementation of nickel with zinc powder from zinc sulfate solutions in the presence of copper. *Canadian Metallurgical Quarterly.* 1999;38(3):207—209. https://doi.org/10.1179/cmq.1999.38.3.207
18. Karavasteva M. The influence of copper on the effect of certain surfactants during the cementation of cadmium by suspended zinc particles. *Hydrometallurgy.* 1998;48(3):361—366. https://doi.org/10.1016/S0304-386X(98)00009-7
19. Wang T., Lin G., Gu L., Hu T., Xie T., Qu H., Wang S., Zhang L., Cheng S., Liu J. Role of organics on the purification process of zinc sulfate solution and inhibition mechanism. *Materials Research Express.* 2019;6(10):106588. https://doi.org/10.1088/2053-1591/ab3dc5
20. Dai J., Wang D., Q. Jiang L., Jin M. Removal of cobalt from zinc sulfate solutions using the addition of antimony trioxide. *Transactions of Nonferrous Metals Society of China*. 2002;12(6):1172—1175.
21. Ragyavan R., Mohanan P.K., Verma S.K. Modified zinc sulphate solution purification technique to obtain low levels of cobalt for the zinc electrowinning process. *Hydrometallurgy.* 1999;51(2):187—206. https://doi.org/10.1016/S0304-386X(98)00076-0
22. Jiang L., Wang D., Dai J., Jin M., Wei X. Zinc powder consumption decrease in cobalt removal from zinc leaching solution with arsenic oxide. *Nonferrous Metals (China).* 2003;55(1):90—95.
23. Dreher T.M., Nelson A., Demopoulos G.P., Filippou D. The kinetics of cobalt removal by cementation from an industrial zinc electrolyte in the presence of Cu, Cd, Pb, Sb and Sn additives. *Hydrometallurgy.* 2001;60(2):105—116. https://doi.org/10.1016/S0304-386X(00)00152-3
24. Guo Zhang-cheng, Yan Jiang-fend, Yang Xian-wan. Mechanism of Sb_2O_3 in removal of cobalt in zinc sulfate solutions. *The Chinese Journal of Nonferrous Metals.* 2000;10(5):697—700.
25. Liu Z., Tang C., Zhang D., Guo X., Chen H. Study on the purifying processes for zinc leach solutions with antimony trioxides. *Journal of Central South University of Technology (China).* 2000;31(3):225—227.
26. Boyanov B.S., Konareva V.V., Kolev N.K. Purification of zinc sulfate solutions from cobalt and nickel through activated cementation. *Hydrometallurgy.* 2004;73(1-2):163—168. https://doi.org/10.1016/j.hydromet.2003.09.002
27. Tozawa K., Nishimura T., Akahori M., Malaga M.A. Comparison between purification processes for zinc leach

solutions with arsenic and antimony trioxides. *Hydrometallurgy.* 1992;30(1-3):445—461.
https://doi.org/10.1016/0304-386X(92)90099-L

28. Bøckman O., Østvold T., Voyiatzis G.A., Papatheodorou G.N. Raman spectroscopy of cemented cobalt on zinc substrates. *Hydrometallurgy.* 2000;55(1):93—105.
https://doi.org/10.1016/S0304-386X(99)00080-8

29. Bagaev A.S. Optimal content of copper ions and the degree of cobalt extraction during cementation cleaning of zinc solutions. *Izvestiya. Non-Ferrous Metallurgy.* 1981;(4):57—58. (In Russ.).
Багаев А.С. Оптимальное содержание ионов меди и степень извлечения кобальта при цементационной очистке цинковых растворов. *Известия вузов. Цветная металлургия*. 1981;(4):57—58.

30. Kolesnikov A.V., Tsyganova I.V. Investigation of flocculant influence on the kinetic parameters of copper recovery in aqueous solution with metal zinc. *Izvestiya. Non-Ferrous Metallurgy.* 2019;(3):4—11. (In Russ.).
https://doi.org/10.17073/0021-3438-2019-3-4-11
Колесников А.В., Цыганова И.В. Исследование влияния флокулянтов на кинетические параметры восстановления меди в водном растворе металлическим цинком. *Известия вузов. Цветная металлургия.* 2019;(3):4—11.
https://doi.org/10.17073/0021-3438-2019-3-4-11

31. Zahmati F., Shayesteh K., Vahidfard V. Removal of cadmium in process of nickel production out of cold purification waste of zinc factories. *Journal of The Institution of Engineers (India): Series D.* 2024:1—10.
https://doi.org/10.1007/s40033-023-00617-0

32. Abbasi P., Shayesteh K., Vahidfard V., Jangara H. Removal of cadmium in the cold purification step by semibatch process. *Chemical Review and Letters.* 2023;6(4):449—460.
https://doi.org/10.22034/crl.2023.408052.1234

33. Granata G., Tsendorj U., Liu W., Tokoro C. Direct recovery of copper nanoparticles from leach pad drainage by surfactant-assisted cementation with iron powder. *Colloids and Surfaces A: Physicochemical and Engineering Aspects.* 2019;580:123719.
https://doi.org/10.1016/j.colsurfa.2019.123719

34. Kolesnikov A.V., Pratskova S.E. Theory and practice of cleaning solutions with zinc dust in hydrometallurgy. Experimental and theoretical data. Riga: Palmarium Academic Publishing, 2017. 130 p. (In Russ.).
Колесников А.В., Працкова С.Е. Теория и практика очистки растворов цинковой пылью в гидрометаллургии. Экспериментальные и теоретические данные. Рига: Palmarium Academic Publishing, 2017. 130 с.

Information about the authors

Alexander V. Kolesnikov – Dr. Sci. (Eng.), Head of the Department of analytical and physical chemistry of Chelyabinsk State University.
https://orcid.org/0000-0002-9747-1241
E-mail: avkzinc@csu.ru

Egor I. Ageenko – Senior Lecturer at the Department of analytical and physical chemistry of Chelyabinsk State University.
https://orcid.org/0000-0002-2701-9831
E-mail: ag-40@mail.ru

Информация об авторах

Александр Васильевич Колесников – д.т.н., заведующий кафедрой аналитической и физической химии Челябинского государственного университета (ЧелГУ).
https://orcid.org/0000-0002-9747-1241
E-mail: avkzinc@csu.ru

Егор Игоревич Агеенко – ст. преподаватель кафедры аналитической и физической химии ЧелГУ.
https://orcid.org/0000-0002-2701-9831
E-mail: ag-40@mail.ru

Contribution of the authors

A.V. Kolesnikov – development of the main concept, setting the goals and objectives of the study.

E.I. Ageenko – conducting calculations and analyzing the research results.

Вклад авторов

А.В. Колесников – формирование основной концепции, постановка цели и задачи исследования.

Е.И. Агеенко – осуществление расчетов, анализ результатов исследования.

The article was submitted 14.02.2024, revised 04.07.2024, accepted for publication 08.07.2024

Статья поступила в редакцию 14.02.2024, доработана 04.07.2024, подписана в печать 08.07.2024

METALLURGY OF NON-FERROUS METALS / МЕТАЛЛУРГИЯ ЦВЕТНЫХ МЕТАЛЛОВ

UDC 669.63
https://doi.org/10.17073/0021-3438-2024-4-22-32

Research article
Научная статья

Effect of ultrasonic treatment on tin recovery from decommissioned displays in sulphuric, hydrochloric, and methanesulphonic acid solutions

E.B. Kolmachikhina, O.B. Kolmachikhina, Ya.A. Yankina, Z.M. Golibzoda, P.A. Brizhevataya, D.S. Sedel'nikova, R.E. Khabibulina

Ural Federal University n.a. the First President of Russia B.N. Eltsin
19 Mira Str., Ekaterinburg 620002, Russia

✉ Elvira B. Kolmachikhina (e.b.khazieva@urfu.ru)

Abstract: The study investigates the physicochemical patterns of tin leaching from the surface of glass substrates from decommissioned displays in hydrochloric, sulphuric, and methanesulphonic acids. The effects of acid concentration (0.1–1.0 N), duration (10–60 min), temperature (298–353 K), and ultrasonic treatment intensity (UST) (120–300 W/cm^2) on leaching performance were evaluated. It was demonstrated that ultrasonic treatment positively impacts sulphuric acid leaching of tin, increasing its recovery by 14–16 %. However, during leaching in hydrochloric and methanesulphonic acid solutions, UST led to a reduction in tin recovery to 28 % and 1.7 %, respectively, due to acid decomposition under ultrasound. The partial reaction orders for tin leaching in HCl, H_2SO_4, and CH_3SO_3H were determined to be 0.8, 1.4, and 1.1, respectively, and changed to 1.5, 1.1, and 0.3 under ultrasound for the corresponding acids. An increase in temperature from 298 K to 333 K significantly improved tin recovery in sulphuric and hydrochloric acids. However, raising the temperature to 353 K led to a decrease in tin ion concentration after 10–20 min, likely due to tin hydrolysis and precipitation. The calculated apparent activation energies of tin oxide dissolution in HCl solutions were 40.4 kJ/mol without UST and 22.9 kJ/mol with UST. For H_2SO_4, the apparent activation energy was 4.0 kJ/mol, increasing to 29.0 kJ/mol under ultrasonic treatment. Therefore, the study showed that tin leaching from glass substrates of decommissioned displays proceeds in a kinetic regime when HCl is used and in a diffusion regime in H_2SO_4 solutions, with ultrasonic treatment facilitating the transition to a mixed regime.

Keywords: tin, sulphuric acid, hydrochloric acid, methanesulphonic acid, leaching, ultrasound.

Acknowledgements: This research was funded by a grant from the Russian Science Foundation, Project No. 22-79-00129, https://rscf.ru/en/project/22-79-00129/

For citation: Kolmachikhina E.B., Kolmachikhina O.B., Yankina Ya.A., Golibzoda Z.M., Brizhevataya P.A., Sedel'nikova D.S., Khabibulina R.E. Effect of ultrasonic treatment on tin recovery from decommissioned displays in sulphuric, hydrochloric, and methanesulphonic acid solutions. *Izvestiya. Non-Ferrous Metallurgy.* 2024;30(4):22–32. https://doi.org/10.17073/0021-3438-2024-4-22-32

Влияние ультразвуковой обработки на выщелачивание олова из отслуживших дисплеев в растворах серной, соляной и метансульфоновой кислот

Э.Б. Колмачихина, О.Б. Колмачихина, Я.А. Янкина, З.М. Голибзода, П.А. Брижеватая, Д.С. Седельникова, Р.Э. Хабибулина

Уральский федеральный университет (УрФУ) им. первого Президента России Б.Н. Ельцина
Россия, 620002, г. Екатеринбург, ул. Мира, 19

✉ Эльвира Барыевна Колмачихина (e.b.khazieva@urfu.ru)

Аннотация: Изучены физико-химические закономерности выщелачивания олова с поверхности стеклянных подложек отслуживших дисплеев в соляной, серной и метансульфоновой кислотах. Установлено влияние концентрации указанных кислот (0,1–

1,0 н), продолжительности (10—60 мин), температуры (298—353 K) и интенсивности ультразвуковой обработки (УЗО) (120—300 Вт/см^2) на показатели выщелачивания. Показано, что ультразвуковое воздействие оказывает положительное влияние на сернокислотное выщелачивание олова, позволяя повышать его извлечение на 14—16 %. При выщелачивании в растворах соляной и метансульфоновой кислот УЗО приводила к снижению извлечения олова до 28 и 1,7 % соответственно, что связано с их разложением под действием ультразвука. Частные порядки реакций выщелачивания олова по HCl, H_2SO_4 и CH_3SO_3H составили 0,8, 1,4 и 1,1, при воздействии ультразвука частные порядки изменялись следующим образом для соответствующих кислот: 1,5, 1,1 и 0,3. Увеличение температуры с 298 до 333 K значительно повышало извлечение олова в серной и соляной кислотах. Повышение температуры до 353 K приводило к снижению концентрации ионов олова через 10—20 мин процесса, что, вероятнее всего, связано с гидролизом и осаждением олова. Рассчитанные величины кажущейся энергии активации растворения оксида олова без и с использованием УЗО в растворах HCl составили 40,4 и 22,9 кДж/моль соответственно. В случае использования H_2SO_4 кажущаяся энергия активации составила 4,0 кДж/моль, а при акустическом воздействии – 29,0 кДж/моль. Таким образом, проведенные исследования показали, что выщелачивание олова из стекол отслуживших дисплеев протекает в кинетическом режиме при использовании HCl и в диффузионном режиме в растворах H_2SO_4, а УЗО способствует переходу процессов в смешанный режим.

Ключевые слова: олово, серная кислота, соляная кислота, метансульфоновая кислота, выщелачивание, ультразвук.

Благодарности: Исследование выполнено за счет гранта Российского научного фонда № 22-79-00129, https://rscf.ru/project/22-79-00129/

Для цитирования: Колмачихина Э.Б., Колмачихина О.Б., Янкина Я.А., Голибзода З.М., Брижеватая П.А., Седельникова Д.С., Хабибулина Р.Э. Влияние ультразвуковой обработки на выщелачивание олова из отслуживших дисплеев в растворах серной, соляной и метансульфоновой кислот. *Известия вузов. Цветная металлургия*. 2024;30(4):22—32.
https://doi.org/10.17073/0021-3438-2024-4-22-32

Introduction

One of the main types of decommissioned electronic devices consists of screens and monitors. This category accounts for approximately 10 % of the total mass of generated electronic waste. Nearly all screens and monitors contain indium tin oxide (ITO) in their displays. ITO (90 % In_2O_3, 10 % SnO_2) is transparent to visible light, possesses electrical conductivity, and is used as a conductive layer applied to the glass substrate of the display [1]. Additionally, ITO is widely used in the production of solar panels, optical coatings, antistatic films, and thermal protection.

Approximately 75 % of the ITO produced is used in the manufacture of flat panel displays. These displays consist of multiple layers, including polarisation filters, glass substrates, and liquid crystals. A layer of ITO, 50—200 nm thick, is applied to the surface of the glass substrate [2], while a polariser made of polyvinyl acetate film is attached to the opposite side. The indium content in the glass substrates ranges from 100—350 mg/kg [3, 4], and the tin content ranges from 25—60 mg/kg [5, 6]. Although the indium content in glass substrates is relatively low, it is comparable to that found in zinc concentrates extracted from sulphide ores [7]. This makes decommissioned monitors a highly promising secondary source of indium.

Tin is a scarce metal [8, 9], classified as a strategic metal in many countries. With the accelerating development of the semiconductor and electric vehicle industries, tin consumption has also increased. Recovering tin from secondary sources will help alleviate the shortage of mineral resources and reduce environmental pollution.

In studies focused on the recycling of liquid crystal displays, the emphasis is often placed on the behaviour of indium due to its high content in ITO. Although the tin content in ITO is relatively low, exploring ways to extract it will provide a comprehensive solution for recycling decommissioned displays.

The recycling of glass substrates begins with pre-treatment, which may include steps such as polariser removal, crushing, grinding, and beneficiation [10—13]. Subsequent metallurgical processing can be carried out using pyrometallurgical methods (reduction and distillation of indium and tin compounds) [14] and/or hydrometallurgical methods (leaching, liquid recovery, cementation, etc.) [15—19].

In this study, a comparative assessment of the tin leaching rate from the surface of glass substrates in hydrochloric, sulphuric, and methanesulphonic acids was conducted. The acids used in the study are strong acids and can be arranged in the following order based on increasing strength, as expressed by the dissociation constant (pK_{d1}): CH_3SO_3H (–1.86), H_2SO_4 (–3), HCl (–7) [20—22]. Ultrasonic treatment (UST) was used to accelerate the ITO leaching process, providing thermal, mechanical, and sonochemical effects [23—30].

The aim of this work was to investigate the influence of ultrasonic treatment, temperature, concentration, and type of acids on the physicochemical patterns of tin dissolution from the surface of crushed glass substrates from decommissioned liquid crystal displays.

Experimental methodology

Researmh materials, equipment, and methods

The glass substrates from decommissioned liquid crystal displays were pre-washed with water, air-dried, and then heated to 463 K to soften and manually remove the film. The cleaned glass substrates were crushed in a rod mill. A fraction of the crushed material smaller than 1 mm was separated by sieving and used for further experiments. After thoroughly homogenising the material, a representative sample was taken by quartering for subsequent chemical analysis using an atomic absorption spectrophotometer (AAS) "novAA 300" (Analytik Jena, Germany). The particle size distribution of the material was determined using a HELOS&RODOS laser diffraction particle size analyser (Sympatec GmbH, Germany). The morphology of the crushed material samples and their chemical composition were examined with a JSM-6390LA scanning electron microscope (JEOL, Japan), equipped with a JED-2300 energy-dispersive microanalysis system (JEOL, Japan).

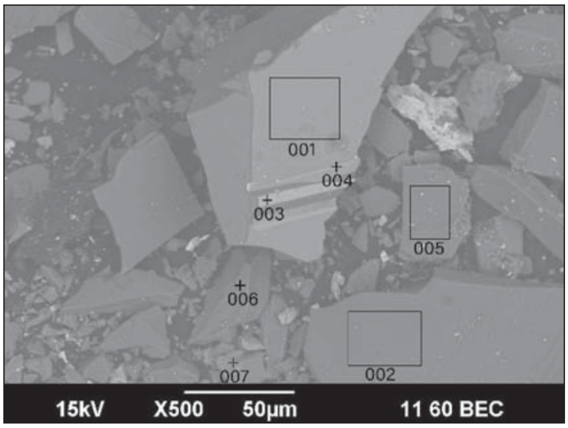

Element	Measurement area number						
	001	002	003	004	005	006	007
Mg	2.1	1.7	0.9		1.6		4.0
Al	10.3	19.0	5.0	23.3	18.3	12.8	19.8
Si	77.8	67.2	73.2	61.7	67.8	48.8	69.5
Ca	2.9	12.1	2.1	1.3	12.3	38.5	6.7
Cr	–	–	12.7	–	–	–	–
Fe	–	–	3.2	–	–	–	–
Mo	–	–	2.3	13.7	–	–	–
In	5.5	–	–	–	–	–	–
Sn	1.3	–	–	–	–	–	–

Fig. 1. SEM image and elemental composition (%) of crushed glass substrates from displays

Рис. 1. СЭМ-изображение и элементный состав (%) измельченных стеклянных подложек дисплеев

The majority of the material (>85 %) consisted of irregularly shaped particles smaller than 300 μm (Fig. 1). Elemental analysis, along with previous studies, showed that the material was primarily composed of aluminium, silicon, and calcium oxides. Indium and tin compounds were detected on the glass surface (Fig. 1, point *1*), while molybdenum compounds were found on the surface of the conductive tracks (Fig. 1, points *3* and *4*). The crushed glass substrates from the displays contained the following concentrations, in mg/kg: indium — 174.8, tin — 1.7.

The experiments used sulphuric acid (H_2SO_4, chemically pure), hydrochloric acid (HCl, chemically pure), and methanesulphonic acid (CH_3SO_3H, chemically pure). The initial acid solutions were prepared by diluting concentrated acids with stirring on a magnetic stirrer.

Ultrasonic treatment was performed using the UZTA-0.1/28-O apparatus (LLC Ultrasound Technology Centre, AltSTU, Biysk), equipped with an immersion-type emitter, at a frequency of 28 ± 2.5 kHz and ultrasonic intensity (I) ranging from 120 to 300 W/cm^2.

Crushed glass leaching

Leaching experiments were conducted in a thermostatically controlled reactor with a volume of 0.5 dm^3 at a temperature of T = 298÷353 K, a duration of τ = 10÷60 min, and acid concentrations of 0.1—1.0 N. The liquid-to-solid ratio (L : S) was 10 : 1 (cm^3/g).

Acid solutions with the required concentration were poured into the reactor, sealed, and heated to the desired temperature under constant stirring. Then, the ultrasonic emitter was immersed in the reactor to a fixed depth, 20 g of material was loaded, and the ultrasonic generator was turned on, with the pulp temperature being automatically maintained with an accuracy of ±2 K.

After leaching, the pulp was filtered, and the cake was washed with distilled water. The cake was then subjected to acid treatment at T = 363 K in a 20 % hydrochloric acid solution for several hours to ensure the complete dissolution of metals into the solution. After acid treatment, the cake was again filtered and washed with distilled water. Samples taken during leaching, the filtrates after leaching and acid treatment, and the wash waters were analyzed for tin ion content using atomic absorption spectrophotometry (AAS) (novAA300, Analytik Jena, Germany). The overall tin recovery (α_{Sn}) was assessed based on its content in the filtrates and wash waters.

Experimental data processing

The degree of tin recovery was calculated, taking into account the volumes of collected samples, using the following formula:

$$\alpha_{Sn}^{i} = \frac{C^{i}(V_{\text{initial}} - V_{\text{sample}}(i-1)) + \sum_{1}^{i-1}(C^{i}V_{\text{sample}})}{G_{Sn}} \cdot 100, \quad (1)$$

where α^{i}_{Sn} is the degree of tin recovery at the moment of the i-th sample collection, %; C^{i} is the concentration of tin in the i-th sample, g/dm^3; V_{sample} is the volume of the sample, dm^3; V_{init} is the initial volume of the leaching solution, dm^3; G_{Sn} is the mass of tin in the material sample, g.

Kinetic characteristics (reaction orders and apparent activation energies) were determined by calculating the instantaneous leaching rate at the initial moment of time (υ_0) by constructing tangents to the curves $\alpha_{Sn} = f(\tau)$. The tangents were drawn through the origin of the coordinate system.

Results and discussion

Effect of ultrasonic treatment intensity on tin recovery

The intensity of ultrasonic treatment had varying effects on the systems under investigation (Table 1). In the case of sulphuric acid leaching, increasing the ultrasonic treatment intensity to I = 120 W/cm^2 improved tin recovery by 14.5 %. Further increasing the intensity did not result in a significant rise in tin recovery, which can be attributed to the weakening of cavitation processes due to the excessive growth of cavitation bubble radius [31].

In hydrochloric acid leaching with ultrasonic treatment, tin recovery decreased to 28—29 %, which was comparable to the results of sulphuric acid leaching. The reduction in the efficiency of hydrochloric acid leaching with ultrasonic treatment is likely due to a decrease in hydrogen chloride solubility in the aqueous solution, caused by local overheating at the hot spots formed by the collapse of cavitation bubbles [32].

During ITO leaching in methanesulphonic acid, ultrasonic treatment reduced tin recovery across the entire studied range of ultrasonic intensities to 1.7—4.3 %. This could indicate thermal decomposition of methanesulphonic acid during acoustic cavitation [33]. The slight increase in tin recovery with rising ultrasonic intensity is likely related to the weakening of cavitation processes.

Table 1. **Effect of ultrasonic treatment intensity on tin recovery during leaching in sulphuric, hydrochloric, and methanesulphonic acids (C_{acids} = 0.2 N, T = 333 K, τ = 60 min)**

Таблица 1. Влияние интенсивности УЗО на извлечение олова при выщелачивании в серной, соляной и метансульфоновой кислотах ($C_{\text{кислот}}$ = 0,2 н, T = 333 K, τ = 60 мин)

I, W/cm^2	Tin recovery, %		
	H_2SO_4	HCl	CH_3SO_3H
0	14.9	47.5	5.6
120	29.4	28.0	1.7
180	29.0	28.5	2.8
240	31.6	28.8	2.8
300	31.2	29.3	4.3

Subsequent investigations into the effect of acid concentration and temperature were conducted at a constant ultrasonic intensity of I = 180 W/cm^2.

Effect of acid type and concentration on tin recovery

According to the obtained data (Fig. 2), during ITO leaching without ultrasonic treatment in hydrochloric (Fig. 2, *a*) and sulphuric (Fig. 2, *c*) acid solutions, the most intensive dissolution of tin occurred in the first 20—40 min, after which the process rate significantly decreased due to the reduction in unreacted ITO and the concentration of H$^+$ ions. When leaching in methanesulphonic acid solutions (without ultrasonic treatment), the graphs of $\alpha_{Sn} = f(\tau)$ showed linear behaviour (Fig. 2, *e*) due to the low recovery and the large amount of unreacted tin oxide.

Tin dissolution without ultrasonic treatment was most intensive in hydrochloric acid solutions, where recovery reached 76 % in a 1.0 N HCl solution. In sulphuric and methanesulphonic acid solutions, the maximum tin recovery was 53 % and 48.5 %, respectively (C_{acid} = 1.0 N). It is clear that the high tin recovery in hydrochloric acid is due to its higher degree of dissociation compared to sulphuric and methanesulphonic acids.

Ultrasonic treatment enhanced tin leaching in sulphuric acid, increasing recovery by 13—30 %, with a maximum of 66% (Fig. 2, *d*). In contrast, acoustic treatment reduced tin recovery in both hydrochloric (Fig. 2, *b*) and methanesulphonic (Fig. 2, *f*) acids. For example,

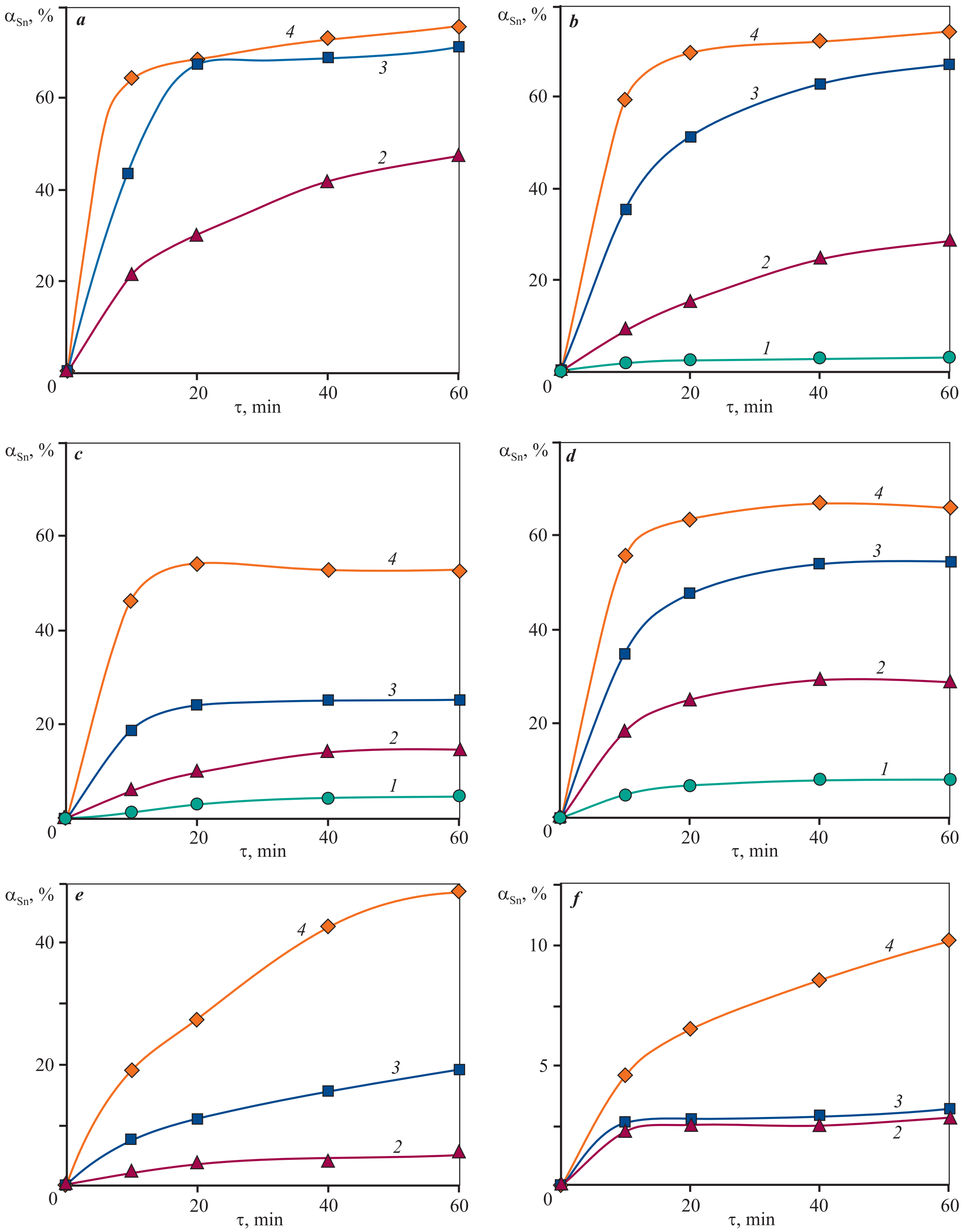

Fig. 2. Effect of leaching duration on tin recovery at various concentrations of hydrochloric (***a***, ***b***), sulphuric (***c***, ***d***) and methanesulphonic (***e***, ***f***) acids without (***a***, ***c***, ***e***) and with (***b***, ***d***, ***f***) ultrasonic treatment

$T = 333$ K; $I = 180$ W/cm^2; C_{acids}, N: 0.1 (*1*), 0.2 (*2*), 0.4 (*3*), and 1.0 (*4*)

Рис. 2. Влияние продолжительности выщелачивания на извлечение олова при различных концентрациях соляной (***a***, ***b***), серной (***c***, ***d***) и метансульфоновой (***e***, ***f***) кислот без использования (***a***, ***c***, ***e***) и с использованием (***b***, ***d***, ***f***) УЗО

$T = 333$ K; $I = 180$ Вт/см^2; $C_{\text{кислот}}$, н: 0,1 (*1*), 0,2 (*2*), 0,4 (*3*) и 1,0 (*4*)

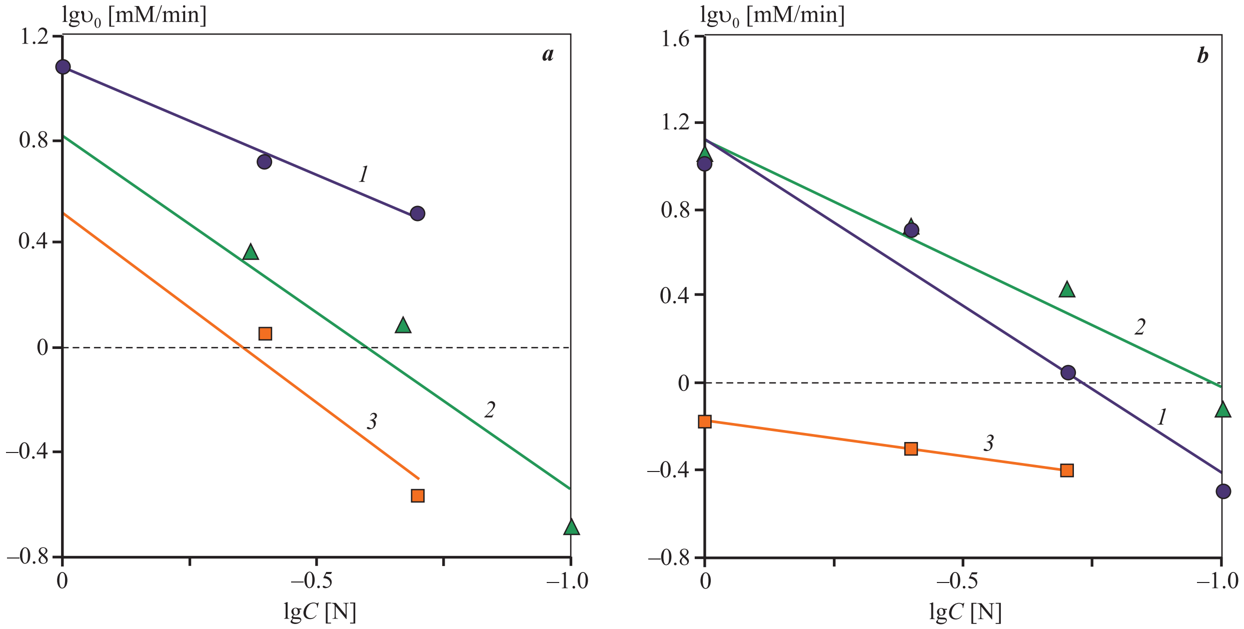

Fig. 3. Evaluation of the partial reaction orders for tin dissolution in hydrochloric (*1*), sulphuric (*2*), and methanesulphonic (*3*) acid solutions without (***a***) and with (***b***) ultrasonic treatment

Рис. 3. Определение частного порядка реакций растворения олова в растворах соляной (*1*), серной (*2*) и метансульфоновой (*3*) кислот без использования (***a***) и с использованием (***b***) УЗО

without ultrasonic treatment, tin recovery in a 0.2 N hydrochloric acid solution reached 48 %, while with ultrasonic treatment, it decreased by 20 %. In methanesulphonic acid, ultrasonic treatment reduced tin recovery by 2 to 6 times, with only 10 % of tin entering the solution after 60 min of leaching in a 1.0 N solution. This significant reduction in tin recovery in hydrochloric and methanesulphonic acids is most likely due to acid decomposition under ultrasonic influence.

The partial reaction orders for tin oxide leaching in the studied acids change significantly under the influence of ultrasound (Fig. 3, Table 2). This effect is especially pronounced in hydrochloric and methanesulphonic acids, which undergo the most significant decomposition under acoustic treatment.

Table 2. **Partial orders of tin oxide leaching reactions by sulphuric, hydrochloric, and methanesulphonic acids**

Таблица 2. Частные порядки реакций выщелачивания оксида олова по серной, соляной и метансульфоновой кислотам

Acid	Reaction order by acids	
	Without ultrasonic treatment	With ultrasonic treatment
HCl	0.8	1.5
H_2SO_4	1.4	1.1
CH_3SO_3H	1.5	0.3

Effect of leaching temperature on tin recovery

Increasing the temperature from 298 to 333 K significantly intensified tin leaching in sulphuric (Fig. 4, *c*) and hydrochloric (Fig. 4, *a*) acid solutions. However, at $T = 353$ K, after 10—20 min of leaching, the concentration of tin ions in the solutions decreased (Fig. 4, *a*, *c*, curve *4*), possibly indicating tin hydrolysis and precipitation at higher temperatures [34].

In the absence of ultrasonic treatment, tin recovery from ITO was highest in hydrochloric acid solutions, reaching 47 % at $T = 333$ K. The application of ultrasound reduced the efficiency of hydrochloric acid leaching compared to experiments conducted without ultrasound: tin recovery decreased by 19—22 % at $T = 333$—353 K (Fig. 4, *b*).

In contrast, sulphuric acid leaching of tin was intensified by ultrasonic treatment across the entire temperature range studied, with tin recovery increasing by 2.0—3.4 times, reaching 30.5 % at $T = 313{\div}333$ K (Fig. 4, *d*). Tin dissolution in methanesulphonic acid was minimal, and tin ions were only detected in solutions after leaching at $T = 333$ K: without ultrasound,

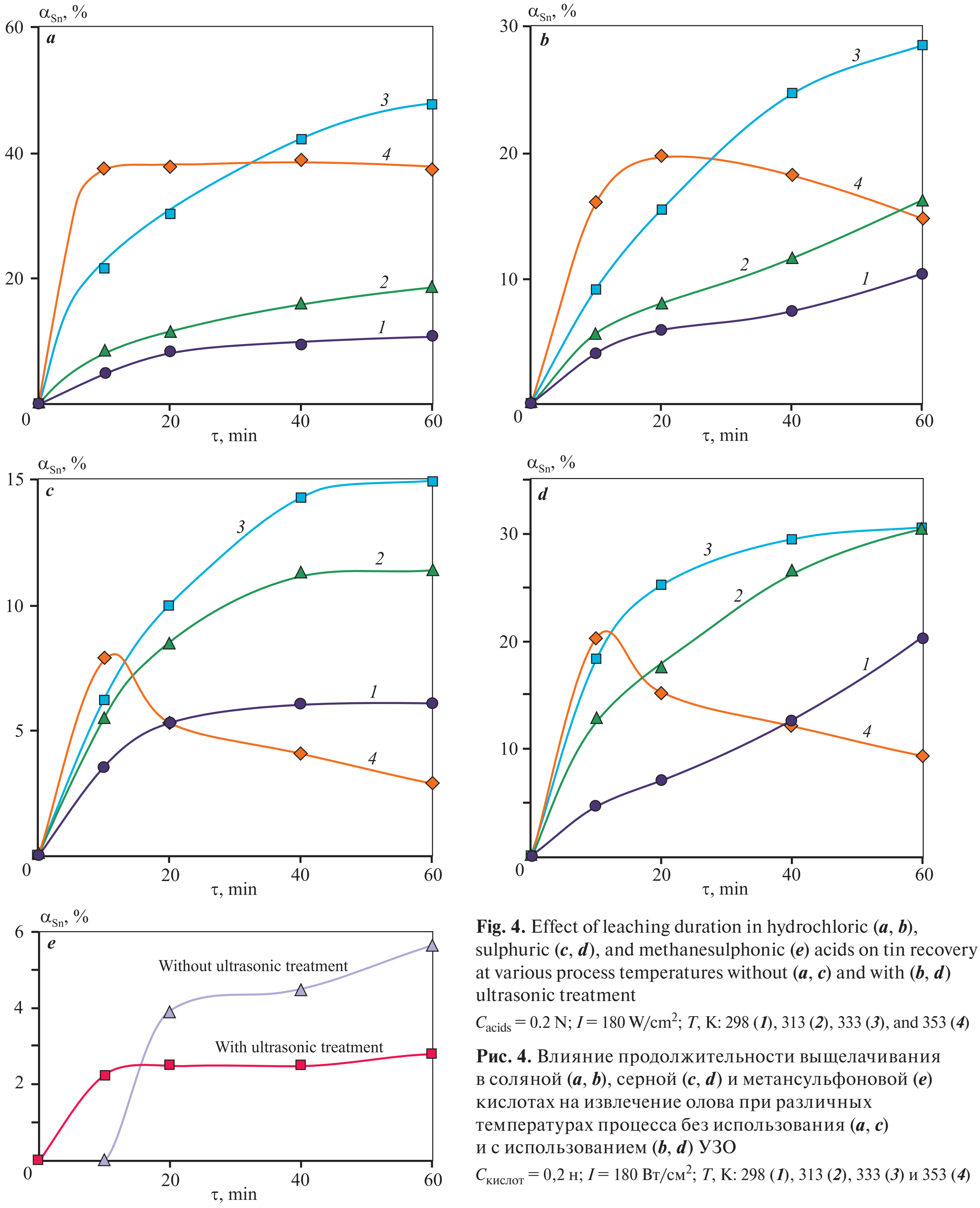

Fig. 4. Effect of leaching duration in hydrochloric (***a***, ***b***), sulphuric (***c***, ***d***), and methanesulphonic (***e***) acids on tin recovery at various process temperatures without (***a***, ***c***) and with (***b***, ***d***) ultrasonic treatment

C_{acids} = 0.2 N; I = 180 W/cm^2; T, K: 298 (***1***), 313 (***2***), 333 (***3***), and 353 (***4***)

Рис. 4. Влияние продолжительности выщелачивания в соляной (***a***, ***b***), серной (***c***, ***d***) и метансульфоновой (***e***) кислотах на извлечение олова при различных температурах процесса без использования (***a***, ***c***) и с использованием (***b***, ***d***) УЗО

$C_{кислот}$ = 0,2 н; I = 180 Вт/см^2; T, K: 298 (***1***), 313 (***2***), 333 (***3***) и 353 (***4***)

α_{Sn} = 5.6 %, and with ultrasound, it dropped to 2.8 % (Fig. 4, *e*).

Based on the obtained kinetic patterns, the apparent activation energy (E_a) for the dissolution of tin oxide in hydrochloric and sulphuric acids was calculated (Fig. 5): HCl — 40.4 (22.9) kJ/mol, H_2SO_4 — 4.0 (29.0) kJ/mol (the values in parentheses correspond to leaching with ultrasonic treatment). The E_a value and the partial reaction order for tin oxide leaching in hydrochloric acid (without ultrasound) indicate that the process occurs in a kinetic-controlled regime. Under acoustic treatment, the E_a value for hydrochloric

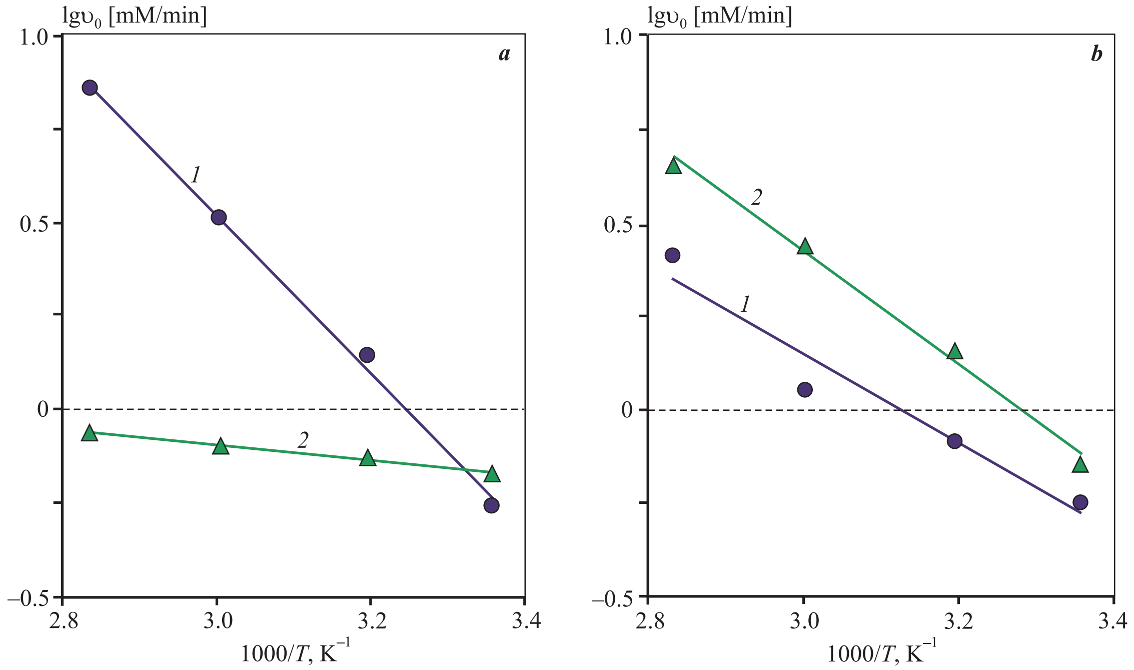

Fig. 5. Evaluation of the apparent activation energy for tin leaching reactions in hydrochloric (***1***) and sulphuric (***2***) acids without (***a***) and with (***b***) ultrasonic treatment

Рис. 5. Определение кажущейся энергии активации реакций выщелачивания олова в соляной (***1***) и серной (***2***) кислотах без использования (***а***) и с использованием (***b***) УЗО

acid leaching of tin oxide decreases, suggesting a shift to a mixed control regime. Sulphuric acid leaching of tin oxide (without ultrasound) likely occurs in a diffusion-controlled regime, while ultrasonic treatment reduces the influence of diffusion factors, leading to a transition to a mixed control regime.

Conclusions

The conducted studies aimed at determining the effects of acid selection, their concentrations, temperature regimes, ultrasonic treatment, and leaching duration of decommissioned displays on leaching performance revealed the following patterns:

1. Ultrasonic treatment intensified the dissolution of tin oxide in 0.2 N sulphuric acid solutions, increasing tin recovery by 14—16 %. However, the application of ultrasound during the leaching of indium tin oxide in hydrochloric and methanesulphonic acids reduced tin recovery to 28 % and 1.7 %, respectively.

2. The maximum tin recovery (76 %) without acoustic treatment was achieved in hydrochloric acid solutions (C_{HCl} = 1.0 N) at T = 333 K over 60 min. With ultrasonic treatment, the highest tin recovery (66 %) was obtained in a 1.0 N sulphuric acid solution at T = 333 K over 60 min.

3. Increasing the leaching temperature significantly enhanced the initial tin dissolution rates. The calculated apparent activation energies for tin leaching in hydrochloric acid indicate a kinetic-controlled process without ultrasonic treatment and a mixed control regime when ultrasound is applied. In sulphuric acid, tin leaching occurs in a diffusion-controlled regime, while ultrasonic treatment transitions the process to a mixed control regime.

References

1. Pasquarelli R.M., Ginley D.S., O'Hayre R. Solution processing of transparent conductors: from flask to film. *Chemical Society Reviews.* 2011;40(11):5406—5441. https://doi.org/10.1039/c1cs15065k
2. Illés I.B., Nagy S., Kékesi T. The recycling of pure metallic indium from waste LCD screens by a combined hydro-electrometallurgical method. *Hydrometallurgy.* 2022;213:105945. https://doi.org/10.1016/j.hydromet.2022.105945
3. Wang H.Y. A study of the effects of LCD glass sand on the properties of concrete. *Waste Management.* 2009;29(1):335—341. https://doi.org/10.1016/j.wasman.2008.03.005
4. Lee C.H., Popuri S.R., Peng Y.H. Analysis of indium and

tin in different scrap liquid crystal display glass by heavy metal digestion method. *Journal of Sustainable Metallurgy*. 2019;5(4):617—626.
https://doi.org/10.1007/s40831-019-00254-6

5. Mineral commodity summaries 2022. URL: https://pubs.usgs.gov/periodicals/mcs2022/mcs2022.pdf (accessed: 12.02.2024).
6. Mineral commodity summaries 2024. URL: https://pubs.usgs.gov/periodicals/mcs2024/mcs2024.pdf (accessed: 12.02.2024).
7. Savvilotidou V., Kousaiti A., Batinic B., Vaccari M., Kastanaki E., Karagianni K., Gidarakos E. Evaluation and comparison of pre-treatment techniques for recovering indium from discarded liquid crystal displays. *Waste Management*. 2019;87:51—61.
https://doi.org/10.1016/j.wasman.2019.01.029
8. Li J., Gao S., Duan H., Liu L. Recovery of valuable materials from waste liquid crystal display panel. *Waste Management*. 2009;29(7):2033—2039.
https://doi.org/10.1016/j.wasman.2008.12.013
9. Lahtela V., Virolainen S., Uwaoma A., Kallioinen M., Kärki T., Sainio T. Novel mechanical pre-treatment methods for effective indium recovery from end-of-life liquid-crystal display panels. *Journal of Cleaner Production*. 2019;230:580—591.
https://doi.org/10.1016/j.jclepro.2019.05.163
10. Wang S., He Y., Yang J., Feng Y. Enrichment of indium tin oxide from colour filter glass in waste liquid crystal display panels through flotation. *Journal of Cleaner Production*. 2018;189:464—471.
https://doi.org/10.1016/j.jclepro.2018.04.096
11. Zheng K., Benedetti M.F., van Hullebusch E.D. Recovery technologies for indium, gallium, and germanium from end-of-life products (electronic waste) — A review. *Journal of Environmental Management*. 2023;347:119043.
https://doi.org/10.1016/j.jenvman.2023.119043
12. Wang Y., Wang R., Zhang C., Wang J. Full components recovery of organic matter and indium from discarded liquid crystal display panels. *Journal of Cleaner Production*. 2021;299:126862.
https://doi.org/10.1016/j.jclepro.2021.126862
13. Zhang L., Wu B., Chen Y., Xu Z. Energy and valuable resource recovery from waste liquid crystal display panels by an environment-friendly technological process: pyrolysis of liquid crystals and preparation of indium product. *Journal of Cleaner Production*. 2017;162:141—152.
https://doi.org/10.1016/j.jclepro.2017.06.031
14. Park K.S., Sato W., Grause G., Kameda T., Yoshioka T. Recovery of indium from In_2O_3 and liquid crystal display powder via a chloride volatilization process using polyvinyl chloride. *Thermochimica Acta*. 2009;493(1-2):105—108. https://doi.org/10.1016/j.tca.2009.03.003
15. Assefi M., Maroufi S., Nekouei R.K., Sahajwalla V. Selective recovery of indium from scrap LCD panels using macroporous resins. *Journal of Cleaner Production*. 2018;180:814—822.
https://doi.org/10.1016/j.jclepro.2018.01.165
16. Schuster J., Ebin B. Investigation of indium and other valuable metals leaching from unground waste LCD screens by organic and inorganic acid leaching. *Separation and Purification Technology*. 2021;279:119659.
https://doi.org/10.1016/j.seppur.2021.119659
17. Qin J., Ning S., Zeng J., He Z., Hu F., Li Y., Fujita T., Wei Y. Leaching behavior and process optimization of tin recovery from waste liquid crystal display under mechanical activation. *Journal of Cleaner Production*. 2023;399:136640.
https://doi.org/10.1016/j.jclepro.2023.136640
18. Houssaine Moutiy E, Tran L.H., Mueller K.K., Coudert L., Blais J.F. Optimized indium solubilization from LCD panels using H_2SO_4 leaching. *Waste Management*. 2020;114:53—61.
https://doi.org/10.1016/j.wasman.2020.07.002
19. Kato T., Igarashi S., Ishiwatari Y., Furukawa M., Yamaguchi H. Separation and concentration of indium from a liquid crystal display via homogeneous liquid—liquid extraction. *Hydrometallurgy*. 2013;137:148—155.
https://doi.org/10.1016/j.hydromet.2013.06.004
20. Guthrie J.P. Hydrolysis of esters of oxy acids: pK_a values for strong acids; Brønsted relationship for attack of water at methyl; free energies of hydrolysis of esters of oxy acids; and a linear relationship between free energy of hydrolysis and pK_a holding over a range of 20 pK units. *Canadian Journal of Chemistry*. 1978;56(17):2342—2354.
https://doi.org/10.1139/v78-385
21. Levanov A.V., Isaikina O.Y., Gurbanova U.D., Lunin V.V. Dissociation constants of perchloric and sulfuric acids in aqueous solution. *The Journal of Physical Chemistry B*. 2018;122(23):6277—6286.
https://doi.org/10.1021/acs.jpcb.8b01947
22. Zinchenko A.V., Izotova S.G., Rumyantsev A.V. The new handbook of the chemist and technologist. Chemical equilibrium. Properties of solutions. Saint Petersburg: ANO NPO “Professional”, 2004. 998 p. (In Russ.).
Зинченко А.В., Изотова С.Г., Румянцев А.В. Новый справочник химика и технолога. Химическое равновесие. Свойства растворов. С.-Пб.: АНО НПО «Профессионал», 2004. 998 с.
23. Vyas S., Ting Y.P. A review of the application of ultrasound in bioleaching and insights from sonication in (bio) chemical processes. *Resources*. 2017;7(1):3.
https://doi.org/10.3390/resources7010003

24. Bang J.H., Suslick K.S. Applications of ultrasound to the synthesis of nanostructured materials. *Advanced Materials.* 2010;22(10):1039—1059. https://doi.org/10.1002/adma.200904093
25. He C., Liu L., Fang Z., Li J., Guo J., Wei J. Formation and characterization of silver nanoparticles in aqueous solution via ultrasonic irradiation. *Ultrasonics Sonochemistry.* 2014;21(2):542—548. https://doi.org/10.1016/j.ultsonch.2013.09.003
26. Gungoren C., Ozkan S.G., Ozdemir O. Use of ultrasound in physical and chemical mineral processing operations. In: *Advances in minerals research. Advances in material research and technology.* Ed. S.R. Ikhmayies. Cham: Springer, 2024. P. 25—54.
27. Yuan Y., Yu X., Shen Q., Zhao Q., Li Y., Wu T. A novel approach for ultrasonic assisted organic acid leaching of waste lithium-containing aluminum electrolyte and recovery of lithium. *Chemical Engineering and Processing — Process Intensification*. 2023;192:109508. https://doi.org/10.1016/j.cep.2023.109508
28. Delmas H., Barthe L., Cleary R. Ultrasonic mixing, homogenization, and emulsification in food processing and other applications. In: *Power ultrasonics.* Eds. J.A. Gallego-Juárez, K.F. Graff, M. Lucas. Amsterdam: Elsevier B.V., 2023. P. 665—685.
29. Rahimi M.R., Mosleh S. Intensification of sorption processes. Amsterdam: Elsevier B.V., 2022. 258 p.
30. Zhang K., Li B., Wu Y., Wang W., Li R., Zhang Y.N., Zuo T. Recycling of indium from waste LCD: A promising non-crushing leaching with the aid of ultrasonic wave. *Waste Management.* 2017;64:236—243. https://doi.org/10.1016/j.wasman.2017.03.031
31. Merouani S., Hamdaoui O., Rezgui Y., Guemini M. Effects of ultrasound frequency and acoustic amplitude on the size of sonochemically active bubbles — Theoretical study. *Ultrasonics Sonochemistry.* 2013;20(3):815—819. https://doi.org/10.1016/j.ultsonch.2012.10.015
32. Bu X., Tong Z., Bilal M., Ren X., Ni M., Ni C., Xie G. Effect of ultrasound power on HCl leaching kinetics of impurity removal of aphanitic graphite. *Ultrasonics Sonochemistry.* 2023;95:106415. https://doi.org/10.1016/j.ultsonch.2023.106415
33. Binnemans K., Jones P.T. Methanesulfonic acid (MSA) in hydrometallurgy. *Journal of Sustainable Metallurgy.* 2023;9:26—45. https://doi.org/10.1007/s40831-022-00641-6
34. Rudnik E., Wincek D. Preliminary studies on hydrometallurgical tin recovery from waste of tin stripping of copper wires. *Metallurgy and Foundry Engineering.* 2017;43(1):7—20. https://doi.org/10.7494/mafe.2017.43.1.7

Information about the authors

Elvira B. Kolmachikhina – Cand. Sci. (Eng.), Researcher of the Laboratory of advanced technologies for complex processing of mineral and technogenic raw materials of non-ferrous and ferrous metals, Ural Federal University n.a. the First President of Russia B.N. Eltsin (UrFU).
https://orcid.org/0000-0002-6007-498X
E-mail: e.b.khazieva@urfu.ru

Olga B. Kolmachikhina – Cand. Sci. (Eng.), Associated Professor of the Department of non-ferrous metallurgy of UrFU.
https://orcid.org/0000-0002-7879-8791
E-mail: o.b.kolmachikhina@urfu.ru

Yana A. Yankina – Student of the Department of non-ferrous metallurgy of UrFU.
E-mail: yankina.1999@mail.ru

Zamira M. Golibzoda – Student of the Department of non-ferrous metallurgy of UrFU.
E-mail: golibzoda@mail.ru

Polina A. Brizhevataya – Student of the Department of non-ferrous metallurgy of UrFU.
E-mail: Polina.brizhevataya@mail.ru

Информация об авторах

Эльвира Барыевна Колмачихина – к.т.н., науч. сотрудник лаборатории перспективных технологий комплексной переработки минерального и техногенного сырья цветных и черных металлов Уральского федерального университета им. первого Президента России Б.Н. Ельцина (УрФУ).
https://orcid.org/0000-0002-6007-498X
E-mail: e.b.khazieva@urfu.ru.

Ольга Борисовна Колмачихина – к.т.н., доцент кафедры металлургии цветных металлов (МЦМ) УрФУ.
https://orcid.org/0000-0002-7879-8791
E-mail: o.b.kolmachikhina@urfu.ru

Яна Александровна Янкина – студентка кафедры МЦМ, УрФУ.
E-mail: yankina.1999@mail.ru

Замира Мирзомурод Голибзода – студентка кафедры МЦМ, УрФУ.
E-mail: golibzoda@mail.ru.

Полина Александровна Брижеватая – студентка кафедры МЦМ, УрФУ.
E-mail: Polina.brizhevataya@mail.ru

Daria S. Sedel'nikova – Student of the Department of non-ferrous metallurgy of UrFU.
E-mail: d.s.sedelnikova@mail.ru

Raisa E. Khabibulina – Assistant of the Department of non-ferrous metallurgy of UrFU.
E-mail: raisa.khabibulina@urfu.ru

Дарья Сергеевна Седельникова – студентка кафедры МЦМ, УрФУ.
E-mail: d.s.sedelnikova@mail.ru

Раиса Энверовна Хабибулина – ассистент кафедры МЦМ, УрФУ.
E-mail: raisa.khabibulina@urfu.ru

Contribution of the authors

E.B. Kolmachikhina – defined the objectives of the study, conducted experiments and analyses, and wrote the article.

O.B. Kolmachikhina – contributed to the discussion of the results and co-authored the article.

Ya.A. Yankina – performed experiments, conducted chemical analysis, and participated in the discussion of the results.

Z.M. Golibzoda – carried out experiments and contributed to the discussion of the results.

P.A. Brizhevataya – carried out experiments and contributed to the discussion of the results.

D.S. Sedel'nikova – carried out experiments and contributed to the discussion of the results.

R.E. Khabibulina – carried out experiments and contributed to the discussion of the results.

Вклад авторов

Э.Б. Колмачихина – определение цели работы, проведение экспериментов и анализов, написание статьи.

О.Б. Колмачихина – участие в обсуждении результатов, написание статьи.

Я.А. Янкина – проведение экспериментов и химического анализа, участие в обсуждении результатов.

З.М. Голибзода – проведение экспериментов, участие в обсуждении результатов.

П.А. Брижеватая – проведение экспериментов, участие в обсуждении результатов.

Д.С. Седельникова – проведение экспериментов, участие в обсуждении результатов.

Р.Э. Хабибуллина – проведение экспериментов, участие в обсуждении результатов.

The article was submitted 14.02.2024, revised 18.03.2024, accepted for publication 27.03.2024

Статья поступила в редакцию 14.02.2024, доработана 18.03.2024, подписана в печать 27.03.2024

METALLURGY OF NON-FERROUS METALS / МЕТАЛЛУРГИЯ ЦВЕТНЫХ МЕТАЛЛОВ

UDC 66.046.4.094.3 + 661.856.532
https://doi.org/10.17073/0021-3438-2024-4-33-42

Research article
Научная статья

Processing of chalcopyrite concentrate by sulfating roasting

A.Yu. Sokolov, A.G. Kasikov

Tananaev Institute of Chemistry of the Kola Science Centre of the Russian Academy of Sciences
26a Akademgorodok Str., Apatity 184209, Russia

✉ Артем Юрьевич Соколов (aiu.sokolov@ksc.ru)

Abstract: Chalcopyrite ($CuFeS_2$) is one of the primary minerals processed on an industrial scale for copper production and often dominates copper concentrates sent for pyrometallurgical processing. This study demonstrates the efficient and selective extraction of copper from chalcopyrite concentrate through sulfating roasting, sulfuric acid leaching, and solvent extraction. At a roasting temperature of 700 °C for 1.5 h, chalcopyrite fully decomposes into hematite (Fe_2O_3) and chalcanthite ($CuSO_4$). Leaching the calcine with a 0.02 M sulfuric acid solution transfers most of the copper to the aqueous phase, while iron concentrates in the solid residue. Additionally, precious metals concentrate in the residue after leaching of the calcine, with the following content in g/t: Pd – 41.61, Pt – 5.65, Ag – 96.22, Au – 4.81. The removal of iron from the leach solution using solvent extraction with di-2-ethylhexyl phosphoric acid was highly effective: with a 25 % extractant solution and an organic-to-aqueous ratio of 1:1 over two stages, the iron concentration in the aqueous phase dropped from 3.05 to 0.01 g/dm^3, and with an organic-to-aqueous ratio of 1:2 over four stages, it decreased to 0.006 g/dm^3. After iron purification and solution evaporation, copper sulfate was obtained with the following composition (%): $CuSO_4 \cdot 5H_2O$ – 99.84 (equivalent to 25.42 % copper), Ni – 0.014, Al – 0.007, Fe – 0.0003, As – 0.0002.

Keywords: copper concentrate, chalcopyrite, roasting, copper, iron, extraction, precious metals.

For citation: Sokolov A.Yu., Kasikov A.G. Processing of chalcopyrite concentrate by sulfating roasting. *Izvestiya. Non-Ferrous Metallurgy.* 2024;30(4):33–42. https://doi.org/10.17073/0021-3438-2024-4-33-42

Переработка халькопиритового концентрата с применением сульфатизирующего обжига

А.Ю. Соколов, А.Г. Касиков

Институт химии и технологии редких элементов и минерального сырья им. И.В. Тананаева Кольского научного центра Российской академии наук
Россия, 184209, г. Апатиты, ул. Академгородок, 26а

✉ Артем Юрьевич Соколов (aiu.sokolov@ksc.ru)

Аннотация: Халькопирит ($CuFeS_2$) является одним из основных минералов, перерабатываемых в промышленном масштабе для получения меди, который зачастую превалирует в медных концентратах, поступающих на последующую пирометаллургическую переработку. В работе показана возможность эффективного и селективного выделения меди из халькопиритового концентрата с применением сульфатизирующего обжига, сернокислотного выщелачивания и жидкостной экстракции. Установлено, что при температуре обжига 700 °С в течение 1,5 ч происходит полное разложение халькопирита с образованием гематита (Fe_2O_3)

и халькоцианита ($CuSO_4$). В результате выщелачивания огарка раствором серной кислоты концентрацией 0,02 М в водную фазу переходит большая часть меди, в то время как железо концентрируется в твердом остатке. Кроме того, в результате выщелачивания огарка в остатке концентрируются и благородные металлы, содержание которых составляет, г/т: Pd – 41,61, Pt – 5,65, Ag – 96,22, Au – 4,81. Очистка раствора выщелачивания от железа посредством жидкостной экстракции ди-2-этилгексилфосфорной кислотой показала высокую эффективность: при использовании 25 %-ного раствора экстрагента при соотношении O : B = 1 : 1 на двух ступенях концентрация железа в водной вазе снижается с 3,05 до 0,01 г/дм^3, а при O : B = 1 : 2 на четырех ступенях – до 0,006 г/дм^3. После железоочистки и упаривания раствора получен медный купорос, содержащий, %: $CuSO_4·5H_2O$ – 99,84 (в пересчете на медь – 25,42), Ni – 0,014, Al – 0,007, Fe – 0,0003, As – 0,0002.

Ключевые слова: медный концентрат, халькопирит, обжиг, медь, железо, экстракция, благородные металлы.

Для цитирования: Соколов А.Ю., Касиков А.Г. Переработка халькопиритового концентрата с применением сульфатизирующего обжига. *Известия вузов. Цветная металлургия*. 2024;30(4):33–42. https://doi.org/10.17073/0021-3438-2024-4-33-42

Introduction

Chalcopyrite ($CuFeS_2$) is one of the main industrial copper-bearing minerals, accounting for approximately 70 % of the world's copper reserves. The predominant method for extracting copper from chalcopyrite ores is froth flotation, which yields a copper-rich concentrate [1]. Most of the copper is produced using the metallurgical process of smelting—converting—refining. During the smelting of high-grade sulfide ores or concentrates, a matte containing up to 40 % Cu is obtained [2].

Despite the high efficiency of conventional pyrometallurgical methods for processing copper concentrates (CC) [3], alternative processing methods are currently being actively studied, although they have not yet found widespread industrial application. For example, various methods of leaching chalcopyrite-containing concentrates are being investigated to reduce sulfur dioxide emissions into the atmosphere [4]: pressure acid leaching [5], microwave acid leaching [6], chloride leaching [5], and leaching with mineral salt solutions combined with sulfuric acid [7], among others. Hydrometallurgical methods also help to prevent arsenic, which is often present in sulfide copper concentrates, from entering the gas phase, reducing the cost of copper production by eliminating the need for specialised dust and gas cleaning systems [8]. However, hydrometallurgical processing of chalcopyrite is challenging due to the formation of a passivating layer on the mineral surface, necessitating the use of strong oxidants such as hydrogen peroxide [9] or ozone [10], or its preliminary treatment, such as mechanoactivation [11], which significantly complicates its processing. The intensification of hydrometallurgical processing of sulfide CCs can also be achieved through the application of pressure leaching [12; 13].

Bacterial leaching of chalcopyrite-containing materials is developing rapidly [13—15], but bioleaching is characterised by a slow reaction rate and the need to maintain optimal conditions for bacterial activity, which limits the practical application of this method.

In addition to the methods mentioned above, sulfating roasting can be used to process sulfide and chalcopyrite CCs by converting copper and iron from sulfides to sulfates [16—19]. The advantage of this method is the use of lower temperatures compared to conventional oxidative roasting [20]. However, when such a concentrate is leached, both metals are transferred to the aqueous phase, leading to the challenge of separating iron and copper by hydrometallurgical means. According to literature data, chalcopyrite decomposition into iron and copper sulfides occurs at roasting temperatures of 330—357 °C, and these sulfides are converted into the corresponding sulfates between 357—555 °C [21]. As the roasting temperature increases to 555—613 °C, iron sulfate decomposes into iron and sulfur oxides, while a higher temperature is required for copper sulfate decomposition [21], indicating the potential for selective copper extraction from chalcopyrite concentrate during the leaching stage. Additionally, the behaviour of precious metals, often present in sulfide CCs, during roasting and leaching of chalcopyrite concentrate is of interest. Therefore, the aim of this study is to investigate the behaviour of copper, iron, and precious metals during the roasting of chalcopyrite concentrate and leaching of the calcine, followed by iron removal to obtain copper sulfate of the required quality.

Experimental technique

The study used chalcopyrite copper concentrate obtained from the beneficiation of copper-sulfide ore from the Chineyskoe deposit, with the following composition (%): Cu — 20.35, Fe — 23.07, S — 22.91, Ni — 0.47, Ca — 0.75, Al — 0.87, Co — 0.05, and trace elements (g/t): As — 138.95, Se — 98.31, Te — 15.74,

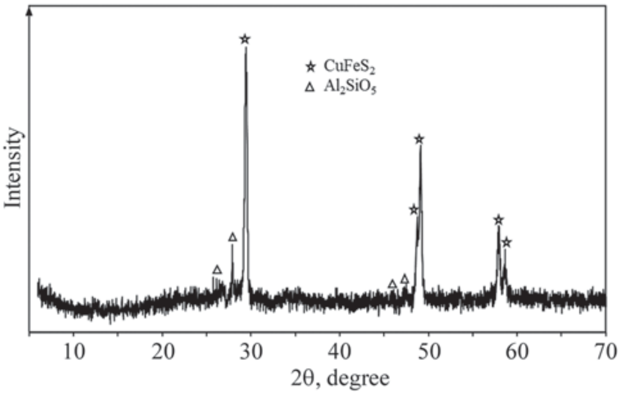

Fig. 1. Phase composition of the initial CC

Рис. 1. Фазовый состав исходного МК

V — 128.12, Mo — 249.18, Pd — 25.95, Pt — 2.84, Au — 2.97, Ag — 60.58. The low arsenic content in the concentrate allows for the use of pyrometallurgical processing methods. The phase composition of the initial concentrate is primarily chalcopyrite with a kyanite (Al_2SiO_5) admixture (Fig. 1).

The concentrate was ground to a size of <74 μm and held in a laboratory electric furnace (SNOL 7.2/1300, Umega Group, Lithuania) for 0.25 to 2.0 h at temperatures ranging from 650 to 900 °C. The heating rate to the required temperature was 10 °C/min, and the sample mass was 50 g. The resulting calcine was leached with sulfuric acid solutions of various concentrations. Iron (III) extraction from the leach solution was carried out using di-2-ethylhexyl phosphoric acid (D2EHPA) (Volgogradpromproject, Russia) in an inert aliphatic diluent RJ-3 (Volganeftchem, Russia) for 5 minutes at different organic-to-aqueous ratios and temperatures. The concentrations of non-ferrous metals and iron were determined using atomic absorption spectrometry ("AAnalyst 400", Perkin Elmer, USA), while concentrations of precious metals and trace elements were measured by inductively coupled plasma mass spectrometry (ICP-MS) on an ELAN 9000 DRC-e instrument (Perkin Elmer, USA). The phase composition of the samples was assessed by *X*-ray phase analysis (XRD) using an XRD-6000 diffractometer (Shimadzu, Japan).

Results and discussion

1. Thermal treatment of the copper concentrate

The roasting of the copper concentrate was conducted for 120 min at temperatures ranging from 650 to 900 °C. *X*-ray diffraction (XRD) patterns of the concentrates roasted at different temperatures are shown in Fig. 2. It was found that at lower roasting temperatures (650—750 °C), the main iron-bearing phase is hematite (Fe_2O_3), while the copper-bearing phase is chalcocyanite ($CuSO_4$). However, at 800 °C, copper oxide (CuO) and copper ferrite ($CuFe_2O_4$), begin to form, which is associated with the decomposition of copper sulfate and the initial interaction between copper oxide and iron oxide. This interaction is confirmed by the XRD pattern of the sample roasted at 900 °C, where characteristic peaks of hematite are absent, and copper ferrite becomes the primary iron-containing phase. Additionally, copper is present in the form of oxide.

Thus, the processes occurring at different roasting temperatures can be summarised in the following equations:

$$\textbf{650—750 °C:}\quad 2CuFeS_2 + 7{,}5O_2 \rightarrow \rightarrow 2CuSO_4 + Fe_2O_3 + 2SO_2, \qquad (1)$$

$$\textbf{800 °C:}\quad 4CuFeS_2 + 13O_2 \rightarrow \rightarrow 3CuO + Fe_2O_3 + CuFe_2O_4 + 8SO_2, \qquad (2)$$

$$\textbf{900 °C:}\quad 2CuFeS_2 + 6{,}5O_2 \rightarrow \rightarrow CuO + CuFe_2O_4 + 4SO_2. \qquad (3)$$

The changes in the phase composition of the calcine over time were studied at a temperature of 700 °C. It was found that chalcopyrite ($CuFeS_2$) could no longer be identified after 90 min of roasting, with copper and iron present only as chalcocyanite and hematite (Fig. 3), indicating the potential for effective separation of iron and copper from the roasted concentrate during leaching.

2. Sulfuric acid leaching of the roasted concentrate

During the study of the leaching process of the calcine obtained after roasting at 700 °C, using sulfuric acid solutions of various concentrations, it was found that leaching with a solution containing 0.02 M H_2SO_4, resulted in copper extraction of $E(Cu) = 83$ % and iron extraction of $E(Fe) = 4{,}6$ % (Fig. 4). As the acid concentration increased to 1.5 M, copper and iron extraction increased to 93 % and 14 %, respectively. These results are consistent with those shown in Figs. 2 and 3: during roasting, copper transitions into water-soluble chalcanthite, while iron remains as insoluble hematite. As the acid concentration increases, hematite reacts with sulfuric acid to form soluble iron (III) sulfate, leading to an increase in Fe(III) concentration in the leach solu-

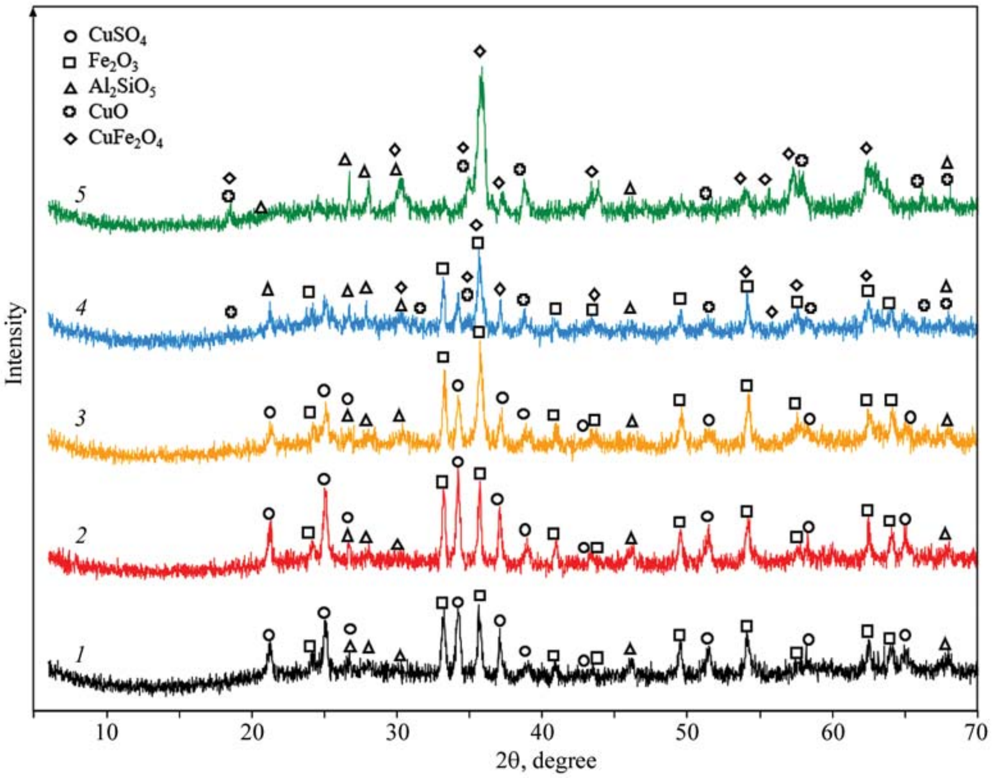

Fig. 2. Phase composition of the calcine after roasting for 120 min at various temperatures
t, °C: ***1*** – 650, ***2*** – 700, ***3*** – 750, ***4*** – 800, ***5*** – 900

Рис. 2. Фазовый состав огарка после обжига в течение 120 мин при различных температурах
t, °C: ***1*** – 650, ***2*** – 700, ***3*** – 750, ***4*** – 800, ***5*** – 900

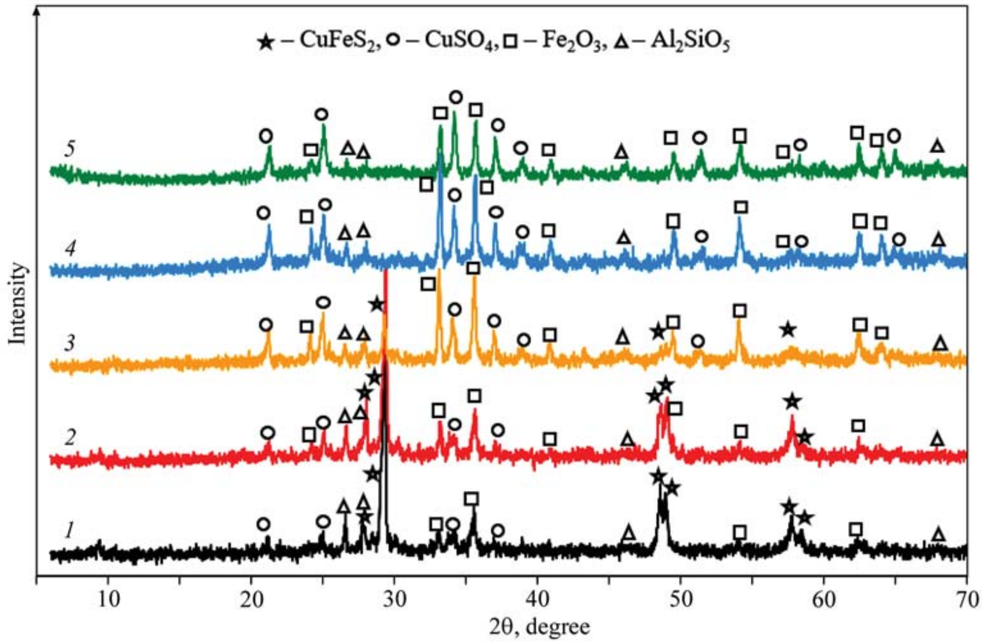

Fig. 3. Phase composition of the calcine at different roasting times at 700 °C
τ, min: ***1*** – 15, ***2*** – 30, ***3*** – 60, ***4*** – 90, ***5*** – 120

Рис. 3. Фазовый состав огарка в зависимости от времени обжига при *t* = 700 °C
τ, мин: ***1*** – 15, ***2*** – 30, ***3*** – 60, ***4*** – 90, ***5*** – 120

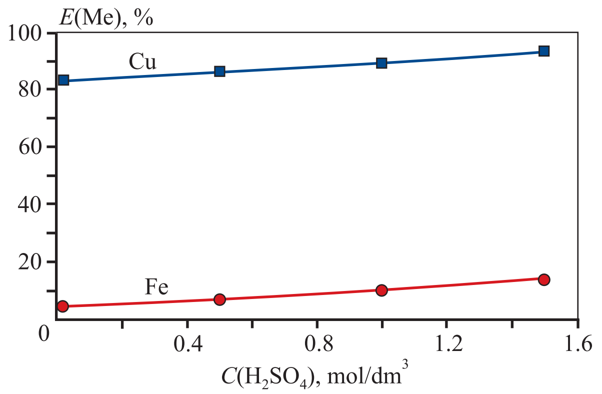

Fig. 4. Effect of H_2SO_4 concentration on the leaching of copper concentrate calcine
t = 60 °C, τ = 1 h, S : L = 1 : 5

Рис. 4. Влияние концентрации H_2SO_4 на выщелачивание огарка МК
t = 60 °C, τ = 1 ч, Т : Ж = 1 : 5

tion. The increase in copper concentration in the solution may be related to the presence of copper oxide in the calcine, which is not detectable by XRD but reacts with sulfuric acid during leaching, resulting in higher copper concentrations in the solution. Although higher acid concentrations improve copper extraction, the use of a less concentrated leaching solution is preferable, as increasing the acid concentration complicates the subsequent separation of iron and copper.

In addition to the behavior of the major components during sulfuric acid leaching of the calcine, the distribution of precious metals and other impurities in the concentrate is also of significant interest. Analysis of the composition of the leaching residues showed that approximately 60 % of nickel is transferred into the solution, while precious metals almost entirely remain in the solid residue (Table 1). Other trace elements, such as arsenic, selenium, tellurium, vanadium, and molybdenum, are barely leached by 0.02 M H_2SO_4, concentrating in the leach residue. The content of trace elements in the residue after leaching with 1.5 M H_2SO_4 is lower than after leaching with 0.02 M H_2SO_4, especially noticeable for arsenic and molybdenum. Thus, with increasing acid concentration, more of these components are extracted into the solution, reducing the selectivity of the leaching process. Based on the data in Fig. 4 and Table 2, 0.02 M H_2SO_4 was chosen as the leaching solution for the roasted concentrate.

A study of the leaching kinetics of the calcine showed that copper extraction into the solution in the first 15 min reaches 72.4 %, gradually increasing to 83.5 % after 60 min (Fig. 5). In contrast, iron extraction in the first 15 min is only 0.9 %, but after 60 min, it increases to 4.6 %. Extending the leaching time does not significantly enhance the extraction of either copper or iron, so subsequent leaching processes were conducted for 60 min to maximize copper extraction.

An investigation of the effect of the solid-to-liquid ratio on concentrate leaching showed that copper extraction decreases slightly: at an S : L ratio of 1 : 10, copper extraction is 85.9 %, while at S : L = 1 : 2, it is 74.6 %, corresponding to copper concentrations of 17.46 and 75.96 g/dm^3, respectively (Fig. 6). Throughout the S : L range, iron extraction does not exceed 5.6 %, which is observed at S : L = 1 : 10, and its maximum concen-

Table 1. **Metals distribution during leaching of copper concentrate calcine (S : L = 1 : 10, *t* = 60 °C, τ = 1 h)**

Таблица 1. Распределение металлов при выщелачивании огарка МК (Т : Ж = 1 : 10, *t* = 60 °C, τ = 1 ч)

Me	Unit	$C(Me)_{initial}$	Composition of leaching residues of the calcine	
			$C(H_2SO_4)$ = = 0.02 M	$C(H_2SO_4)$ = = 1.5 M
Ni	%	0.47	0.31	0.30
Cu		20.35	2.0	1.6
Ca		0.75	0.70	0.70
Co		0.05	0.02	0.01
Al		0.87	1.30	1.62
Fe		23.07	40.8	40.1
As	г/т	138.95	257.80	134.20
Se		98.31	128.30	97.30
Te		15.74	22.63	25.96
Ag		60.58	96.22	101.49
Pd		25.95	41.61	45.44
Au		2.97	4.81	5.59
Pt		2.84	5.65	5.06
V		128.12	208.3	192.9
Mo		249.18	349.8	217.1

Table 2. **Effect of temperature on the leaching of copper concentrate calcine (S : L = 1 : 5, $C(H_2SO_4)$ = 0.02 M, τ = 1 h)**

Таблица 2. Влияние температуры на выщелачивание огарка МК (Т : Ж = 1 : 5, $C(H_2SO_4)$ = 0,02 M, τ = 1 ч)

t, °C	*E*(Cu), %	*E*(Fe), %
20	81.5	4.5
40	82.3	4.6
60	83.2	4.6

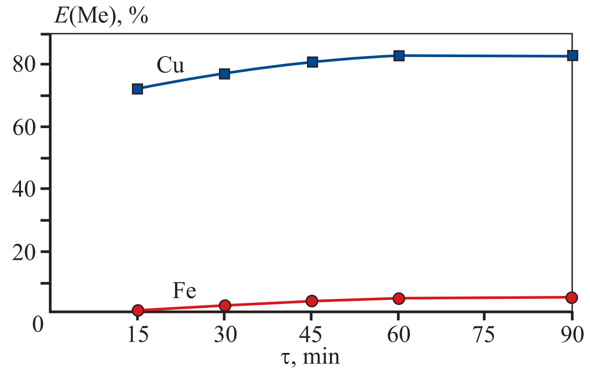

Fig. 5. Kinetics of calcine leaching
S : L = 1 : 5, $C(H_2SO_4)$ = 0.02 M, t = 60 °C

Рис. 5. Кинетика выщелачивания огарка
Т : Ж = 1 : 5, $C(H_2SO_4)$ = 0,02 М, t = 60 °C

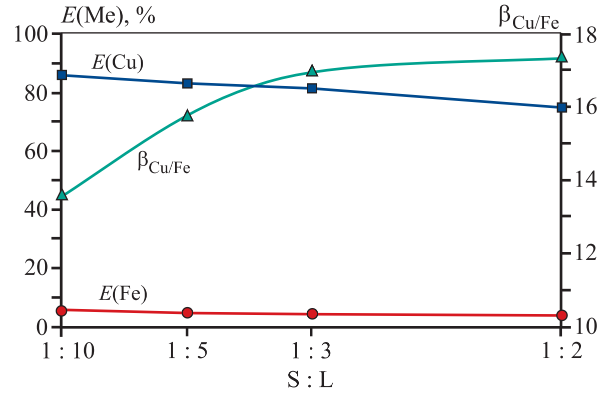

Fig. 6. Effect of S : L on the extraction and separation of Fe and Cu during leaching
$C(H_2SO_4)$ = 0.02 M, τ = 1 h, t = 60 °C

Рис. 6. Влияние Т : Ж на извлечение и разделение Fe и Cu при выщелачивании
$C(H_2SO_4)$ = 0,02 М, τ = 1 ч, t = 60 °C

tration is 4.38 g/dm^3 at S : L = 1 : 2. Notably, copper extraction at S : L = 1 : (3÷5) is 81.2 % and 83.1 %, respectively, indicating a more efficient process than leaching at S : L = 1 : 2. However, at S : L = 1 : 10, the copper concentration in the solution (17.46 g/dm^3) is insufficient for further processing.

The S : L ratio also plays a crucial role in the separation of copper and iron during leaching. While the initial Cu/Fe ratio in the concentrate is 0.88, during leaching, it increases in the solution to 13.5 and 17.3 at S : L = = 1 : 10 and 1 : 2, respectively, with a non-linear dependence (see Fig. 6). The lack of direct proportionality can be explained by the increased copper concentration in the solution at lower S : L ratios, which likely reduces the activity of sulfuric acid, leading to less interaction with hematite. Consequently, the optimal S : L ratio range is 1 : (5÷3), where copper and iron concentrations in the solution are 33.8—55.0 g/dm^3 and 2.15—3.25 g/dm^3, respectively, with a separation coefficient ($\beta_{Cu/Fe}$) of 15.7—16.9.

It was found that increasing the leaching temperature slightly improves copper extraction into the solution and has little effect on iron extraction (Table 2). The minimal effect of temperature on copper extraction is due to the lack of a chemical reaction during copper leaching, as the process is based on the dissolution of chalcocyanite in the liquid phase. The lack of temperature influence on iron extraction is explained by the low acid concentration in the leaching solution.

3. Iron solvent extraction from the leach solution

To separate iron (III) and copper (II) in sulfate solutions, the hydrolytic method of precipitating iron as an insoluble hydroxide (iron cake) is often used [22]. However, some copper co-precipitates with the cake, leading to copper losses in the waste. Therefore, it was proposed to separate iron (III) and copper (II) by extracting Fe(III) from the copper solution using extractants based on D2EHPA, which has proven effective for extracting iron (III) from a copper electrolyte [23]. A 25 % solution of technical-grade D2EHPA in an inert aliphatic diluent was used for extraction. Based on the McCabe-Thiele plot for Fe(III) solvent extraction from the leach solution, it was found that iron is nearly quantitatively extracted in two stages at O : A = 1 : 1 and in four stages at O : A = 1 : 2, with residual Fe(III) concentrations in the raffinates of 0.01 and 0.006 g/dm^3, respectively (Fig. 7), corresponding to extraction rates of 99.7 % and 99.8 %. Notably, copper (II) extraction does not exceed 2.7 %, as under the studied conditions, D2EHPA has a higher affinity for iron (III) than for copper (II) [24], ensuring more efficient Fe(III) extraction. As a result, the organic phase is saturated with iron (III), which prevents the co-extraction of copper (II).

The organic phase saturated with iron (III) can be regenerated by stripping using hydrochloric [25] or oxalic [26] acids, allowing the extractant to be recycled back into the extraction stage. After thorough iron extraction, the obtained raffinate was evaporated and cooled, leading to the precipitation of copper sulfate, which contained (%): $CuSO_4 \cdot 5H_2O$ — 99.84 (equivalent to 25.42% copper), Ni — 0.014, Al — 0.007, Fe — 0.0003, As — 0.0002. The resulting mother liquor can be either evaporated further or used for leaching roasted concentrate. If nickel impurities concentrate in the solution during further processing, the filtrate can be treated for effec-

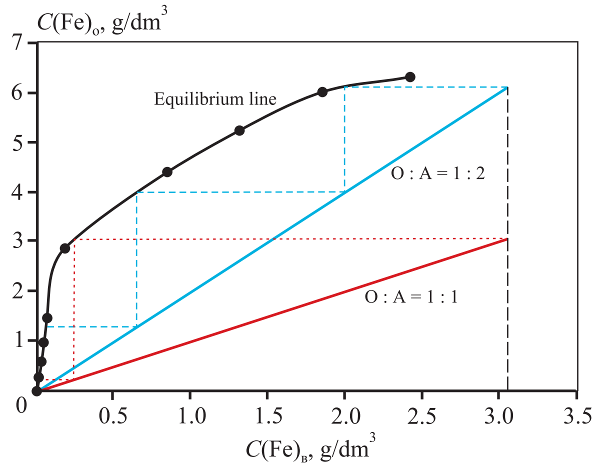

Fig. 7. McCabe-Thiele plot for Fe(III) solvent extraction by D2EHPA

$C(Cu) = 35$ g/dm^3, $C(Fe^{3+}) = 3.05$ g/dm^3, $C(H_2SO_4) = 0.02$ M, $t = 20$ °C, $\tau = 5$ min

Рис. 7. Изотерма экстракции Fe(III) Д2ЭГФК

$C(Cu) = 35$ г/дм^3, $C(Fe^{3+}) = 3{,}05$ г/дм^3, $C(H_2SO_4) = 0{,}02$ М, $t = 20$ °C, $\tau = 5$ мин

tive copper and nickel separation, for example, by solvent extraction [27].

Thus, sulfating roasting allows for not only the effective separation of copper from iron and precious metals during leaching but also the production of copper sulfate with less than 0.16 % impurities after iron solvent extraction from the copper sulfate solution.

Conclusion

The method for processing chalcopyrite copper concentrate presented in this study allows for avoiding one of the main challenges in non-ferrous hydrometallurgy — the stage of iron removal from solutions via hydrolytic means. The difference in the thermal stability of iron and copper sulfates within the temperature range of 650—750 °C enables the conversion of most of the iron into oxide, while copper remains in the form of sulfate after roasting. As a result, during sulfuric acid leaching, copper transitions into the aqueous phase, and iron remains in the insoluble residue. It was established that leaching is best performed with a 0.02 M sulfuric acid solution for 1 hour at a solid-to-liquid ratio of 1 : (3÷5) and a temperature of 20 °C. The possibility of separating copper and precious metals, which concentrate in the solid phase along with iron during leaching, is also significant. he low content of iron and sulfuric acid in the leach solution enables iron removal via selective cation exchange solvent extraction. Using a 25 % D2EHPA solution in an inert aliphatic diluent at O : A = 1 : 1 over two stages results in 99.7 % iron extraction. The obtained raffinate can be further used for copper sulfate production or for copper electrodeposition.

References

1. Faris N., Rama R., Chena M., Tardio J., Pownceby M.I., Jones L.A., McMaster S., Webster N.A.S., Bhargava S. The effect of thermal pre-treatment on the dissolution of chalcopyrite ($CuFeS_2$) in sulfuric acid media. *Hydrometallurgy.* 2017;169: 68—78.
https://doi.org/10.1016/j.hydromet.2016.12.006
2. Medvedev A.S., So Tu, Khamkhash A., Gosteeva N.V., Ptitsyn A.M. Option for processing copper sulfide concentrate using a combined method (For discussion). *Tsvetnye Metally.* 2010;(1):33—36. (In Russ.).
Медведев А.С., Со Ту, Хамхаш А., Гостеева Н.В., Птицын А.М. Вариант переработки сульфидного медного концентрата комбинированным способом (В порядке обсуждения). *Цветные металлы.* 2010;(1):33—36.
3. Ding Z., Yang C., Zhang H., Mei J., Wang J., Yang S. New utilizations of natural $CuFeS_2$ as the raw material of Cu smelting for recovering Hg^0 from Cu smelting flue gas. *Fuel.* 2023;34:126997.
https://doi.org/10.1016/j.fuel.2022.126997
4. Khamkhash A., Medvedev A.S., Krylova L.N. Changes in the mineral phases during the processing of a copper sulfide concentrate. *Izvestiya. Non-Ferrous Metallurgy.* 2007;(1):35—40. (In Russ.).
Хамхаш А., Медведев А.С., Крылова Л.Н. Изменение фаз минералов при переработке сульфидного медного концентрата. *Известия вузов. Цветная металлургия.* 2007;(1):35—40.
5. Vasilieva A.A., Boduen A.Ya., Vasiliev R.E. The feasibility of hydrometallurgical methods for enhancing the processing of copper concentrates. *iPolytech Journal.* 2022;26(2):320—335. (In Russ.).
https://doi.org/10.21285/1814-3520-2022-2-320-335
Васильева А.А., Бодуэн А.Я., Васильев Р.Е. Анализ возможности применения гидрометаллургических методов с целью улучшения переработки медных концентратов. *iPolytech Journal.* 2022;26(2):320—335.
https://doi.org/10.21285/1814-3520-2022-2-320-335
6. Turkmen Y., Kaya E. Leaching of chalcopyrite concentrate in sulphuric acid with the aid of mechanical activation and microwave energy. *Asian Journal of Chemistry.* 2010;22(10):8107—8116.

7. Neira A., Pizarro D., Quezada V., Velásquez-Yévenes L. Pretreatment of copper sulphide ores prior to heap leaching: A review. *Metals*. 2021;11:1067. https://doi.org/10.3390/met11071067
8. Olubambi P.A., Potgieter J.H. Investigations on the mechanisms of sulfuric acid leaching of chalcopyrite in the presence of hydrogen peroxide. *Mineral Processing and Extractive Metallurgy Review: An International Journal*. 2009;30:327—345. https://doi.org/10.1080/08827500902958191
9. Ter-Organesyan A.K., Netrusov A.O., Milman B.M., Vasiliev R.E. Complex hydrometallurgical processing of high-arsenic copper concentrates containing noble metals. In: *Proceedings XXIII International Chernyaev Conference in chemistry, analytics and technology of platinum metals* (Novosibirsk, 3–7 October 2022). Novosibirsk: IIC SB RAS, 2022. P. 92. (In Russ.). https://doi.org/10.26902/Chern-2022-068

   Тер-Органесян А.К., Нетрусов А.О., Мильман Б.М., Васильев Р.Е. Комплексная гидрометаллургическая переработка высокомышьяковистых медных концентратов, содержащих благородные металлы. В сб.: *Тезисы докладов XXIII Международной Черняевской конференции по химии, аналитике и технологии платиновых металлов* (г. Новосибирск, 3—7 октября 2022 г.). Новосибирск: ИНХ СО РАН, 2022. С. 92. https://doi.org/10.26902/Chern-2022-068
10. Wang J., Faraji F., Ghaherman A. Evaluation of ozone as an efficient and sustainable reagent for chalcopyrite leaching: Process optimization and oxidative mechanism. *Journal of Industrial and Engineering Chemistry*. 2021;104:333—344. https://doi.org/10.1016/j.jiec.2021.08.036
11. Vafaeian S., Ahmadian M., Rezaei B. Sulphuric acid leaching of mechanically activated copper sulphidic concentrate. *Minerals Engineering*. 2011;24:1713—1716. https://doi.org/10.1016/j.mineng.2011.09.010
12. Zaitsev P.V., Shneerson Ya.M. Autoclave processes for treatment copper-containing raw materials. *Tsvetnye Metally*. 2016;(1):26—31. (In Russ.). https://doi.org/10.17580/tsm.2016.01.04

    Зайцев П.В., Шнеерсон Я.М. Автоклавные процессы переработки медьсодержащего сырья. *Цветные металлы*. 2016;(1):26—31. https://doi.org/10.17580/tsm.2016.01.04
13. Meretukov M.A., Strukov K.I. Modern hydrometallurgical methods for processing gold-copper and copper-gold ores. Foreign experience. *Tsvetnye Metally*. 2023;(1): 21—37. (In Russ.). https://doi.org/10.17580/tsm.2023.01.03

    Меретуков М.А., Струков К.И. Современные гидрометаллургические способы переработки золото-медных и медно-золотых руд. Зарубежный опыт. *Цветные металлы*. 2023;(1):21—37. https://doi.org/10.17580/tsm.2023.01.03
14. Nasirov U.F., Ochilov Sh.A., Umirzakov A.A., Turdikulova G.I., Botirov E.A. Bacterial heap leaching method for processing low-grade primary copper sulfide ore. *Journal of Advanced Research and Stability*. 2022;Special Issue:259—264. (In Russ.).

    Насиров У.Ф., Очилов Ш.А., Умирзаков А.А., Турдикулова Г.И., Ботиров Э.А. Метод бактериального кучного выщелачивания для обработки из низкосортной первичной сульфидной медной руды. *Journal of Advanced Research and Stability*. 2022;Special Issue:259—264.
15. Yanishevskya E.S., Goryachev A.A. Bioleaching of major sulfide minerals of copper-nickel ores: A review. In: *Proceedings of Fersman Scientific Session of the GI KSC RAS*. Apatity: Kola Sci. Center RAS, 2019;(16):637–642. (In Russ.). https://doi.org/10.31241/FNS.2019.16.131

    Янишевская Е.С., Горячев А.А. Бактериальное выщелачивание основных сульфидных минералов медно-никелевых руд: Обзор. В сб.: *Труды Ферсмановской научной сессии ГИ КНЦ РАН*. Апатиты: Кольский научный центр РАН, 2019;(16):637—642. https://doi.org/10.31241/FNS.2019.16.131
16. Sargsyan L.E., Oganesyan A.M. Activated sulfatizing roasting of chalcopyrite concentrate for sulfuric acid leaching. *Izvestiya. Non-Ferrous Metallurgy*. 2010;(5):11—13. (In Russ.).

    Саргсян Л.Е., Оганесян А.М. Активированный сульфатизирующий обжиг халькопиритового концентрата для сернокислотного выщелачивания. *Известия вузов. Цветная металлургия*. 2010;(5):11—13.
17. Rogozhnikov D.A., Karimov K.A., Dizer O.A., Mamyachenkov S.V., Naboichenko S.S. Complex processing of polymetallic sulfide industrial products of non-ferrous metallurgy enterprises. Ekaterinburg: UMTs UPI, 2022. 142 p. (In Russ.).

    Рогожников Д.А., Каримов К.А., Дизер О.А., Мамяченков С.В., Набойченко С.С. Комплексная переработка полиметаллических сульфидных промпродуктов предприятий цветной металлургии. Екатеринбург: УМЦ УПИ, 2022. 142 с.

18. Bumazhnov F.T. Study of the physico-chemical laws of sulfatizing roasting. *Zapiski Gornogo Instituta*. 1966;46(3):47—57. (In Russ.).

    Бумажнов Ф.Т. Исследование физико-химических закономерностей сульфатизирующего обжига. *Записки Горного института*. 1966;46(3):47—57.

19. Khudyakov I.F., Tikhonov A.I., Deev V.I., Naboichenko S.S. Metallurgy of copper, nickel and cobalt. T. 1: Metallurgy of copper. Moscow: Metallurgiya, 1977. 295 p. (In Russ.).

    Худяков И.Ф., Тихонов А.И., Деев В.И., Набойченко С.С. Металлургия меди, никеля и кобальта. Т. 1: Металлургия меди. М.: Металлургия, 1977. 295 с.

20. Vanyukov A.V., Utkin N.I. Complex processing of copper and nickel raw materials. Chelyabinsk: Metallurgiya, 1988. 432 p. (In Russ.).

    Ванюков А.В., Уткин Н.И. Комплексная переработка медного и никелевого сырья. Челябинск: Металлургия, 1988. 432 с.

21. Atesoglu G., Atilgan I. Effect of roasting temperature on the leaching of chalcopyrite concentrate in sulphuric acid. *Mining, Metallurgy & Exploration*. 2022;39:2199—2208. https://doi.org/10.1007/s42461-022-00669-y

22. Zhunusova G.Zh., Altaibaev B.T., Kalyanova O.A., Serkebaeva S.K., Sydykanov M.M. Hydrolytic purification of sulfate solutions from impurities of iron, arsenic, antimony, aluminum and silicon. *Prioritetnye nauchnye napravleniya: ot teorii k praktike*. 2013;(8):123—129. (In Russ.).

    Жунусова Г.Ж., Алтайбаев Б.Т., Кальянова О.А., Серкебаева С.К., Сыдыканов М.М. Гидролитическая очистка сульфатных растворов от примесей железа, мышьяка, сурьмы, алюминия и кремния. *Приоритетные научные направления: от теории к практике*. 2013;(8):123—129.

23. Sokolov A.Yu., Kasikov A.G., Bagrova E.G. Solvent extraction purification of sulfuric acid solutions from iron with di-2-ethylhexyl phosphoric acid. In: *Proceedings of International Conference “Innovative processes of complex treatment of natural and man- made mineral raw materials”* (Plaksinsky Readings) (Apatity, 21–26 September 2020). Apatity: Publ. KSC RAS, 2020. P. 270–272. (In Russ.).

    Соколов А.Ю., Касиков А.Г., Багрова Е.Г. Экстракционная очистка сернокислых растворов от железа ди-2-этилгексилфосфорной кислотой. В сб.: *Материалы Международной конференции «Инновационные процессы комплексной переработки природного и техногенного минерального сырья»* (Плаксинские чтения) (г. Апатиты, 21—26 сентября 2020 г.). Апатиты: Издательство КНЦ РАН, 2020. С. 270—272.

24. Corrae M.M.J., Silvas F.P.C., Aliprandini P., de Moraes V.T., Dreisinger D., Espinosa D.C.R. Separation of copper from a leaching solution of printed circuit boards by using solvent extraction with D2EHPA. *Brazilian Journal of Chemical Engineering*. 2018;35(3): 919—930.
    https://doi.org/10.1590/0104-6632.20180353s20170144

25. Hirato T., Wu Z.-C., Yamada Y., Majima H. Improvement of the stripping characteristics of Fe(III) utilizing a mixture of di(2-ethylhexyl) phosphoric acid and tri-n-butyl phosphate. *Hydrometallurgy*. 1992;28:81—93.
    https://doi.org/10.1016/0304-386X(92)90066-9

26. Singh D.K., Mishra S.L., Singh H. Stripping of iron (III) from the D2EHPA + TBP extract produced during uranium recovery from phosphoric acid by oxalic acid. *Hydrometallurgy*. 2006;81:214—218.
    https://doi.org/10.1016/j.hydromet.2005.12.006

27. Devi N.B., Nayak B. Liquid-liquid extraction and separation of copper (II) and nickel (II) using LIX®984N. *Journal of the Southern African Institute of Mining and Metallurgy*. 2008;114(11):937—943.

Information about the authors

Artem Yu. Sokolov – Cand. Sci. (Eng.), Junior Researcher, Tananaev Institute of Chemistry of the Kola Science Centre of the Russian Academy of Sciences (ICT KSC RAS).
https://orcid.org/0000-0002-0281-5284
E-mail: aiu.sokolov@ksc.ru

Alexandr G. Kasikov – Cand. Sci. (Chem.), Leading Researcher, ICT KSC RAS.
https://orcid.org/0000-0001-7694-0910
E-mail: a.kasikov@ksc.ru

Информация об авторах

Артем Юрьевич Соколов – к.т.н., мл. науч. сотрудник Института химии и технологии редких элементов и минерального сырья им. И.В. Тананаева Кольского научного центра Российской академии наук (ИХТРЭМС КНЦ РАН).
https://orcid.org/0000-0002-0281-5284
E-mail: aiu.sokolov@ksc.ru

Александр Георгиевич Касиков – к.х.н., вед. науч. сотрудник ИХТРЭМС КНЦ РАН.
https://orcid.org/0000-0001-7694-0910
E-mail: a.kasikov@ksc.ru

Contribution of the authors

A.Yu. Sokolov – defined the objectives of the study, conducted the experiments, contributed to the discussion of the results, and wrote the article.

A.G. Kasikov – defined the objectives of the study, provided the source materials, contributed to the discussion of the results, and wrote the article.

Вклад авторов

А.Ю. Соколов – определение цели работы, проведение экспериментов, участие в обсуждении результатов, подготовка статьи.

А.Г. Касиков – определение цели работы, предоставление исходного материала для работы, участие в обсуждении результатов, подготовка статьи.

The article was submitted 21.02.2024, revised 01.07.2024, accepted for publication 03.07.2024

Статья поступила в редакцию 21.02.2024, доработана 01.07.2024, подписана в печать 03.07.2024

PRESSURE TREATMENT OF METALS / ОБРАБОТКА МЕТАЛЛОВ ДАВЛЕНИЕМ

UDC 621.77
https://doi.org/10.17073/0021-3438-2024-4-43-53

Research article
Научная статья

Capabilities of asymmetric rolling of single-layer and laminated materials made from aluminum and its alloys

O.D. Biryukova[1], **A.E. Mogilnykh**[1], **A.M. Pesin**[1], **D.O. Pustovoytov**[1], **I.A. Pesin**[1], **M.A. Biryukov**[2]

[1] **Nosov Magnitogorsk State Technical University**
38 Lenin Prosp., Magnitogorsk, Chelyabinsk Region 455000, Russia

[2] **PJSC "Magnitogorsk Iron and Steel Works"**
93 Kirov Str., Magnitogorsk, Chelyabinsk Region 455000, Russia

✉ Olesya D. Biryukova (fimapatisonchik@inbox.ru)

Abstract: Asymmetric rolling of aluminum alloys is one of the methods for improving their mechanical and performance characteristics. Kinematic asymmetry during rolling is achieved by varying the roll speed ratios (V_1 / V_2). It is believed that when $V_1 / V_2 > 3$, the process of asymmetric rolling, by combining significant compression and shear deformations, approximates the processes of severe plastic deformation. It has been found that the majority of studies are based on data obtained within a limited roll speed ratio range, $V_1 / V_2 < 2$, in asymmetric rolling. This article examines the effects observed at $V_1 / V_2 = 1 \div 7.7$. The implementation of this condition became possible thanks to a unique scientific facility – the 400 laboratory-industrial asymmetric rolling mill at the Zhilyaev laboratory "Mechanics of Gradient Nanomaterials" at Nosov Magnitogorsk State Technical University Experiments were conducted on asymmetric thin-sheet rolling of aluminum alloys 2024, 5083, and 6061, as well as accumulative roll bonding to produce laminated sheet aluminum composites 5083/2024, 5083/1070, and 6061/5083. The disadvantages of asymmetric rolling compared to symmetric rolling were identified: sample failure was observed at single relative reductions of 37 % for layered sheet aluminum composites (5083/2024) and 40 % for thin-sheet aluminum alloys (6061). The nuances of material preparation for processing were described, including the necessity of cleaning and degreasing the alloy surfaces before bonding into a composite. The rolling temperature regimes were selected, determining cold asymmetric thin-sheet rolling (room temperature processing) and warm asymmetric accumulative roll bonding (heating of the workpieces in the furnace before rolling at 320–350 °C). A reduction in rolling force (by a minimum of 1.3 times), the ability to vary hardness (including an increase by a minimum of 30 %), and technological plasticity with changes in the roll speed ratios within the range of 2 to 7.7 were demonstrated. Options were proposed for reducing the processing cycles of aluminum alloys without compromising the quality of the finished product by reducing the number of rolling passes and annealing steps in the standard process scheme.

Key words: asymmetric rolling, accumulative roll bonding, severe plastic deformation, technological plasticity, hardness, kinematic asymmetry, rolling force.

Acknowledgements: This research was supported by the Russian Science Foundation grant (agreement No. 23-79-30015).

For citation: Biryukova O.D., Mogilnykh A.E., Pesin A.M., Pustovoytov D.O., Pesin I.A., Biryukov M.A. Capabilities of asymmetric rolling of single-layer and laminated materials made from aluminum and its alloys. *Izvestiya. Non-Ferrous Metallurgy.* 2024;30(4):43–53.
https://doi.org/10.17073/0021-3438-2024-4-43-53

Возможности асимметричной прокатки однослойных и слоистых материалов из алюминия и его сплавов

О.Д. Бирюкова[1], **А.Е. Могильных**[1], **А.М. Песин**[1], **Д.О. Пустовойтов**[1], **И.А. Песин**[1], **М.А. Бирюков**[2]

[1] **Магнитогорский государственный технический университет им. Г.И. Носова**
Россия, 455000, Челябинская обл., г. Магнитогорск, пр. Ленина, 38

[2] **ПАО «Магнитогорский металлургический комбинат»**
Россия, 455000, Челябинская обл., г. Магнитогорск, ул. Кирова, 93

✉ Олеся Дмитриевна Бирюкова (fimapatisonchik@inbox.ru)

Аннотация: Асимметричная прокатка алюминиевых сплавов является одним из способов улучшения их механических и эксплуатационных характеристик. Кинематическая асимметрия при прокатке осуществляется при варьировании отношений скоростей рабочих валков (V_1/V_2). Считается, что при $V_1/V_2 > 3$ процесс асимметричной прокатки по механизму совмещения больших деформаций сжатия и сдвига приближен к процессам интенсивной пластической деформации. Выявлено, что большее количество исследований основано на данных, полученных при ограниченном диапазоне соотношения скоростей валков $V_1/V_2 < 2$ при асимметричной прокатке. В статье рассмотрены эффекты, полученные при $V_1/V_2 = 1 \div 7{,}7$. Реализация данного условия стала возможна благодаря уникальной научной установке – лабораторно-промышленному стану 400 асимметричной прокатки лаборатории «Механика градиентных наноматериалов им. А.П. Жиляева» МГТУ им. Г.И. Носова. Проведены эксперименты по асимметричной тонколистовой прокатке алюминиевых сплавов 2024, 5083 и 6061 и аккумулирующей прокатке с получением листовых слоистых алюминиевых композитов 5083/2024, 5083/1070 и 6061/5083. Выявлены недостатки асимметричной прокатки по сравнению с симметричной: наблюдалось разрушение образцов при единичных относительных обжатиях от 37 % для листовых слоистых алюминиевых композитов (5083/2024) и от 40 % – для тонколистовых алюминиевых сплавов (6061). Описаны нюансы подготовки материала к обработке, в том числе необходимость зачистки и обезжиривания поверхности сплавов перед соединением в композит. Подобраны температурные режимы прокатки, определившие холодную асимметричную тонколистовую прокатку (комнатная температура обработки) и теплую асимметричную аккумулирующую прокатку (температура нагрева заготовок в печи перед прокаткой 320–350 °С). Показаны снижение силы прокатки (минимально в 1,3 раза), возможность варьирования твердости (в том числе увеличения минимально на 30 %) и технологической пластичности при изменении отношений скоростей валков в пределах от 2 до 7,7. Предложены варианты сокращения технологических циклов обработки алюминиевых сплавов без снижения качества готовой продукции путем уменьшения количества прокаток и отжигов в стандартной схеме.

Ключевые слова: асимметричная прокатка, аккумулирующая прокатка, интенсивная пластическая деформация, технологическая пластичность, твердость, кинематическая асимметрия, сила прокатки.

Благодарности: Исследования выполнены за счет гранта РНФ (соглашение № 23-79-30015).

Для цитирования: Бирюкова О.Д., Могильных А.Е., Песин А.М., Пустовойтов Д.О., Песин И.А., Бирюков М.А. Возможности асимметричной прокатки однослойных и слоистых материалов из алюминия и его сплавов. *Известия вузов. Цветная металлургия.* 2024;30(4):43–53. https://doi.org/10.17073/0021-3438-2024-4-43-53

Introduction

In line with the Metallurgical Industry Development Strategy of the Russian Federation through 2030[1], a series of objectives has been set, focusing on the production of high-quality metal products. Notably, under these conditions, the non-ferrous metallurgy sector is expected to achieve production growth, not only to meet import substitution goals but also to support the export of high-quality, competitive products. The development of new ultra-strong yet lightweight materials is crucial for driving technological progress in industries such as aerospace, electrical engineering, automotive, and aviation manufacturing. Aluminum and its alloys

---

[1] Order of the Government of the Russian Federation of December 28, 2022 No. 4260-r “On approval of the strategy for the development of the metallurgical industry of the Russian Federation for the period up to 2030”.

are the primary materials of choice for structural design in these fields.

Achieving high-quality aluminum rolled products depends on processing methods that aim to comprehensively improve the materials' properties, structure, and geometric parameters. For instance, asymmetric rolling is a promising technique for producing high-quality materials, as it improves mechanical properties such as strength, hardness, and plasticity, along with performance characteristics like formability under pressure and technological plasticity [1—10]. Asymmetry during rolling can be achieved in several ways: varying the roll speed ratio to induce kinematic asymmetry; changing the roll diameter ratio to create geometric asymmetry; or modifying the surface of the working rolls or the material itself to introduce physical-mechanical or contact asymmetry [11—14]. Among these, kinematic asymmetry is the most technologically viable and often preferred. Currently, asymmetric rolling with a roll speed ratio of $V_1/V_2 > 3$ is regarded as a metal forming process that closely approximates the effects of severe plastic deformation. Its key feature lies in the ability to combine significant compression and shear deformations by employing a simple and pure shear scheme, which impacts the deformability of metals and alloys.

It has been established that asymmetric rolling significantly increases the hardness and strength of materials [15—19], though plasticity tends to decrease, necessitating intermediate and final heat treatments of the rolled metal. However, combining high levels of reduction with specific roll speed ratios can maintain or even It's important to note that in most foreign publications [20—23], researchers typically explore a narrow range of roll speed ratios, with V_1/V_2 not exceeding 2. There is a noticeable lack of data on the effects of a broader roll speed ratio range ($V_1/V_2 = 2 \div 10$) in both Russian and international studies, making this an area of significant interest.

The implementation of asymmetric rolling with kinematic asymmetry and roll speed ratios ranging from 1.05 to 10.0 has been made possible thanks to a unique scientific facility (USF)[1] — the 400 laboratory-industrial asymmetric rolling mill[2] at the Zhilyaev laboratory "Mechanics of Gradient Nanomaterials" at Nosov Magnitogorsk State Technical University. This equipment has no equivalent in Russia, with the most similar system located in South Korea, where the roll speed ratio can reach up to 2.

Research methodology

The study investigated the effect of kinematic asymmetry during thin-sheet and accumulative rolling on the changes in mechanical properties of aluminum alloys. The asymmetric rolling was carried out on the USF "Asymmetric Rolling Mill 400" at room temperature. No lubricants were used; however, pre-rolling of aluminum was performed to promote its adhesion to the roll surfaces, thereby increasing friction coefficient. The aluminum alloys subjected to rolling were from the 1xxx, 2xxx, 5xxx, and 6xxx series, specifically 1070, 2024, 5083, and 6061, whose chemical compositions are presented in Table 1. The selection of these alloys was based on their widespread use and popularity in the manufacturing industries for which this research was conducted (automotive, aerospace, etc.).

Aluminum alloys 2024, 5083, and 6061 were processed using asymmetric rolling with relative reductions ranging from 5 to 89 % and roll speed ratios V_1/V_2 from 1 to 7.7. The workpiece dimensions were as follows, in mm: thickness — from 1.9 to 6, width — 25, length — 100. No additional heat treatment or preheating was applied prior to rolling.

Certain parameters of asymmetric thin-sheet and asymmetric accumulative roll bonding differed, which was determined by the technological features of the process: thin-sheet rolling involved processing single-layer aluminum alloys, while accumulative roll bonding, the general scheme of which is shown in Fig. 1 [24], was intended for laminated materials forming a composite.

These methods are used to obtain an ultrafine-grained structure, with the accumulative roll bonding process involving not only the combined and simple shear schemes but also the accumulation of stresses after each processing cycle. However, the complexity of this process, compared to asymmetric thin-sheet rolling, lies in the necessity of preparing the alloy surfaces for bonding during processing. Some studies [24—27] describe the requirement for preliminary mechanical joining of the sheets, which improves the adhesion level during rolling. This was performed on several workpieces, as shown in Fig. 2.

During asymmetric accumulative roll bonding, aluminum alloys 1070, 2024, 5083, and 6061 were used to create laminated sheet aluminum composites 5083/1070, 5083/2024, and 6061/5083. For these materials, two rolling cycles were conducted in all cases, with relative reductions ranging from 45 to 75 % (except in cases where samples were destroyed after the first

---

[1] https://ckp-rf.ru/catalog/usu/3206908

[2] http://lmgn.magtu.ru/ru/oborudovanie.html

Table 1. **Chemical composition (%) of aluminum alloys from various series**

Таблица 1. Химический состав (%) алюминиевых сплавов различных серий

Alloy	Mn	Mg	Si	Fe	Cu	Cr	Ti	Zn	Al
1070	0.03	0.02	0.15	0.16	0.01	–	0.01	0.04	99.70
2024	0.019	0.473	0.422	0.178	0.02	0.001	0.15	0.25	98.487
5083	0.682	4.479	0.091	0.285	0.027	0.104	0.007	0.014	94.282
6061	0.90	1.00	0.60	0.70	0.32	0.22	0.15	0.25	95.86

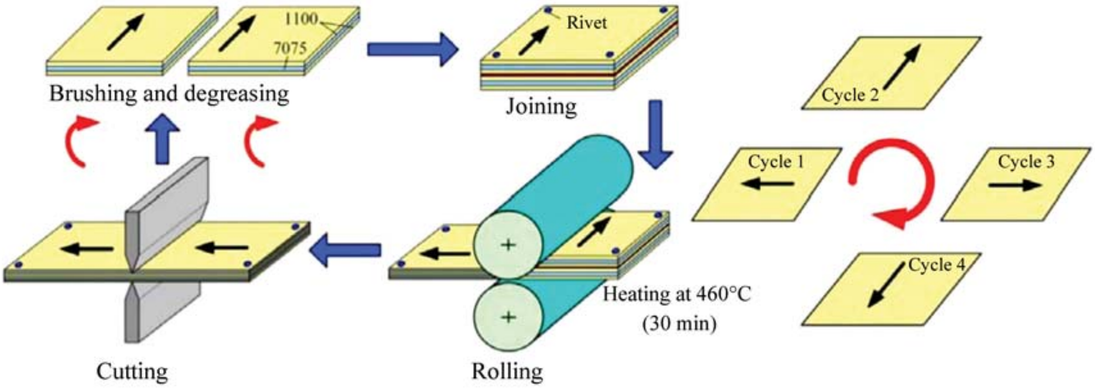

Fig. 1. Scheme of accumulative roll bonding [24]

Рис. 1. Схема аккумулирующей прокатки [24]

Fig. 2. Workpieces prepared for asymmetric accumulative roll bonding with preliminary joining using thin wire

Рис. 2. Образцы, подготовленные для асимметричной аккумулирующей прокатки с предварительным соединением их тонкой проволокой

rolling cycle). The roll speed ratio V_1/V_2 ranged from 1 to 5. The workpieces had the following dimensions, in mm: the thickness of individual layers composing the composite ranged from 1 to 2, with the total thickness of the two alloys being between 2 and 4; the width was 50, and the length was 100. The rolling temperature conditions varied from cold to hot, with preheating of the workpieces to 320—350 °C typically applied. The surface of each alloy (only for the cold asymmetric accumulative roll bonding method) was pre-treated by cleaning with wire brushes or sandpaper, followed by degreasing with a solvent. Subsequent transport to the rolling mill was carried out immediately to prevent the formation of a new thick oxide layer.

Results and discussion

In symmetric cases (при $V_1/V_2 = 1$), all workpieces failed during the first pass, both in thin-sheet rolling and cold accumulative roll bonding, when the single relative reduction was 40 % or higher. The results are shown in Table 2 and Fig. 3.

The study also revealed that improper or insufficiently thorough pre-cleaning and subsequent degreasing of the surface before accumulative roll bonding (at any roll speed ratio) negatively affected the formation of the transition layer, which is created through diffusion interactions. This resulted in a low degree of layer interpenetration between the base metals and alloys, leading to microcracks at the layer interfaces and areas with partial lack of bonding between the layers.

The necessity of pre-joining the alloys to form a laminated material, as shown in Fig. 2, was not confirmed — at low reductions, this "bond" had no positive effect, as the layers would separate, and the wire would break. For reductions exceeding 50 %, such pre-joining was unnecessary, as the layers bonded equally well regardless of the presence or absence of wire. In some cases, the wire had a negative effect, leading to defects at the front and rear ends of the rolled material.

It was also found that the formation of laminated sheet composites in the cold processing mode is only possible when joining identical alloys in the first cycle (e.g., alloy 5083 + alloy 5083 or alloy 1070 + alloy 1070). The first and second cycles with dissimilar alloys (e.g., alloy 5083 + alloy 2024 or alloy 6061 + alloy 5083) must be conducted in the warm rolling mode with preheating to 320—350 °C (considering material cooling during transport from the furnace to the rolling mill). Hot deformation of laminated sheet aluminum composites was performed by heating the workpieces to 420—500 °C, which produced unsatisfactory results, as all workpieces developed defects such as "over-squeezing" and "waviness". Table 3 presents some parameters of the asymmetric accumulative roll bonding modes—preheating temperatures for different types of materials (homogeneous 6061/6061, 5083/5083, 1070/1070, and heterogeneous 5083/1070, 5083/2024, 6061/5083) prior

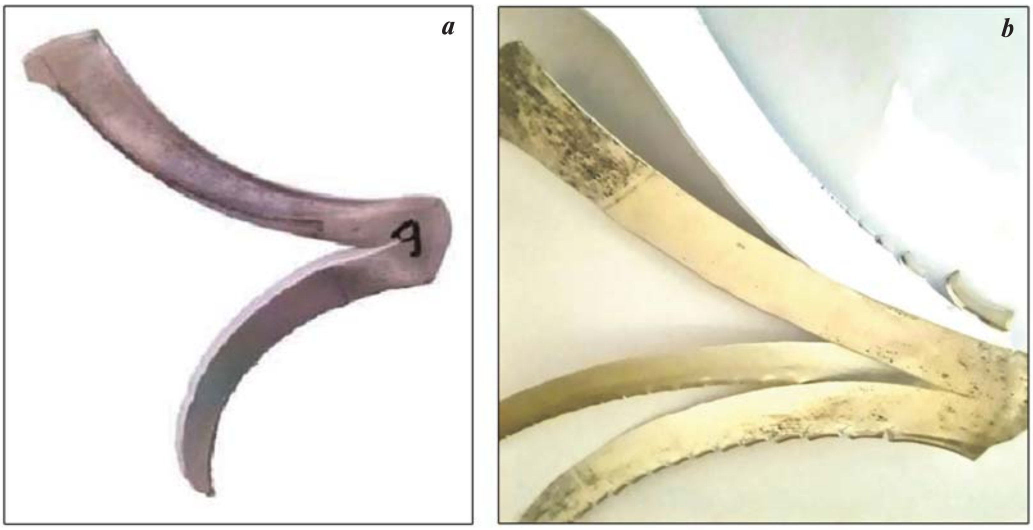

Fig. 3. Workpieces after symmetrical thin-sheet rolling (***a***) and accumulative (***b***) roll bonding

Рис. 3. Образцы после симметричной тонколистовой (***a***) и аккумулирующей (***b***) прокаток

Table 2. **Results of symmetrical thin-sheet rolling and accumulative roll bonding of aluminum alloys**

Таблица 2. Результаты симметричной тонколистовой и аккумулирующей прокаток алюминиевых сплавов

Material	Thickness, mm		Relative reduction, %	Force, kN
	Initial	Final		
2024	6.00	3.10	48	464
5083	1.90	0.95	50	290
6061	2.00	1.20	40	353
5083/2024	3.00	1.90	37	1330
5083/1070	3.00	1.60	47	900
6061/5083	3.00	1.55	48	1200

to rolling, the cycle number of asymmetric accumulative roll bonding, the relative reduction, and the integrity of the workpieces after processing, including the likelihood of defects that could affect further material processing.

The key advantages of asymmetric rolling compared to symmetric rolling have been identified: a reduction in rolling force, the ability to control mechanical properties (including hardness, strength, and plasticity) depending on the level of asymmetry, and an increase in technological plasticity. These advantages are characteristic of both thin-sheet rolling and accumulative roll bonding, as shown in Table 4 (using alloy 6061 processed in one pass and laminated sheet composite 6061/5083 processed in two cycles as examples). During asymmetric accumulative roll bonding, the preheating of the workpieces was carried out for 10—15 minutes at a temperature of 320 °C. All the presented workpieces maintained their integrity after processing.

It is important to note that asymmetric rolling significantly increases technological plasticity. This parameter is taken into account when developing new technical and technological solutions for material processing. Below are experimental data comparing symmetric and asymmetric rolling (using aluminum alloy 6061 as an example), clearly demonstrating the difference in the deformability of the workpieces. The ultimate goal of the experiment was to obtain a strip with a thickness of 0.5 mm. In the case of symmetric rolling, this result was achieved in 4 passes. After each pass, heat treatment, specifically annealing, was required, meaning it was performed 4 times. The roll gap was set to a relative reduction of 35 % for the first three passes and 9 % for the final pass. Any reduction greater than 35 % led to the workpiece's integrity being compromised, i.e., resulting in its failure. The results are presented in Table 5.

During asymmetric rolling, the roll speed ratio was $V_1/V_2 = 2$ (in passes 1 and 2), allowing the rolling process to be carried out with a relative reduction of 63 % without damaging the workpieces. As shown by the data in Table 6, the target was achieved in just two passes. The number of annealing treatments was also reduced to two.

With a further increase in kinematic asymmetry to $V_1/V_2 = 4$, the relative reduction without material

Table 3**. Parameters of the asymmetric accumulative roll bonding modes for aluminum alloys (comparison of temperature conditions)**

Таблица 3. Параметры режимов асимметричной аккумулирующей прокатки алюминиевых сплавов (сравнение температурных условий)

Material	Preheating temperature of the aluminum composite, °C	Cycle No.	Relative reduction, %	Defects Preservation of workpiece integrity
6061/6061 5083/5083 1070/1070	–	1	50	+
5083/1070 5083/2024 6061/5083	–	1	50	Delamination (integrity not preserved)
5083/1070 5083/2024 6061/5083	320–350	1	50	+
5083/1070 5083/2024 6061/5083	320–350	2	50	+
5083/1070 5083/2024 6061/5083	420–500	1	50	Waviness and over-squeezing (integrity preserved, but cycle 2 is not possible)

failure reached 75 %. It is clear that with asymmetric rolling at a roll speed ratio of $V_1/V_2 = 4$, only one pass and one final annealing were required (see Table 6).

Similar results were observed during accumulative roll bonding. It was shown that in cold symmetric accumulative roll bonding, the workpieces failed at a relative reduction of 42 %. Additionally, this level of relative reduction was insufficient for bonding the workpieces in the deformation zone, which resulted in either incomplete bonding of the metal layers or tears in the middle of the samples, along with the "crescent-shaped" defect. Cold asymmetric rolling was characterized by a reduction in defect formation. All workpieces demonstrated good pressure weldabil-

Table 4. **Results of asymmetrical thin-sheet rolling and accumulative roll bonding of aluminum alloys (comparison of rolling force and hardness)**

Таблица 4. Результаты асимметричной тонколистовой и аккумулирующей прокаток алюминиевых сплавов (сравнение силы прокатки и твердости)

Material	Roll speed ratio	Relative reduction, %	Force, kN	Hardness, HB
6061	2	63	320	118
6061	3	70	228	121
6061	4	75	166	100
6061/5083	2	53	640	65/78
6061/5083	3	62	558	73/89
6061/5083	4	67	490	93/100

Table 5. **Experimental data on symmetrical rolling of aluminum strip made from alloy 6061**

Таблица 5. Экспериментальные данные симметричной прокатки алюминиевой ленты из сплава 6061

Pass No.	Thickness, mm		Relative reduction, %	Force, kN
	Initial	Final		
1	2.00	1.30	35	337
2	1.30	0.85	35	272
3	0.85	0.55	35	275
4	0.55	0.50	9	151

Table 6. **Experimental data on asymmetric rolling of aluminum strip made from alloy 6061**

Таблица 6. Экспериментальные данные асимметричной прокатки алюминиевой ленты из сплава 6061

Pass No.	Thickness, mm		Relative reduction, %	Force, kN
	Initial	Final		
$V_1/V_2 = 2$				
1	2.00	0.74	63	320
2	0.74	0.50	32	234
$V_1/V_2 = 4$				
1	2.00	0.50	75	166

ity. Technological plasticity increased significantly, making it possible to roll laminated aluminum composites with single relative reductions ranging from 75 to 95 %.

In warm asymmetric accumulative roll bonding, the maximum single relative reduction reached 98 %. At lower reductions (up to 75 %), an increase in the drawing ratio (calculated using the formula $\mu = l1/l0$ was observed with an increase in kinematic asymmetry to $V_1/V_2 = 4$ (the preheating temperature of the workpieces was 320 °C, and the initial total thickness of the alloys in the composite was 3 mm). The values of the drawing ratio for the laminated aluminum composite 5083/2024 at various roll speed ratios are presented below:

V_1/V_2	1.0	2.0	2.5	3.0	3.5	4.0
μ	1.60	3.00	3.58	3.92	4.40	5.06

Conclusion

In both Russia and abroad, a limited range of roll speed ratios is considered in asymmetric rolling. Thanks to modern equipment, specifically the USF — 400 laboratory-industrial asymmetric rolling mill at the Zhilyaev laboratory “Mechanics of Gradient Nanomaterials”, it has become possible to process metals and alloys at roll speed ratios $V_1/V_2 > 2$. Based on the results of experimental studies on asymmetric thin-sheet rolling and accumulative roll bonding, the following were demonstrated:

1. An increase in the technological plasticity of aluminum alloys (as exemplified by alloys 2024, 5083, and 6061) and laminated sheet aluminum composites (as exemplified by 5083/1070, 5083/2024, and 6061/5083). In thin-sheet rolling, it became possible to shorten the technological cycle of cold material processing, including reducing the number of rolling passes and annealing without compromising the quality of the rolled product. It was shown that instead of four standard passes in the symmetric mode, a single pass in the asymmetric mode is permissible. In accumulative roll bonding, a single relative reduction of 98 % can be achieved without material failure in the asymmetric mode, compared to 42 % in the symmetric mode. The drawing ratio increased from 1.60 to 5.06 as the roll speed ratio V_1/V_2 increased from 1 to 4 (as demonstrated with the laminated sheet aluminum composite 5083/2024).

2. The ability to control mechanical properties (as demonstrated with hardness) by adjusting the level of asymmetry at roll speed ratios V_1/V_2 in the range of 2 to 4.

3. A reduction in rolling force with an increase in the level of asymmetry: for example, for aluminum alloy 6061, the force decreased from 320 to 166 kN as the roll speed ratio V_1/V_2 increased from 2 to 4, and for the laminated sheet aluminum composite 6061/5083, the force decreased from 640 to 490 kN, respectively. Similar results were observed for other aluminum alloys and laminated sheet aluminum composites considered.

4. Specifics of preparing aluminum alloys for the production of laminated sheet aluminum composites, which include proper surface treatment before bonding and the lack of necessity for additional wire-based bonding of layers.

References

1. Youzhi Li, Yongfeng Shen, Sixin Zhao, Weina Zhang, Xue W.Y. Strengthening a medium-carbon low-alloy steel by nanosized grains: The role of asymmetrical rolling. *Nanomaterials*. 2023;13(5):956.
https://doi.org/10.3390/nano13050956
2. Muñoz J.A., Avalos M., Schell N., Brokmeier H.G., Bolmaro R. Comparison of a low carbon steel processed by cold rolling (CR) and asymmetrical rolling (ASR): Heterogeneity in strain path, texture, microstructure and mechanical properties. *Journal of Manufacturing Processes*. 2021;64:557—575.
https://doi.org/10.1016/j.jmapro.2021.02.017
3. Graça A., Vincze G., Wen W., Butuc M.C., Lopes A.B. Numerical study on asymmetrical rolled aluminum alloy sheets using the visco-plastic self-consistent (VPSC) method. *Metals*. 2022;12(6):979.
https://doi.org/10.3390/met12060979
4. Tao Zhang, Lei Li, Shi-hong Lu, Jia-bin Zhang, Hai Gong. Comparisons of flow behavior characteristics and microstructure between asymmetrical shear rolling and symmetrical rolling by macro/micro coupling simulation. *Journal of Computational Science*. 2018;29:142—152.
https://doi.org/10.1016/j.jocs.2018.10.005
5. Guofu Xu, Xiaowu Cao, Tao Zhang, Yulu Duan, Xiaoyan Peng, Ying Deng, Zhimin Yin. Achieving high strain rate superplasticity of an Al—Mg—Sc—Zr alloy by a new asymmetrical rolling technology. *Materials Science and Engineering: A*. 2016;672:98—107.
https://doi.org/10.1016/j.msea.2016.06.070

6. Ji Wang, Xianghua Liu, Xiangkun Sun. Study on asymmetrical cold rolling considered sticking friction. *Journal of Materials Research and Technology*. 2020;9(6):14131—14141. https://doi.org/10.1016/j.jmrt.2020.10.027
7. Amegadzie M.Y., Bishop D.P. Effect of asymmetric rolling on the microstructure and mechanical properties of wrought 6061 aluminum. *Materials Today*. 2020;25:101283. https://doi.org/10.1016/j.mtcomm.2020.101283
8. Tao Zhang, Lei Li, Shi-Hong Lu, Hai Gong, Yun-Xin Wu. Comparisons of different models on dynamic recrystallization of plate during asymmetrical shear rolling. *Materials*. 2018;11(1):151. https://doi.org/10.3390/ma11010151
9. Cunqiang Ma, Longgang Hou, Jishan Zhang, Linzhong Zhuang. Influence of thickness reduction per pass on strain, microstructures and mechanical properties of 7050 Al alloy sheet processed by asymmetric rolling. *Materials Science and Engineering: A*. 2016;650(5):454—468. https://doi.org/10.1016/j.msea.2015.10.059
10. Šlapáková M., Kihoulou B., Grydin O. Development of microstructure of asymmetrically rolled AA3003 aluminium sheets with Zr addition. *Journal of Alloys and Metallurgical Systems*. 2023;2:100012. https://doi.org/10.1016/j.jalmes.2023.100012
11. Muñoz J.A., Khelfa T., Duarte G.A., Avalos M., Bolmaro R., Cabrera J.M. Plastic behavior and microstructure heterogeneity of anAA6063-T6 aluminum alloy processed by symmetric and asymmetric rolling. *Metals*. 2022;12(10):1551. https://doi.org/10.3390/met12101551
12. Vincze G., Simões F., Butuc M.C. Asymmetrical rolling of aluminum alloys and steels: A review. *Metals*. 2020;10(9):1126. https://doi.org/10.3390/met10091126
13. Sułek B., Krawczyk J., Majewski M., Nawida N., Plewa K. Analysis of the influence of kinematic and frictionasymmetry on the curvature of the strip and forceparameters of the rolling process. *Tribologia*. 2023;305(3):81—94. https://doi.org/10.5604/01.3001.0053.9439
14. Sai Wang, Xianlei Hu, Xiaogong Wang, Jingqi Chen, Xianghua Liu, Changsheng Li. Design and experiment of V-shaped variable thickness rolling for rolled profiled strips. *Journal of Materials Research and Technology*. 2021;15:4381—4396. https://doi.org/10.1016/j.jmrt.2021.10.067
15. Biryukova O.D., Pesin A.M., Pustovoytov D.O. Investigation of the influence of kinematic asymmetry on the properties of laminated materials. *Materials Research Proceedings*. 2023;32:287—293. https://doi.org/10.21741/9781644902615-33
16. Biryukova O., Pesin A., Pustovoitov D. Experience in obtaining laminated aluminum composites by asymmetric accumulative roll bonding. *Letters on Materials*. 2022;12(4):373—378. https://doi.org/10.22226/2410-3535-2022-4-373-378
17. Pustovoytov D., Pesin A., Tandon P. Asymmetric (hot, warm, cold, cryo) rolling of light alloys: A review. *Metals*. 2021;11(6):956. https://doi.org/10.3390/met11060956
18. Biryukova O., Pesin A., Pustovoytov D., Kozhemiakina A., Nosov L. Obtaining laminated aluminum composites with a gradient structure based on asymmetric deformation. *METAL*. 2021;496—501. https://doi.org/10.37904/metal.2021.4133
19. Pesin A., Raab G., Sverchkov A., Pustovoytov D., Kornilov G., Bochkarev A., Pesin I., Nosov L. Development of asymmetric cold rolling technology of high-strength steel grades in order to exclude intermediate annealing operations. *Materials Research Proceedings*. 2023;32:355—361.
20. Kosturek R., Mróz S., Stefanik A., Szota P.L., Gębara P., Merda A., Wachowski M., Gloc M. Study on symmetry and asymmetry rolling of AA2519-T62 alloy at room-temperature and cryogenic conditions. *Materials*. 2022;15(21):7712. https://doi.org/10.3390/ma15217712
21. Pan D., Sansome D.H. An experimental study of the effect of roll-speed mismatch on the rolling load during the cold rolling of thin strip. *Journal of Mechanical Working Technology*. 1982;6(4):361—377. https://doi.org/10.1016/0378-3804(82)90034-1
22. Aboutorabi A., Assempour A., Afrasiab H. Analytical approach for calculating the sheet output curvature in asymmetrical rolling: In the case of roll axis displacement as a new asymmetry factor. *International Journal of Mechanical Sciences*. 2016;105:11—22. https://doi.org/10.1016/j.ijmecsci.2015.10.016
23. Qilin Zhao, Xianlei Hu, Xianghua Liu. Analysis of mechanical parameters in multi-pass asymmetrical rolling of strip by slab method. *Materials*. 2023;16(18):6286. https://doi.org/10.3390/ma16186286
24. Zejun Chen, Hongbo Hu, Xia Wu, Minhong Zhou, Kawunga Nyirenda, Qing Liu, Guojun Wang, Deman

Wang. Effect of cross accumulative roll bonding process on microstructure and mechanical properties of laminated 1100/7075 composite sheets. *TMS (The Minerals, Metals and Society).* 2013;2285—2295. https://doi.org/10.1002/9781118792148.ch284

25. Mehtedi M.E., Lai D., Mohtadi R.E., Carta M., Buonadonna P., Aymerich F. Bonding of similar AA3105 aluminum alloy by accumulative roll bonding process. *ESAFORM*. 2021;942/1—942/11. https://doi.org/10.25518/esaform21.942

26. Seleznev M., Renzing C., Schmidtchen M., Prahl U., Biermann H., Weidner A. Deformation lenses in a bonding zone of high-alloyed steel laminates manufactured by cold roll bonding. *Metals.* 2022;12:590. https://doi.org/10.3390/met12040590

27. Karganroudi S.S., Nasab B.H., Rahmatabadi D., Ahmadi M., Gholami M.D., Kasaeian-Naeini M., Hashemi R., Aminzadeh A., Ibrahim H. Anisotropic behavior of Al1050 through accumulative roll bonding. *Materials.* 2021;14:6910. https://doi.org/10.3390/ma14226910

Information about the authors

Olesya D. Biryukova – Cand. Sci. (Eng.), Senior Research Scientist, Zhilyaev laboratory of mechanics of gradient nanomaterials, Nosov Magnitogorsk State Technical University (NMSTU).
https://orcid.org/0000-0002-3922-9289
E-mail: fimapatisonchik@inbox.ru

Anna E. Mogilnykh – Cand. Sci. (Eng.), Senior Research Scientist, Zhilyaev laboratory of mechanics of gradient nanomaterials, NMSTU.
https://orcid.org/0000-0002-0977-3566
E-mail: kozhemiakina.a@yandex.ru

Alexander M. Pesin – Dr. Sci. (Eng.), Chief Research Scientist, Zhilyaev laboratory of mechanics of gradient nanomaterials, NMSTU.
https://orcid.org/0000-0002-5443-423X
E-mail: pesin@bk.ru

Denis O. Pustovoytov – Cand. Sci. (Eng.), Leading Researcher, Zhilyaev laboratory of mechanics of gradient nanomaterials, NMSTU.
https://orcid.org/0000-0003-0496-0976
E-mail: pustovoitov_den@mail.ru

Ilya A. Pesin – Cand. Sci. (Eng.), Senior Research Scientist, Zhilyaev laboratory of mechanics of gradient nanomaterials, NMSTU.
E-mail: ilya33392@bk.ru

Maxim A. Biryukov – Leading Engineer, PJSC “Magnitogorsk Iron and Steel Works”.
E-mail: bigmax174@gmail.com

Информация об авторах

Олеся Дмитриевна Бирюкова – к.т.н., ст. науч. сотрудник, лаборатория «Механика градиентных наноматериалов им. А.П. Жиляева» Магнитогорского государственного технического университета (МГТУ) им. Г.И. Носова.
https://orcid.org/0000-0002-3922-9289
E-mail: fimapatisonchik@inbox.ru

Анна Евгеньевна Могильных – к.т.н., ст. науч. сотрудник, лаборатория «Механика градиентных наноматериалов им. А.П. Жиляева» МГТУ им. Г.И. Носова.
https://orcid.org/0000-0002-0977-3566
E-mail: kozhemiakina.a@yandex.ru

Александр Моисеевич Песин – д.т.н., гл. науч. сотрудник, лаборатория «Механика градиентных наноматериалов им. А.П. Жиляева» МГТУ им. Г.И. Носова.
https://orcid.org/0000-0002-5443-423X
E-mail: pesin@bk.ru

Денис Олегович Пустовойтов – к.т.н., вед. науч. сотрудник, лаборатория «Механика градиентных наноматериалов им. А.П. Жиляева» МГТУ им. Г.И. Носова.
https://orcid.org/0000-0003-0496-0976
E-mail: pustovoitov_den@mail.ru

Илья Александрович Песин – к.т.н., ст. науч. сотрудник, лаборатория «Механика градиентных наноматериалов им. А.П. Жиляева» МГТУ им. Г.И. Носова.
E-mail: ilya33392@bk.ru

Максим Александрович Бирюков – вед. инженер, ПАО «Магнитогорский металлургический комбинат».
E-mail: bigmax174@gmail.com

Contribution of the authors

O.D. Biryukova – defined the research aim, conducted experiments on accumulative roll bonding and thin-sheet rolling, participated in mechanical testing, analyzed and processed the results, and authored the article.

A.E. Mogilnykh – contributed to defining the research aim, performed experiments on thin-sheet rolling, participated in mechanical testing, and analyzed and processed the results.

A.M. Pesin – led the work on asymmetric rolling, defined the experimental methods, participated in conducting the asymmetric rolling experiments, and evaluated the results.

D.O. Pustovoytov – led the work on asymmetric rolling, defined the experimental methods, participated in conducting the asymmetric rolling experiments, and evaluated the results.

I.A. Pesin – participated in conducting the asymmetric rolling experiments and contributed to the discussion of the results.

M.A. Biryukov – contributed to the discussion of the results and participated in writing the article.

Вклад авторов

О.Д. Бирюкова – определение цели работы, проведение экспериментов по аккумулирующей и тонколистовой прокаткам, участие в проведении механических испытаний, оценка и обработка полученных результатов, написание статьи.

А.Е. Могильных – участие в определении цели работы, проведение экспериментов по тонколистовой прокатке, участие в проведении механических испытаний, оценка и обработка полученных результатов.

А.М. Песин – руководство работой по асимметричной прокатке, определение методик экспериментов, участие в проведении экспериментов по асимметричной прокатке, оценка полученных результатов.

Д.О. Пустовойтов – руководство работой по асимметричной прокатке, определение методик экспериментов, участие в проведении экспериментов по асимметричной прокатке, оценка полученных результатов.

И.А. Песин – участие в проведении экспериментов по асимметричной прокатке, участие в обсуждении результатов.

М.А. Бирюков – участие в обсуждении результатов, участие в написании статьи.

The article was submitted 28.03.2024, revised 03.04.2024, accepted for publication 07.05.2024

Статья поступила в редакцию 28.03.2024, доработана 03.04.2024, подписана в печать 07.05.2024

PHYSICAL METALLURGY AND HEAT TREATMENT / МЕТАЛЛОВЕДЕНИЕ И ТЕРМИЧЕСКАЯ ОБРАБОТКА

UDC 661.665
https://doi.org/10.17073/0021-3438-2024-4-54-65

Research article
Научная статья

Investigating the impact of the porous structure of needle-punched preform-based carbon-carbon composites on the completeness of liquid silicon infiltration

K.V. Petrovskaya, P.A. Timofeev

Joint Stock Company "Kompozit"
4 Pionerskaya Str., Korolev, Moscow Region 141070, Russia

✉ Kristina V. Petrovskaya (info@kompozit-mv.ru)

Abstract: Currently, siliconized carbon-carbon composites (C/C composites) hold a significant position among materials used in non-ferrous metallurgy. The process of Liquid Silicon Infiltration (LSI) for porous C/C composites is strongly influenced by their microstructural characteristics. Studying the effect of the porous structure of various C/C composites on the completeness of silicon infiltration can enable the regulation of the phase composition of siliconized materials over a wide range, as well as the physical, mechanical, and thermophysical properties of C/C–SiC composites. This paper presents the results of analyzing the porous structure and strength characteristics of C/C composites based on needle-punched preforms with different types of carbon matrices (pyrocarbon, natural and synthetic pitch coke, and phenol-formaldehyde resin coke) and the C/C–SiC composites derived from them. Due to the specific features of carbon matrix formation from liquid or gas phases, differences in pore size distribution were observed. A carbon matrix formed by the gas-phase method exhibits fewer nanoscale pores compared to one formed by the liquid-phase method. The influence of the pore structure and the nature of the matrix carbon in various needle-punched preforms on the degree of saturation during LSI, infiltration depth, and mechanical properties was determined.

Keywords: carbon-carbon composites, porous structure, carbon matrix, carbon preform, liquid silicon infiltration (LSI), C/C–SiC composites.

For citation: Petrovskaya K.V., Timofeev P.A. Investigating the impact of the porous structure of needle-punched preform-based carbon-carbon composites on the completeness of liquid silicon infiltration. *Izvestiya. Non-Ferrous Metallurgy*. 2024;30(4):54–65.
https://doi.org/10.17073/0021-3438-2024-4-54-65

Определение влияния пористой структуры углерод-углеродных композиционных материалов на основе иглопробивной преформы на полноту пропитки расплавом кремния

К.В. Петровская, П.А. Тимофеев

АО «Композит»
Россия, 141070, Московская обл., г. Королев, ул. Пионерская, 4

✉ Кристина Владиславовна Петровская (info@kompozit-mv.ru)

Аннотация: В настоящее время особое место среди материалов, используемых в цветной металлургии, занимают силицированные углерод-углеродные композиционные материалы (УУКМ). На процесс силицирования пористого УУКМ значительно влияют его микроструктурные характеристики. Изучение влияния пористой структуры различных УУКМ на полноту пропитки расплавом кремния может позволить регулировать фазовый состав силицированных материалов в широком диапазоне, а также физико-механические и теплофизические свойства углерод-керамического композиционного материала (УККМ). Описаны результаты анализа пористой структуры и прочностных характеристик УУКМ на основе иглопробивной преформы с различными типами углеродных матриц (пироуглеродная, кокс натурального и синтетического пеков, кокс фенолформальдегидной смолы) и УККМ на их основе. В силу особенностей формирования углеродной матрицы из жидкой или газовой фаз наблюдается отличие по границам диапазонов пор. Углеродная матрица, сформированная газофазным методом, оставляет меньше наноразмерных пор в сравнении с матрицей, полученной жидкофазным методом. Установлено влияние структуры порового пространства и природы матричного углерода различных УУКМ на основе иглопробивных преформ на их степень насыщения расплавом кремния, глубину пропитки, а также определены механические свойства.

Ключевые слова: углерод-углеродные композиционные материалы, пористая структура, углеродная матрица, углеродная преформа, силицирование, пропитка расплавом кремния, углерод-керамические композиционные материалы.

Для цитирования: Петровская К.В., Тимофеев П.А. Определение влияния пористой структуры углерод-углеродных композиционных материалов на основе иглопробивной преформы на полноту пропитки расплавом кремния. *Известия вузов. Цветная металлургия*. 2024;30(4):54–65. https://doi.org/10.17073/0021-3438-2024-4-54-65

Introduction

The modern development of materials science is inseparable from the creation and implementation of high-temperature materials that combine heat resistance, excellent thermal stability, high mechanical properties, wear resistance, and durability in aggressive gaseous and liquid environments at elevated temperatures. Siliconized graphite largely meets these requirements, which explains its widespread use in the chemical, metallurgical, and energy industries. Siliconized graphite is utilized as components in friction assemblies (such as sealing rings and sliding bearings) for pumps and reactors, as protective sheaths for immersion thermocouples, and as bottom pouring refractories or stopper rod systems for metallurgical furnaces. Ensuring and enhancing the strength properties of materials under high-temperature conditions necessitates the development of new structural materials [1—3].

Currently, siliconized carbon-carbon composites (C/C composites) hold a significant position among materials used in non-ferrous metallurgy. Liquid silicon infiltration (LSI) is one of the most effective and rapid methods for forming a ceramic matrix. This method involves applying a slip coating based on silicon-containing powder to the surface of a porous C/C composite semi-finished product. At temperatures exceeding 1414 °C, the coating decomposes, producing liquid silicon. The LSI process for porous C/C composites is significantly influenced by their microstructural characteristics. The completeness of silicon infiltration is determined by the nature of the porous structure and the pore distribution in the C/C composite (including pore volume, size, configuration, distribution throughout the material, and accessibility to liquid silicon). Studying the influence of the structural features of porous C/C composites on their reactivity with liquid silicon and the completeness of infiltration enables regulation of the phase composition of siliconized materials over a wide range, as well as the physical, mechanical, and thermophysical properties of C/C—SiC composites [4—14].

Depending on the intended purpose, structural features of the components, and their operating conditions, various methods are used to manufacture reinforcing preforms and form carbon matrices for the production of C/C composites. Each type of carbon-reinforcing framework has its own structural features, and together with the different technological processes for densifying them with a carbon matrix, they exhibit specific ranges of pore sizes and configurations. Over the past decade, significant attention has been devoted to the development of high-speed, fully automated technologies for creating needle-punched reinforcing frameworks from carbon fibers. The emergence of new needle-punched frameworks has necessitated the development of porous C/C composites based on these frameworks and the adjustment of LSI process parameters to produce high-density C/C—SiC composites with uniformly distributed SiC [15—20].

To saturate the reinforcing framework with a carbon matrix, various carbon-containing substances are used. In the case of forming the carbon matrix by the gas-phase method, a carbon-containing gas undergoes pyrolysis, resulting in carbon deposition between the fibers of the framework. The advantages of this method include ensuring uniform distribution of the carbon matrix, high density of deposited carbon, strong adhesion between the matrix and the fibers, and enhanced mechanical and strength characteristics of the C/C composites. However, the gas-phase method is characterized by its long processing time, low raw material utilization efficiency, and consequently, high cost [10; 19; 21—24].

An alternative method for forming the carbon matrix is the impregnation of the framework with a polymer binder. This approach is faster and more cost-effective. The liquid-phase method of forming a carbon matrix involves impregnating carbon frameworks with polymer resin, followed by pyrolysis, carbonization, and high-temperature treatment (HTT). Precursors for this method can include various thermosetting (e.g., phenol-formaldehyde, furan) and thermoplastic (e.g., coal tar pitch, petroleum pitch) resins. The mechanical and thermophysical properties of the resulting composites largely depend on the chemical and physical structure of the coke residue from the polymer binder. The advantages of using pitches include their high coke density, good graphitization tendency, and the elimination of solvents from the technological process. However, their drawbacks include thermoplasticity, which leads to binder migration during heat treatment, and the presence of carcinogenic compounds in pitches, which negatively impacts working conditions. In industrial applications, phenol-formaldehyde resins and coal tar pitches are most commonly used to form the carbon matrix via the liquid-phase method [19; 25—28].

The objective of this study is to determine the influence of the pore structure and the nature of the matrix carbon in various needle-punched preform-based C/C composites on their degree of saturation with silicon melt, infiltration depth, and mechanical properties.

1. Research methodology

For the study, C/C composites were manufactured based on needle-punched preforms (NPPs) produced by JSC “Kompozit” (Korolev, Russia). The needle-punching technology enables the production of layered fibrous preforms with the required level of mechanical properties. NPPs made from continuous carbon fibers were fabricated by sequentially laying the tapes with rotation at a specific angle to reduce anisotropy in the properties. After preparing the reinforcing preform, the space between the fibers was filled with a carbon matrix formed using gas-phase and liquid-phase methods.

Phenol-formaldehyde resin of the BZh grade, produced by LLC “Naukom” (Nizhny Novgorod, Russia), natural and synthetic coal tar pitches produced by LLC “Mini-Max” (Moscow, Russia), and the carbon-containing gas methane (CH_4) were used as precursors for the carbon matrix.

The total open porosity and apparent density were determined using the hydrostatic weighing method in accordance with GOST 15139-69.

Data on the pore size and volumetric content of pores in the studied materials were obtained by the standard contact porometry (SCP) method using the “Porosimeter 3.2” instrument. The SCP method allows for the evaluation of the integral and differential porosity of materials, as well as their density. The measurement range of the pores is from 1 nm to 500 μm. The SCP experiment involves measuring the equilibrium relative moisture content curve (the ratio of the volume of liquid—octane—inside the pores to the weight or volume of the porous sample) between a standard and the test sample. The equilibrium relationship between the relative amount of octane in the test sample and its quantity in the standard, for which the porometric curve is pre-determined, is calculated. From this dependence and the calibration porometric curve of the standard (the distribution curve of pore volumes by their radii), the porometric curve of the test sample can be derived. The obtained integral and differential pore distribution data make it possible to evaluate the volumetric pore content and the porous structure of the material.

To study the porous space and microstructure of C/C composites and C/C—SiC composites, microstructural analysis of cross-sections of the samples was performed using a JCM-6610 LV scanning electron microscope equipped with an “Advanced Aztec” energy-dispersive analyzer. The investigation was conducted at various magnifications under an accelerating voltage of 20 kV. Surface topography analysis was carried out based on the contrast of the microstructure images obtained using secondary electrons (SEI). Imaging with backscattered electrons (BEC) was used to determine the elemental composition and morphology of the sample surfaces based on differences in the electron density distribution of the elements. Heavier elements appear brighter (e.g., Si), while lighter elements appear darker (e.g., C).

Tests to determine the ultimate tensile and compressive strength in the primary reinforcement direction, as well as compressive and shear strength perpendicular to the reinforcement direction, were conducted using a UTS-111 universal testing machine in accordance with OST 92-1459-77, 92-1460-77, and 92-1472-78, respectively. The loading range varied from 50 N to 50 kN. The method involves applying loads at fixation points according to various test schemes at a speed of 2—5 mm/min. The measurement error is ±0.5 %.

The structure of C/C—SiC composites was examined for the absence of hidden macro-defects (such as cracks or delaminations) and to assess the depth of LSI using *X*-ray tomography with an XT H 320 LC *X*-ray tomograph. As *X*-ray radiation passes through each part of the examined object, it loses intensity, which is then recorded by the cells of the receiver matrix. Each element (pixel) of the receiver records the intensity of the *X*-ray radiation. The calculated grayscale values, ranging from 0 (black) to 65536 (white), are proportional to the *X*-ray density of the examined object. This density, in turn, is directly proportional to the atomic numbers of the elements comprising the object, as listed in the Periodic Table of Elements, and to the physical density of the object.

2. Results and discussion

The main characteristics (apparent density — ρ, kg/m^3, and open porosity — OP, %) of various types of C/C composites depending on the type of matrix are presented in Table 1. The initial density of the NPP framework is 720 kg/m^3, and the volumetric fraction of the reinforcing filler is 50 %.

2.1. Porometric analysis of C/C composites

The analysis of the pore space can help in selecting the optimal mode for the subsequent formation of the ceramic matrix. To investigate the volumetric content, distribution, and size of pores, porometric analysis was performed on samples with different carbon matrices, ensuring comparable open porosity. The integral and differential pore distributions as a function of the logarithm of their radius are presented in Fig. 1.

The predominant pore size ranges from 1 to 15 μm, accounting for over 50 % of the total pore volume in the material. At the same time, due to the specific features of carbon matrix formation via liquid- or gas-phase methods, differences are observed in the pore size distribution boundaries. The carbon matrix formed by the gas-phase method contains fewer nanoscale pores (up to 9 %) compared to the matrix formed by the liquid-phase method (ranging from 17 to 36 %). For IPP/V, a higher number of closed pores is characteristic compared to C/C composites with a carbon matrix formed by the liquid-phase method, due to the partial blockage of pores during the deposition of pyrocarbon from the gas phase.

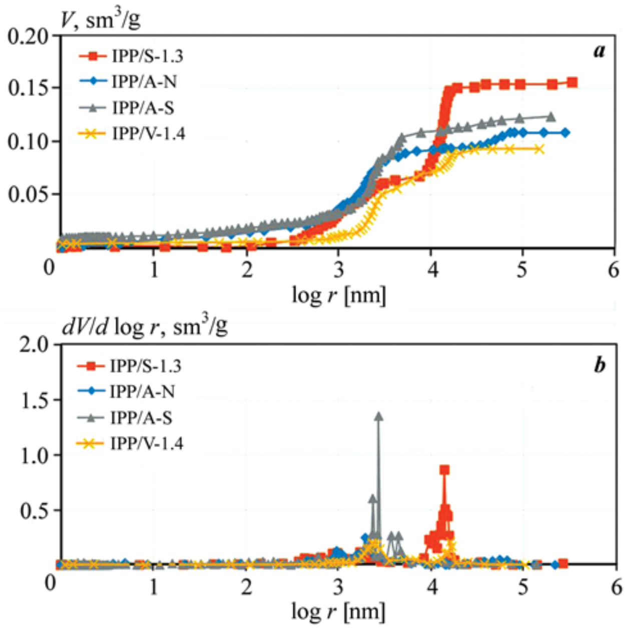

Fig. 1. Integral (***a***) and differential (***b***) pore distributions as a function of the logarithm of their radius in the studied samples

Рис. 1. Интегральное (***a***) и дифференциальное (***b***) распределения пор в зависимости от логарифма их радиуса в исследуемых образцах

2.2. Microstructural analysis of C/C composites

The microstructural analysis of the pore space in C/C composites of grades IPP/S-1.3, IPP/A-N, and IPP/V-1.4 is shown in Fig. 2. The IPP/A-S sample is not included due to the absence of distinctive structural features in the coke on the microphotographs, regardless of the type of pitch used.

Table 1. **The main characteristics of CCCM**

Таблица 1. Основные характеристики УУКМ

Type of precursor	Material grade	ρ, kg/m^3	OP, %
Phenol-formaldehyde resin	IPP/S-1.3	1360	12.1
Natural pitch	IPP/A-N	1590	15.1
Synthetic pitch	IPP/A-S	1580	15.5
Pyrolytic carbon	IPP/V-1.4	1480	15.3

Table 2. **Quantitative analysis of pore distribution in C/C composites**

Таблица 2. Количественный анализ распределения пор УУКМ

Material grade	Pore distribution in range, %			
	1 nm–1 μm	1–15 μm	15–70 μm	>70 μm
IPP/S-1.3	21.4	65.9	10.9	1.8
IPP/A-N	35.8	49.6	13.4	1.2
IPP/A-S	17.3	69.4	10.5	2.8
IPP/V-1.4	9.1	74.2	13.5	3.2

The structure of C/C composites with a matrix formed by the liquid-phase method predominantly exhibits high porosity, with large pores located along the boundaries of fiber bundles and the carbon matrix formed during the pyrolysis of the polymer binder at the carbonization stage (Fig. 2, *a*, *b*). The primary channels in the needle-punched preform are through interbundle pores as well as pores aligned with the needle-punching direction. The interfiber space in C/C composites with a liquid-phase-formed matrix is significantly filled with coke, with the presence of submicron-sized pores. Additionally, in C/C composites with a resin coke matrix (Fig. 2, *a*), as well as those with a pyrocarbon matrix (Fig. 2, *c*), the interbundle pores are clearly visible. In C/C composites with a matrix based on coal tar pitch coke (Fig. 2, *b*), the interbundle pores are largely filled with coke, which may hinder the penetration of silicon melt during subsequent LSI. In C/C composites with a gas-phase-formed matrix (Fig. 2, *c*), interbundle pores with a radius exceeding 15 μm are distinctly observed.

2.3. Evaluation of strength characteristics

The initial C/C composites with various types of carbon matrices were tested to determine the ultimate tensile and compressive strengths in the primary reinforcement direction (*X*), as well as compressive and shear strengths in the plane perpendicular to the primary rein-

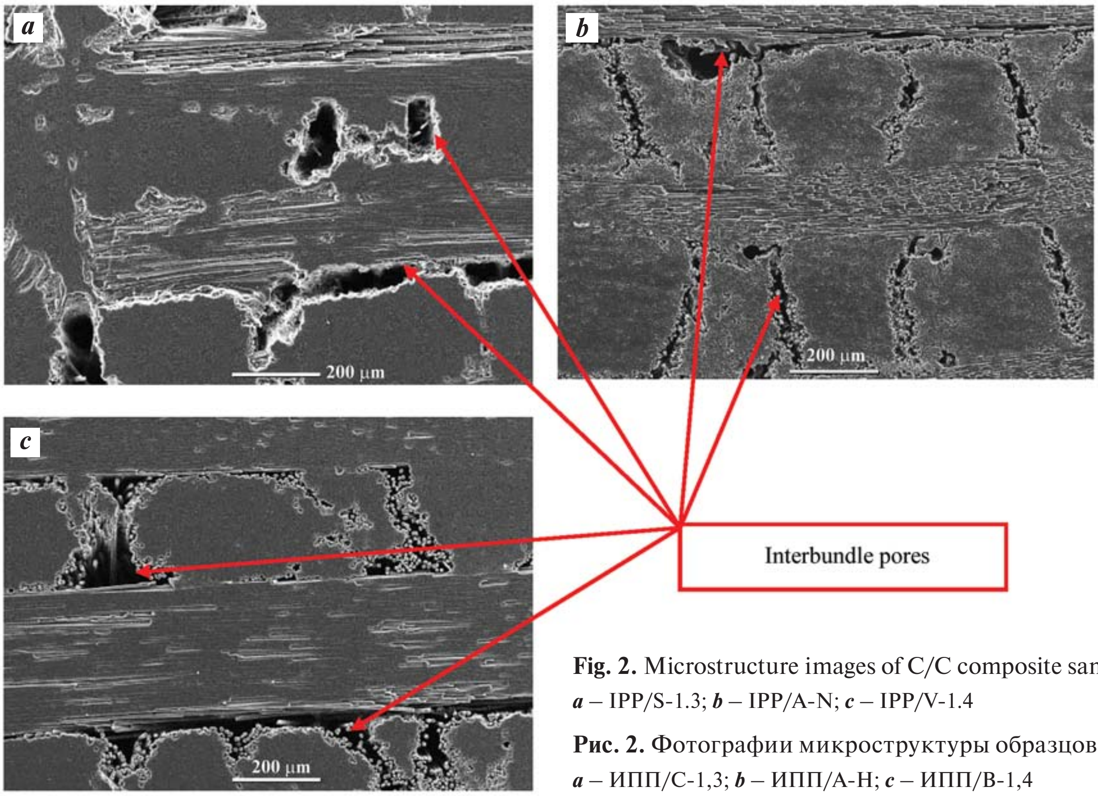

Fig. 2. Microstructure images of C/C composite samples
a – IPP/S-1.3; ***b*** – IPP/A-N; ***c*** – IPP/V-1.4

Рис. 2. Фотографии микроструктуры образцов УУКМ
a – ИПП/С-1,3; ***b*** – ИПП/А-Н; ***c*** – ИПП/В-1,4

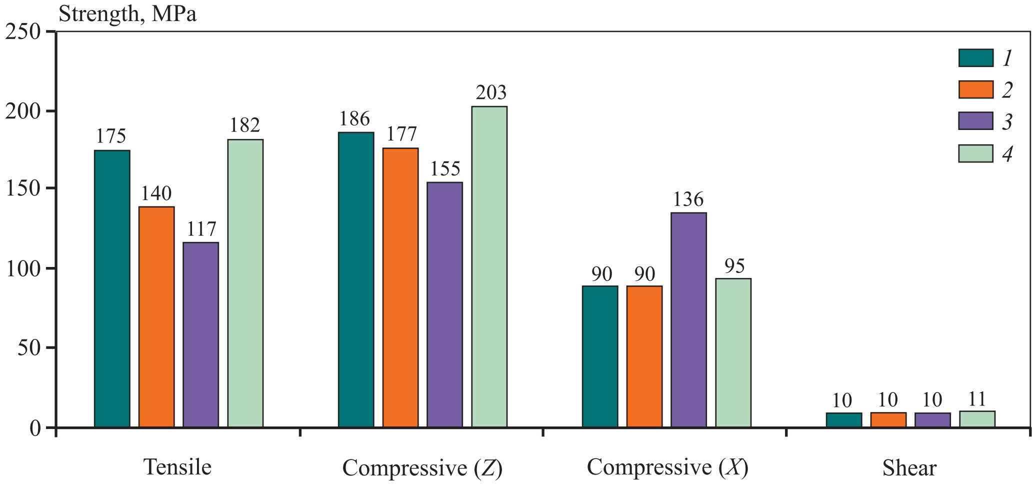

Fig. 3. Tensile, compressive, and shear strengths for various grades of C/C composites
1 – IPP/S-1.3; *2* – IPP/A-N; *3* – IPP/A-S; *4* – IPP/V-1.4

Рис. 3. Пределы прочности при растяжении, сжатии и сдвиге для различных марок УУКМ
1 – ИПП/С-1,3; *2* – ИПП/А-Н; *3* – ИПП/А-С; *4* – ИПП/В-1,4

forcement direction (*Z*). The results of the strength tests for the initial C/C composites are shown in Fig. 3.

Overall, the obtained values of the physical and mechanical characteristics for all C/C composite semi-finished products are relatively high, indicating their suitability for producing C/C—SiC composites with superior strength properties. For all grades of C/C composites, the tensile strength ranges from 117 to 182 MPa, compressive strength along the *X*-axis ranges from 90 to 136 MPa, compressive strength along the *Z*-axis ranges from 155 to 203 MPa, and shear strength ranges from 10 to 11 MPa.

2.4. Results of liquid silicon infiltration (LSI)

During the determination of technological parameters and optimization of the LSI process, adjustments were made to the coefficient of the applied slip, consisting of a silicon-containing powder and binder. The amount of slip was calculated based on the initial characteristics of the C/C composite. Increasing the coefficient allowed for obtaining a denser material in a single infiltration cycle. However, it could result in the formation of residual silicon build-ups, tightly bonded to the sample surface, representing an excess of the melt. The evaluation parameters included weight gain as a percentage of the initial mass and final open porosity not exceeding 5 %. The results of LSI for various samples are presented in Table 3.

C/C—SiC composites of grades IPP/S-1.3 and IPP/A-N exhibit identical weight gains (22.6 and 22.7 %, respectively) and a residual open porosity slightly above 5 %. The lowest residual open porosity (4.1 and 3.3 %) was observed for C/C—SiC composites with initial pyrocarbon and synthetic pitch coke-based matrices, respectively. The highest weight gain and SiC content were observed in C/C—SiC composites with initial pyrocarbon (31.0 and 12.9 %, respectively) and synthetic pitch coke-based matrices (26.0 and 12.2 %, respectively). Similar SiC phase volume fractions were also observed in C/C—SiC composites with matrices based on phenol-formaldehyde resin coke and natural pitch coke (9.6 and 11.2 %, respectively). The dependence of weight gain and silicon carbide content on the type of carbon matrix is shown graphically in Fig. 4.

The intensity and completeness of the bulk LSI process for C/C composites are significantly influenced by the nature of their porous structure, the total pore volume, pore size and configuration, their distribution throughout the entire volume of the material, and their accessibility for liquid silicon infiltration. It is most likely that interbundle pores, once filled, allow the silicon melt to flow further into interfiber pores. The C/C—SiC composite of grade IPP/V-1.4, with a pyrocarbon matrix, exhibits the highest weight gain and SiC content, which is attributed to its more favorable porous structure (interfiber and interbundle pores ranging from 1 to 15 μm account for approximately 75 % of the total pore volume). In the case of carbon matrices formed by the liquid-phase method, the submicron pore fraction for IPP/A-S, IPP/S-1.3, and IPP/A-N materials is 17 %, 21 %, and 36 %, respectively. This high proportion of submicron pores can lead to premature pore blockage

Table 3. **Results of liquid silicon infiltration using the developed technology**

Таблица 3. Результаты пропитки расплавом кремния по отработанной технологии

Material grade	ρ_{initial}, kg/m^3	OP$_{\text{init}}$, %	Weight gain Δm, %	ρ_{final}, kg/m^3	OP$_{\text{final}}$, %	V_{SiC}, vol. %
IPP/S-1,3	1360	12.1	22.6	1740	5.3	9.6
IPP /A-N	1590	15.1	22.7	1950	5.5	11.2
IPP /A-C	1580	15.5	26.0	2010	3.3	12.2
IPP /V-1,4	1480	15.3	31.0	1870	4.1	12.9

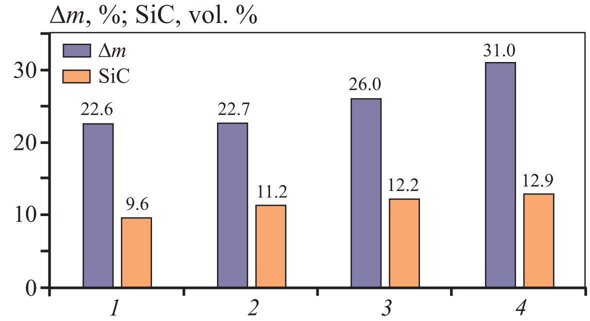

Fig. 4. Dependence of silicon carbide content on the type of carbon matrix

Matrix type: ***1*** – phenol-formaldehyde resin coke; ***2*** – natural pitch coke; ***3*** – synthetic pitch coke; ***4*** – pyrocarbon

Рис. 4. Зависимость содержания карбида кремния от типа углеродной матрицы

Тип матрицы: ***1*** – кокс фенолформальдегидной смолы; ***2*** – кокс натурального пека; ***3*** – кокс синтетического пека; ***4*** – пироуглерод

and unreacted carbon matrix volumes, reducing the effectiveness of LSI.

After LSI, the strength characteristics of the C/C—SiC composites were determined. The test results for the ultimate tensile and compressive strengths in the primary reinforcement direction (*X*), as well as compressive and shear strengths in the plane perpendicular to the primary reinforcement direction (*Z*), are shown graphically in Fig. 5.

The tensile strength of all types of C/C—SiC composites showed only a slight decrease after LSI compared to the initial C/C composites before infiltration, indicating minimal carbidization of carbon fibers. In contrast, the compressive strength along the primary reinforcement direction (*X*-axis) more than doubled, while compressive strength perpendicular to the reinforcement direction (*Z*-axis) increased by up to 70 %. Interlayer shear strength improved by 70—80 %. These significant enhancements in the mechanical properties of all C/C—SiC composite types relative to their initial C/C composite precursors are attributed to the formation of the silicon carbide matrix.

To evaluate the infiltration depth, a tomographic study was conducted on cubic samples measuring 15 × 15 × 15 mm. The tomographic images, presented in Fig. 6, show the non-infiltrated regions marked with dashed lines, facilitating the assessment of infiltration completeness.

Tomographic analysis revealed that samples of C/C—SiC composites with initial pyrocarbon and phenol-formaldehyde resin coke-based matrices were infiltrated to their full depth (7.5 mm from the surface), compared to C/C—SiC composites with initial pitch-based matrices, which showed infiltration depths of up to 5 mm. This difference can be attributed to the porous structure formed during carbonization and high-temperature treatment, characterized by a high fraction of submicron pores and low interbundle porosity, which hinders silicon infiltration.

Notably, a dependence of infiltration depth on the type of pitch was identified. For example, C/C—SiC composites with a synthetic pitch-based matrix exhibited an infiltration depth 1.5 times greater than those with a natural pitch-based matrix, due to a higher proportion of pores with radii ranging from 1 to 15 μm.

For a detailed analysis of the microstructure and overall composition of the C/C—SiC composites, a microstructural analysis was conducted. The microstructural images are shown in Fig. 7.

The distribution of SiC in C/C—SiC composites with a carbon matrix formed by the liquid-phase method is uniform across all pore size ranges. In contrast, C/C—SiC composites with an initial pyrocarbon matrix contain closed macropores (10—50 μm in diameter) that remain unfilled with SiC. This is due to the characteristics of carbon matrix distribution during deposition. Nevertheless, the highest weight gain after LSI in composites with an initial pyrocarbon matrix

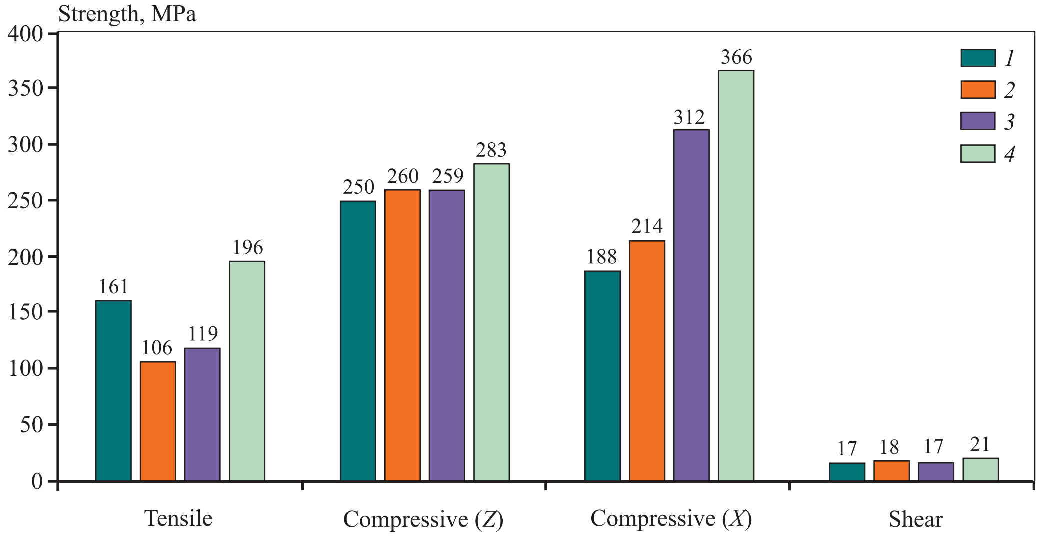

Fig. 5. Tensile, compressive, and shear strengths for various grades of C/C–SiC composites
1 – IPP/S-1.3; ***2*** – IPP/A-N; ***3*** – IPP/A-S; ***4*** – IPP/V-1.4

Рис. 5. Пределы прочности при растяжении, сжатии и сдвиге для различных марок УККМ
1 – ИПП/С-1,3; ***2*** – ИПП/А-Н; ***3*** – ИПП/А-С; ***4*** – ИПП/В-1,4

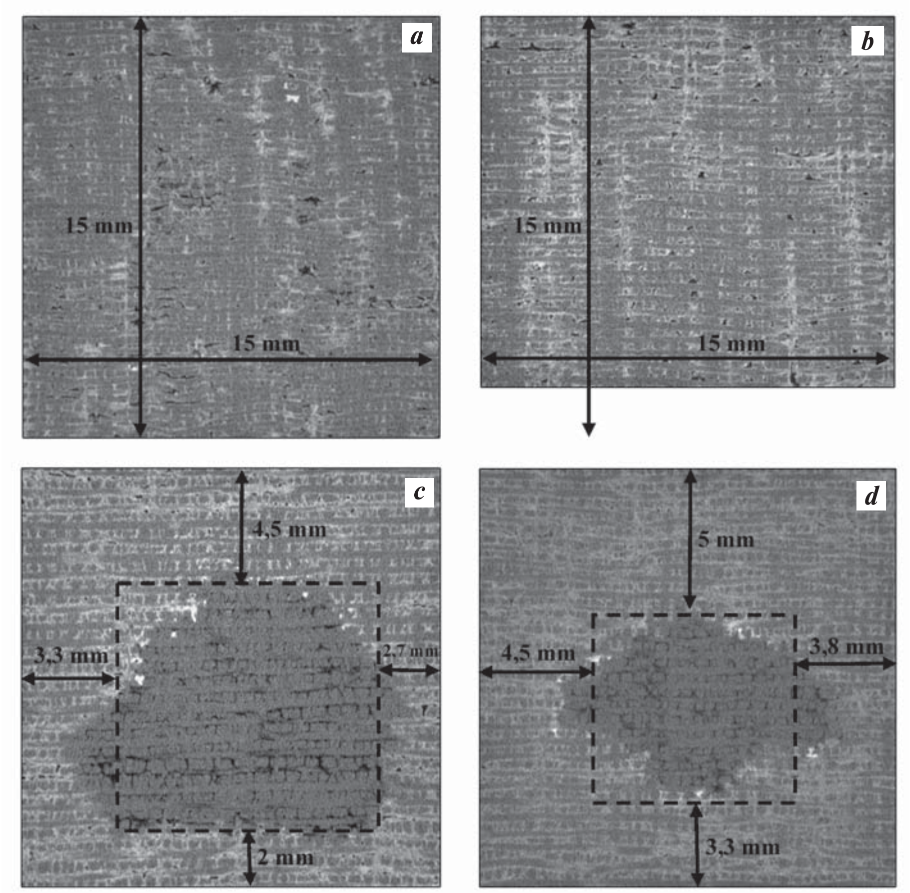

Fig. 6. Tomographic images after LSI of C/C–SiC composite samples
a – IPP/S-1.3; ***b*** – IPP/V-1.4; ***c*** – IPP/A-N; ***d*** – IPP/A-S

Рис. 6. Томографические изображения после силицирования образцов УККМ
a – ИПП/С-1,3; ***b*** – ИПП/В-1,4; ***c*** – ИПП/А-Н; ***d*** – ИПП/А-С

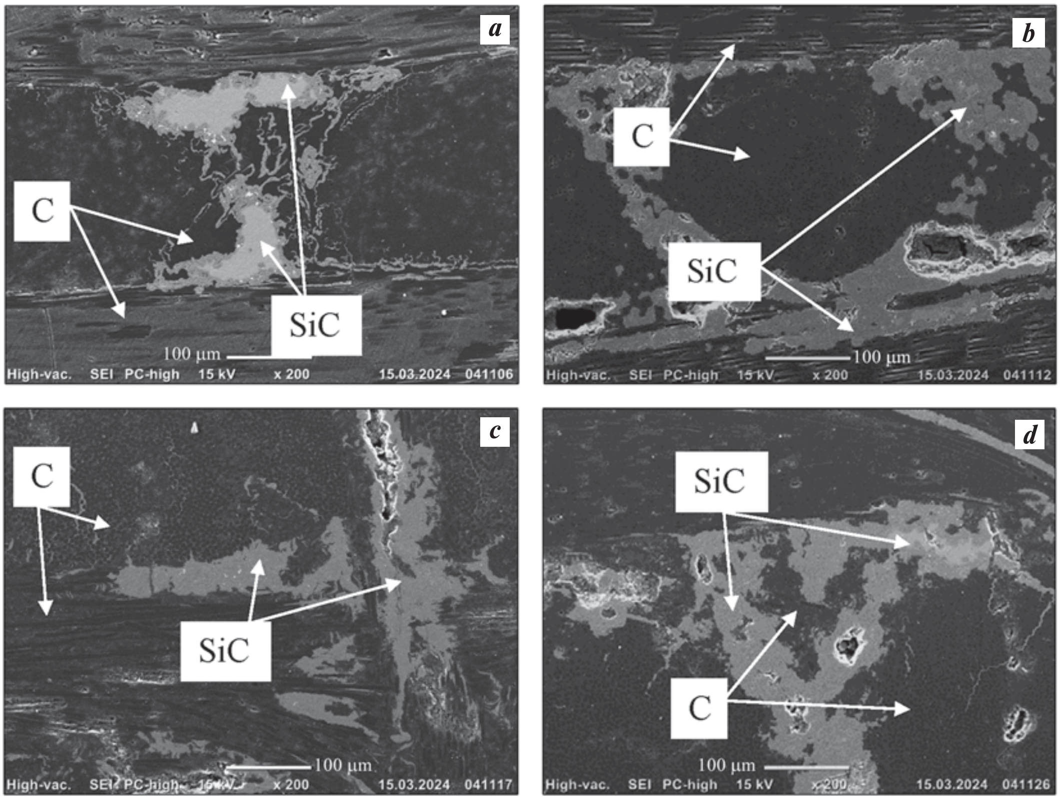

Fig. 7. Microstructural images of C/C–SiC composite samples
a – IPP/S-1.3; ***b*** – IPP/V-1.4; ***c*** – IPP/A-N; ***d*** – IPP/A-S

Рис. 7. Фотографии микроструктуры образцов УККМ
a – ИПП/С-1,3; ***b*** – ИПП/В-1,4; ***c*** – ИПП/А-Н; ***d*** – ИПП/А-С

is achieved due to the predominance of pores in the 1—15 µm range in the initial C/C composites before infiltration.

Conclusion

The microstructural, porometric, and tomographic studies of C/C composites with different initial carbon matrices reveal that the nature of the matrix carbon and the pore distribution in terms of volume and size significantly influence the degree of saturation and infiltration depth during liquid silicon infiltration (LSI). The highest saturation was observed in C/C—SiC composites of grades IPP/V-1.4 with a pyrocarbon matrix and IPP/S-1.3 with a phenol-formaldehyde resin coke-based matrix, owing to their favorable porous structures for siliconization. In composites with pyrocarbon matrices, infiltration depth reached 7.5 mm from the surface, with weight gain and SiC content values of 31.0 and 12.9 %, respectively. For liquid-phase carbon matrices, the greatest infiltration depth (7.5 mm from the surface) was achieved in the IPP/S-1.3 composite with a phenol-formaldehyde resin coke-based matrix, with weight gain and SiC content values of 22.6 and 9.6 %, respectively. For IPP/A-N and IPP/A-S composites, infiltration depths averaged 4.5 mm from the surface, with weight gain and SiC content values of 22.7 and 11.2 % for IPP/A-N (natural pitch-based matrix) and 26.0 and 12.2 % for IPP/A-S (synthetic pitch-based matrix). A direct dependence of the infiltration depth during LSI on the fraction of submicron pores was identified: the smaller the fraction of nanoscale pores, the higher the weight gain, SiC content, and infiltration depth. Mechanical tests of various C/C composites and their corresponding C/C—SiC composites demonstrated high physical and mechanical properties, confirming the applicability of C/C—SiC composites as structural materials. For all grades of C/C—SiC composites, tensile strength ranged from 106 to 196 MPa, compressive strength along the *X*-axis ranged from 188 to 366 MPa, compressive strength along the *Z*-axis ranged from 250 to 283 MPa, and shear strength ranged from 17 to 21 MPa.

References

1. Tarabanov A.S., Kostikov V.I. Siliconised graphite. Moscow: Metallurgiya, 1977. 158 p. (In Russ.).
   Тарабанов А.С., Костиков В.И. Силицированный графит. М.: Металлургия, 1977. 158 с.
2. Bushuev Yu.G. Carbon-carbon composite materials. Moscow: Metallurgiya, 1994. 196 p. (In Russ.).
   Бушуев Ю.Г. Углерод-углеродные композиционные материалы. М.: Металлургия, 1994. 196 с.
3. Deborah D.L. Chung. Carbon composites: composites with carbon fibers, nanofibers, and nanotubes New York; Buffalo: Imprint Butterworth-Heinemann, 2017. 682 p. https://doi.org/10.1016/C2014-0-02567-1
4. Kumar S., Kumar A., Shukla A., Gupta A.K., Devi R. Capillary infiltration studies of liquids into 3D-stitched C—C preforms. Part A: Internal pore characterization by solvent infiltration, mercury porosimetry, and permeability studies. *Journal of the European Ceramic Society.* 2009;29(12):2643—2650. https://doi.org/10.1016/j.jeurceramsoc.2009.03.007
5. Niu Z., Li Z., Xiao P., Li J., Li Z., Ou-yang X., Li Y. Influence of h-BN as additive on microstructure and oxidation mechanism C/C-SiC composites. *Journal of the European Ceramic Society.* 2019;39(15):4634—4644. https://doi.org/10.1016/j.jeurceramsoc.2019.06.032
6. Shvetsov A.A. Research of interaction of carbon with silicon melt in the process of siliconised graphite production: Diss. ... Cand. Sci. (Eng.). Moscow: RKhTU, 2019. (In Russ.).
   Швецов А.А. Исследование взаимодействия углерода с расплавом кремния в процессе получения силицированного графита: Дис. ... канд. техн. наук. М.: РХТУ, 2019.
7. Zhang K.X., Guo X.S., Cheng Y.X., Zhang F.Q., He L.L. TEM study on the morphology and interface microstructure of C/C-SiC composites fabricated by liquid infiltration. *Materials Characterization.* 2021;175:1—7. https://doi.org/10.1016/j.matchar.2021.111055
8. Tong Y., Bai S., Liang X., Qin Q., Zhai J. Reactive melt infiltaration fabrication of C/C-SiC composites: Wetting and infiltration. *Ceramics International.* 2016;42(15):17174—17178. https://doi.org/1016/j.ceramint.2016.08.007
9. Koshelev Yu.I., Bubnenkov I.A., Shvetsov A.A., Bardin N.G. Siliconised graphite: physicochemical bases of obtaining and prospects of development. Part 2. Influence of structural features of carbon materials on the degree of their interaction with silicon. *Silicate Technique and Technology.* 2017;24(2):6—11. URL: https://www.researchgate.net/publication/320148525 (accessed: 05.03.2024). (In Russ.).
   Кошелев Ю.И., Бубненков И.А., Швецов А.А., Бардин Н.Г. Силицированный графит: физико-химические основы получения и перспективы развития. Часть 2. Влияние структурных особенностей углеродных материалов на степень их взаимодействия с кремнием. *Техника и технология силикатов.* 2017;24(2):6—11. URL: https://www.researchgate.net/publication/320148525 (дата обращения: 05.03.2024).
10. Zhang Y., Xiao Z., Wang J., Yang J., Jin Z. Effect of pyrocarbon content in C/C preforms on microstructure and mechanical properties on the C/C-SiC composites. *Materials Science and Engineering: A.* 2009; 502(1-2):64—69. https://doi.org/10.1016/j.msea.2008.11.026
11. Tang J., Liu M., Wei Y., Yang Y., Huang Z. An efficient and low-cost liquid silicon infiltration method to prepare SiC-coated carbon short fiber for fiber protection of Cf/SiC ceramic matrix composites. *Ceramics International.* 2021;47(9):13235—13241. https://doi.org/10.1016/j.ceramint.2021.01.115
12. Tyurina S.A., Yudin G.A., Dalskaya G.Yu., Demin V.L., Andreeva S.A. The specifics of structure-building of composite material C—SiC in the process of Liquid Silicon Infiltration (LSI). *International Research Journal.* 2023;3(129):1—10. (In Russ.). https://doi.org/10.23670/IRJ.2023.129.24
    Тюрина С.А., Юдин Г.А., Дальская Г.Ю., Демин В.Л., Андреева С.А. Особенности структурообразования композиционного материала C—SiC в процессе инфильтрации углеродной основы жидким кремнием (LSI — Liquid Silicon Infiltration). *Международный научно-исследовательский журнал.* 2023;3(129):1—10. https://doi.org/10.23670/IRJ.2023.129.24
13. Garshin A.P., Kulik V.I., Nilov A.S. Analysis of emergence, characterization and methods of imagining technological defects in ceramic composites with SiC-matrix obtained by liquid-phase silicification. *Novye Ogneupory* (New Refractories). 2019;(8):23—33. (In Russ.). https://doi.org/10.17073/1683-4518-2019-8-23-33
    Гаршин А.П., Кулик В.И., Нилов А.С. Анализ возникновения, характеристика и способы минимизации технологических дефектов в керамических композитах с SiC-матрицей, получаемых методом жидкофазного силицирования. *Новые огнеупоры.* 2019;(8):23—33. https://doi.org/10.17073/1683-4518-2019-8-23-33
14. Shikunov S.L. New approaches to preparation of high-temperature carbide-silicon ceramic materials and products from them; Diss. ... Cand. Sci. (Eng.). Chernogolovka: IFTT RAS, 2019. (In Russ.).
    Шикунов С.Л. Новые подходы к получению высокотемпературных карбидокремниевых керами-

ческих материалов и изделий из них: Дис. ... канд. техн. наук. Черноголовка: ИФТТ РАН, 2020.

15. Panin M.I., Gareev A.R., Karpov A.P., Maksimova D.S., Korchinsky N.A. Analysis of textile structures of reinforcing components of composite materials and selection of areas of their application. *MSTU Vestnik. Ser. Mechanical Engineering*. 2023;(2):15—28. (In Russ.). https://doi.org/10.18698/0236-3941-2023-2-15-28
Панин М.И., Гареев А.Р., Карпов А.П., Максимова Д.С., Корчинский Н.А. Анализ текстильных структур армирующих компонентов композиционных материалов и выбор областей их применения. *Вестник МГТУ. Сер. Машиностроение*. 2023;(2):15—28. https://doi.org/10.18698/0236-3941-2023-2-15-28

16. Kolesnikov S.A., Maksimova D.S. Formation of physical and mechanical characteristics of carbon-carbon materials at isostatic technology of carbon matrix production. *Izvestiya vuzov. Chemistry and chemical technology*. 2018;61(11):50—61. (In Russ.). https://doi.org/10.6060/ivkkt.20186111.14
Колесников С.А., Максимова Д.С. Формирование физико-механических характеристик углерод-углеродных материалов при изостатической технологии получения углеродной матрицы. *Известия вузов. Химия и химическая технология*. 2018;61(11):50—61. https://doi.org/10.6060/ivkkt.20186111.14

17. Tzeng S., Pan J. Densification of two-dimensional carbon/carbon composites by pitch impregnation. *Materials Science and Engineering*. 2001;316(1-2): 127—34.
https://doi.org/10.1016/S0921-5093(01)01255-2

18. Casal E., Granda M., Bermejo J., Bonhomme J., Menéndez R. Influence of porosity on the apparent interlaminar shear strength of pitch-based unidirectional C—C composites. *Carbon*. 2001;39(1):73—82.
https://doi.org/10.1016/S0008-6223(00)00085-3

19. Hue R., Wang Z., Zhang Z., Zhang N., Zhang Y., Xia H., Xiao Z., Wang J. Anisotropic tribological behavior of LSI based 2.5D needle-punched carbon fiber reinforced C/C-SiC composites. *Ceramics International*. 2022;48(15):21283—21292.
https://doi.org/10.1016/j.ceramint.2022.04.071

20. Mikheev P.V., Bukharov S.V., Lebedev A.K., Tashchilov S.V. Modeling of spatial reinforcement schemes of multilayer fiber preforms UUKM. *Russian Journal of Cybernatics*. 2022;3(3):63—73. (In Russ.).
https://doi.org/10.51790/2712-9942-2022-3-3-7
Михеев П.В., Бухаров С.В., Лебедев А.К., Тащилов С.В. Моделирование схем пространственного армирования многослойных волокнистых преформ УУКМ. *Успехи кибернетики*. 2022;3(3):63—73. https://doi.org/10.51790/2712-9942-2022-3-3-7

21. Chao X., Qi L., Tian W., Hou X., Ma W., Li H. Numerical evaluation of the influence of porosity on bending properties of 2D carbon/carbon composites. *Composites Part B: Engineering*. 2017;(136):72—80.
https://doi.org/10.1016/j.compositesb.2017.10.027

22. Chaoa X., Qia L., Tiana W., Lub Y., Lib H. Potential of porous pyrolytic carbon for producing zero thermal expansion coefficient composites: A multi-scale numerical evaluation. *Composite Structure*. 2020;(235): 111819.
https://doi.org/10.1016/j.compstruct.2019.111819

23. Papkova M.V., Magnitsky I.V., Tashchilov S.V., Dvoretsky A.E. Determination of pyrocarbon matrix characteristics in carbon/carbon composite materials. *Izvestiya vuzov. Chemistry and chemical technology*. 2018;61(11): 50—61. (In Russ.).
https://doi.org/10.6060/ivkkt.20216405.6352
Папкова М.В., Магнитский И.В., Тащилов С.В., Дворецкий А.Э. Определение характеристик пироуглеродной матрицы в углерод-углеродных композиционных материалах. *Известия вузов. Химия и химическая технология*. 2021;64(5):44—49.
https://doi.org/10.6060/ivkkt.20216405.6352

24. Magnitskaya M.V., Magnitsky M.V., Tashchilov S.V., Tsvetkov D.A. Influence of high-temperature processing on mechanical characteristics of carbon-carbon composite materials based on pyrocarbon matrix. *PNIPU Mechanics Bulletin*. 2022;(4):5—12. (In Russ.).
https://doi.org/10.15593/perm.mech/2022.4.01
Магнитская М.В., Магнитский М.В., Тащилов С.В., Цветков Д.А. Влияние высокотемпературной обработки на механические характеристики углерод-углеродных композиционных материалов на основе пироуглеродной матрицы. *Вестник ПНИПУ. Механика*. 2022;(4):5—12.
https://doi.org/10.15593/perm.mech/2022.4.01

25. Ilyushchenko A.F., Prokhorov O.A., Krivulenko N.V. Increase of compaction efficiency in technologies of manufacturing of high-density carbon/carbon composite materials. *Doklady of the National Academy of Belarus*. 2022;66(5):544—551. (In Russ.).
https://doi.org/10.29235/1561-8323-2022-66-5-544-551
Ильющенко А.Ф., Прохоров О.А., Кривуленко Н.В. Повышение эффективности уплотнения в технологиях изготовления высокоплотных углерод-углеродных композиционных материалов. *Доклады Национальной академии наук Беларуси*. 2022;66(5): 544—551.
https://doi.org/10.29235/1561-8323-2022-66-5-544-551

26. Dang A., Li H., Zhao T., Xiong C., Zhuang Q., Shang Y., Chen X., Ji X. Preparation and pyrolysis behavior of modified coal tar pitch as C/C composites matrix

precursor. *Journal of Analytical and Applied Pyrolysis*. 2016;(119):18—23.
https://doi.org/10.1016/j.jaap.2016.04.002

27. Ren C.Q., Li T.H., Lin Q.L., Li H., Sun X.Y. Preparation of carbon materials by modeling of impregnating coal-tar pitch into carbon preform. *Journal of Materials Processing Technology*. 2006;172(3):424—430.
https://doi.org/10.1016/j.jmatprotec.2005.11.003

28. Timofeev P.A. Formation of matrices of composite materials from silicon carbides, nitrides and borides by pyrolysis of polymer precursors: Diss. ... Cand. Sci. (Eng.). Moscow: MISIS, 2017. (In Russ.).
Тимофеев П.А. Формирование матриц композиционных материалов из карбидов, нитридов и боридов кремния методом пиролиза полимерных прекурсоров: Дис. ... канд. техн. наук. М.: МИСИС, 2017.

Information about the authors

Kristina V. Petrovskaya – Engineer of the JSC "Composite".
https://orcid.org/0009-0006-9074-3060
E-mail: info@kompozit-mv.ru

Pavel A. Timofeev – Cand. Sci. (Eng.), Head of the Department of JSC "Composite".
https://orcid.org/0000-0001-7448-8086
E-mail: info@kompozit-mv.ru

Информация об авторах

Кристина Владиславовна Петровская – инженер-технолог АО «Композит.
https://orcid.org/0009-0006-9074-3060
E-mail: info@kompozit-mv.ru

Павел Анатольевич Тимофеев – к.т.н., начальник отдела АО «Композит».
https://orcid.org/0000-0001-7448-8086
E-mail: info@kompozit-mv.ru

Contribution of the authors

K.V. Petrovskaya – conducted experiments, prepared initial samples, performed microstructural, porometric, and physical-mechanical analysis, and wrote the article.

P.A. Timofeev – defined the research objective and participated in the discussion of results.

Вклад авторов

К.В. Петровская – проведение экспериментов, подготовка исходных образцов, проведение микроструктурного, порометрического, физико-механического анализов, написание статьи.

П.А. Тимофеев – определение цели работы, участие в обсуждении результатов.

The article was submitted 26.04.2024, revised 30.07.2024, accepted for publication 05.08.2024

Статья поступила в редакцию 26.04.2024, доработана 30.07.2024, подписана в печать 05.08.2024

PHYSICAL METALLURGY AND HEAT TREATMENT / МЕТАЛЛОВЕДЕНИЕ И ТЕРМИЧЕСКАЯ ОБРАБОТКА

UDC 669.35 : 539.89
https://doi.org/10.17073/0021-3438-2024-4-66-76

Research article
Научная статья

Effect of annealing on the structure and properties formation of a copper alloy alloyed with palladium and silver

O.S. Novikova, Yu.A. Salamatov, A.E. Kostina, A.Yu. Volkov

M.N. Mikheev Institute of Metal Physics of Ural Branch of the Russian Academy of Sciences
18 Kovalevskaya Str., Ekaterinburg 620108, Russia

✉ Oksana S. Novikova (novikova@imp.uran.ru)

Abstract: A copper alloy with small additions of palladium and silver (Cu–1.5Pd–3Ag (at. %))—which has potential applications as a corrosion-resistant conductor of weak electrical signals—was studied using *X*-ray diffraction analysis, microhardness measurements, specific electrical resistivity, and tensile mechanical properties tests. Samples were examined in several initial states: quenched (from 700 °C) and deformed at room and cryogenic temperatures (with a 90 % reduction in cross-sectional area in both cases). To study the processes of structural reorganization and property evolution, the initial samples were annealed in the temperature range from 150 to 450 °C (in 50 °C increments), followed by cooling in water or air. The duration of the heat treatments ranged from 1 to 48 hours. It was established that annealing the Cu–1.5Pd–3Ag alloy at temperatures below 450 °C leads to the precipitation of silver-based phase particles in the Cu matrix. Annealing of the initially quenched alloy was found to slightly increase its specific electrical resistivity (ρ) from $3.55\cdot10^{-8}$ to $3.8\cdot10^{-8}$ Ohm·m (after 48 h at 250 °C). It was revealed that alloying copper with 1.5 at. % palladium and 3 at. % silver enhances the strength properties (the yield strength of the alloy reaches 500 MPa) and raises the recrystallization temperature, while the electrical conductivity of the alloy remains around 50 % IACS. The optimal combination of properties (strength, ductility, and electrical conductivity) is observed after annealing the pre-cryodeformed alloy at 250 °C for less than 18 h. Extending the annealing time causes overaging, resulting in softening. The results of this study can be applied in the development of a new high-strength material with reduced electrical resistivity.

Keywords: Cu–Pd–Ag alloys, resistometry, microhardness, microstructure, *X*-ray diffraction analysis, cryodeformation.

Acknowledgments: *X*-ray diffraction analysis and scanning electron microscopy were carried out using the equipment of the Center for Collective Use at the Institute of Metal Physics, Ural Branch of the Russian Academy of Sciences.

This work was performed as part of the state assignment from the Ministry of Education and Science of Russia (project “Pressure”, No. 122021000032-5).

For citation: Novikova O.S., Salamatov Yu.A., Kostina A.E., Volkov A.Yu. Effect of annealing on the structure and properties formation of a copper alloy alloyed with palladium and silver. *Izvestiya. Non-Ferrous Metallurgy.* 2024;30(4):66–76.
https://doi.org/10.17073/0021-3438-2024-4-66-76

Влияние отжигов на формирование структуры и свойств сплава меди, легированного палладием и серебром

О.С. Новикова, Ю.А. Саламатов, А.Е. Костина, А.Ю. Волков

Институт физики металлов им. М.Н. Михеева УрО РАН
Россия, 620108, г. Екатеринбург, ул. С. Ковалевской, 18

✉ Оксана Сергеевна Новикова (novikova@imp.uran.ru)

Аннотация: Методами рентгеноструктурного анализа, измерения микротвердости, удельного электросопротивления и механических свойств при растяжении изучали сплав меди с малыми добавками палладия и серебра: Cu–1,5Pd–3Ag (ат. %), который может найти применение в качестве коррозионно-стойкого проводника слабых электрических сигналов. Исследованы образцы, находящиеся в нескольких исходных состояниях: закаленном (от 700 °С), деформированном при комнатной и криогенной температурах (в обоих случаях – на 90 % изменения площади поперечного сечения). Для изучения процессов перестройки структуры и эволюции свойств проводили отжиги исходных образцов в интервале температур от 150 до 450 °С (с шагом в 50 °С) с последующим охлаждением в воде или на воздухе. Продолжительность термообработок (ТО) составляла от 1 до 48 ч. Установлено, что отжиг сплава Cu–1,5Pd–3Ag в температурном интервале ниже 450 °С приводит к выделению в Cu-матрице частиц фазы на основе серебра. Показано, что отжиг исходно закаленного сплава несколько увеличивает значение его удельного электросопротивления (ρ): от $3{,}55\cdot10^{-8}$ до $3{,}8\cdot10^{-8}$ Ом·м (после $t = 250$ °С, 48 ч). Выявлено, что легирование меди палладием (1,5 ат. %) и серебром (3 ат. %) обусловливает повышение прочностных свойств (предел текучести сплава составляет 500 МПа) и температуры рекристаллизации, при этом электропроводность сплава составляет ~50 % IACS. Оптимальный набор свойств (прочности, пластичности и электропроводности) наблюдается после отжигов предварительно криодеформированного сплава при $t = 250$ °С продолжительностью менее 18 ч. Увеличение времени ТО вызывает перестаривание, следствием которого является разупрочнение. Результаты исследования могут быть использованы при разработке нового высокопрочного материала с пониженным электрическим сопротивлением.

Ключевые слова: сплавы Cu–Pd–Ag, резистометрия, микротвердость, микроструктура, рентгеноструктурный анализ, криодеформация.

Благодарности: Рентгеноструктурный анализ, а также сканирующая электронная микроскопия проведены с использованием оборудования ЦКП ИФМ УрО РАН.

Работа выполнена в рамках государственного задания Минобрнауки России (тема «Давление», № 122021000032-5).

Для цитирования: Новикова О.С., Саламатов Ю.А., Костина А.Е., Волков А.Ю. Влияние отжигов на формирование структуры и свойств сплава меди, легированного палладием и серебром. *Известия вузов. Цветная металлургия*. 2024;30(4):66–76.
https://doi.org/10.17073/0021-3438-2024-4-66-76

Introduction

Copper-based alloys are known for their low electrical resistivity, which has made them widely used in electrical engineering applications [1]. One approach to enhancing the mechanical properties of copper alloys without significantly reducing their electrical conductivity, while maintaining sufficient ductility, is alloying. For example, adding elements such as beryllium or niobium to copper can substantially improve its strength properties [2—4]. However, the toxicity and cost of beryllium, as well as the mutual immiscibility of copper and niobium in the solid state [5], limit the use of such alloys in industrial applications. The table below summarizes the physical and mechanical properties of various copper alloys used as electrical conductors [6].

Previous studies have shown [7] that alloying copper with palladium (less than 10 at. %) results in solid-solution strengthening, while simultaneously increasing corrosion resistance. However, as the demand for high-strength electrical conductors continues to rise, strengthening by alloying with a single component may prove insufficient [8]. Therefore, to achieve superior functional properties, modern approaches utilize alloys with two or more alloying elements, as well as severe plastic deformation, including at cryogenic temperatures. This approach allows the combination of different strengthening mechanisms [9]. For example, the authors of [10] combined solid-solution and dispersion strengthening mechanisms to reinforce an Ag—Pd—Cu—Au alloy, while in [11], a method was proposed for strengthening the Cu—Pd—Ag alloy through the simultaneous occurrence of several phase transformations.

It has been found [12] hat small additions of silver (3 at. %) have a negligible effect on the electrical con-

Physical and mechanical properties of low-alloyed copper alloys for electrical conductors [6]

Физические и механические свойства низколегированных медных сплавов
для проводников электрического тока [6]

Alloy	ρ, 10^{-8} Ohm·m	σ_u, MPa	
		Deformation	Deformation + annealing
Cu + 0.4Zr	2.0	–	270
Cu + 0.3Mg	2.2	530	300
Cu + 0.4Cr + 0.2Sn + 0.8Ti	2.6	–	650
Cu + 0.1Ag	1.7	340	200

ductivity of Cu—Pd alloys while significantly enhancing their strength and recrystallization temperature. For instance, the yield strength and ultimate tensile strength of the ternary Cu—3Pd—3Ag (at. %) alloy are higher, while its electrical conductivity is comparable to that of the Cu—3Pd alloy. It is of particular interest to investigate the properties of a ternary Cu—Pd—Ag alloy with a lower palladium content and to determine the effect of cryodeformation on its strength and electrical conductivity.

The aim of the present work was to study the structure and properties of the Cu—1.5Pd—3Ag (at. %) alloy in various initial states, as well as after annealing in the temperature range of 150—450 °C.

Materials and methods

The Cu—1.5Pd—3Ag (at. %) alloy was melted from copper, palladium, and silver with purities of 99.98 %, 99.99 %, and 99.99 %, respectively. The melting was performed under a vacuum of at least 10^{-2} Pa, with the alloy cast into a graphite crucible.

A 5 mm diameter ingot was homogenized at 800 °C for 3 h, then quenched by water cooling and cut into two parts. From one part of the ingot, a wire with a diameter of 1.5 mm was produced through drawing, and samples for tensile testing were cut from this wire. Further drawing to a diameter of 0.22 mm produced thin wire for resistometry. The other part of the ingot was rolled into plates with a thickness of 0.3 mm, which were used to characterize the phase composition at various stages of processing and to measure microhardness.

Cryodeformation of the samples was carried out between two stainless steel plates. This assembly was immersed in liquid nitrogen for about one minute, after which the rolling step was performed. The process was then repeated. The massiveness of this sandwich-like structure ensured the stability of the cooled sample's temperature. Some of the wires and plates deformed at room temperature were annealed at 700 °C (for 1 h) and then quenched in water. Thus, the study investigated samples in several initial states: quenched (from 700 °C), deformed at room and cryogenic temperatures (in both cases, with a 90 % reduction in cross-sectional area).

Both the wire and plate samples had the same degree of preliminary deformation. As we previously demonstrated for various ordered systems, setting aside some differences in microstructure and texture between the samples, the mechanism of deformation-induced structural reorganization, in general, does not depend on whether the preliminary deformation is performed by rolling or drawing [13]. Therefore, the results obtained provide a comprehensive picture of the effect of deformation on the structure and properties of the Cu—1.5Pd—3Ag alloy.

To study the processes of structural reorganization and property evolution, the initial samples were annealed in the temperature range from 150 to 450 °C (in 50 °C increments), followed by cooling in water or air. The duration of the heat treatments ranged from 1 to 48 h. All heat treatments were performed in vacuum-sealed glass or quartz ampoules. In further descriptions of the heat treatment process, including its characteristics (temperature, holding time, etc.), the term "annealing" is used. When emphasizing changes in properties due to the formation of a new phase, the term "aging" is applied.

The specific electrical resistivity (ρ) was measured using the standard four-point probe method (with a constant current of $I = 20$ mA). Measurements of the specific electrical resistivity at room temperature were conducted on wire samples with a diameter of 0.22 mm and a length of 250 mm, fixed in a special conductor as previously described [13]. The absolute measurement error of ρ was $\pm 0.04 \cdot 10^{-8}$ Ohm·m.

Mechanical tests were carried out using a ZD 10/90 tensile testing machine at a strain rate of 3 mm/min. The working length of the samples was 30 mm. At least five samples were tested for each structural state. The absolute measurement error for the yield strength was ±10 MPa, and for elongation to failure, it was ±0.5 %.

X-ray diffraction analysis (XRD) was conducted on alloy plates with a thickness of 0.3 mm. The *X*-ray diffraction measurements were performed using a PANalytical Empyrean Series 2 laboratory diffractometer (Netherlands) equipped with a three-axis Eulerian cradle. Measurements were made in parallel beam geometry using CoK_α radiation with a wavelength of 0.179 nm. The microstructure was studied using a Tescan MIRA LMS scanning electron microscope (SEM) (Czech Republic) with an accelerating voltage of up to 30 kV, magnifications ranging from $20^\times$ to $160\,000^\times$, and a resolution of 1.2 nm. Structural images were obtained in both backscattered and secondary electron modes. The chemical composition of the samples (Cu—2.4Pd—5.2Ag (wt. %) / Cu—1.5Pd—3Ag (at. %)) was monitored using an EDAX energy-dispersive *X*-ray spectrometer (USA) with a resolution of 160 eV.

Vickers microhardness was measured using a PMT-3 device (JSC LOMO, St. Petersburg, Russia) under a load of 50 g with a holding time of 30 s. At least 10 measurements were taken for each structural state.

Results and discussion

Fig. 1 shows the changes in mechanical properties after holding quenched and room-temperature-deformed samples of the Cu—1.5Pd—3Ag alloy for 1 h in the temperature range of 150 to 450 °C.

The quenched sample has a very low yield strength ($\sigma_{0.2}$ = 70 MPa), which remains almost unchanged after aging in the temperature range below 300 °C (Fig. 1, *a*). After heat treatment of the quenched alloy at 400 °C, the yield strength increases significantly to ~170 MPa, while aging at temperatures above 400 °C causes a slight decrease. The increase in strength during aging of quenched Cu—Ag alloys has been observed multiple times before and is attributed to the decomposition of the supersaturated solid solution, accompanied by the precipitation of fine silver particles along grain boundaries and within the grains [14; 15]. The elongation to fracture of the initially quenched Cu—1.5Pd—3Ag alloy is almost independent of the heat treatment temperature and remains at ~40 %.

After 90 % deformation at room temperature, the yield strength of the alloy increases to $\sigma_{0.2}$ = 520 MPa (Fig. 1, *b*), which is about seven times higher than that of the initially quenched sample. Annealing the initially deformed alloy at temperatures below 250 °C does not significantly change its strength properties. Above 250 °C, there is a sharp decline in yield strength due to recrystallization. Since the onset of recrystallization depends on temperature and time conditions [16], comparing this characteristic in different alloys should be done under similar heat treatment conditions. In previous experiments with deformed pure copper samples, it was established that the decrease in strength due to recrystallization begins after annealing for 1 hour at 150 °C [8]. Thus, the recrystallization temperature of the investigated alloy is approximately 100 °C higher than that of pure copper.

After annealing the previously deformed alloy at 425—450 °C, its elongation to failure increases from the initial 2 % to 46—48 %. Notably, after annealing within this temperature range, the mechanical properties of the samples are very similar and practically independent of their initial state. This result suggests that annealing at 425—450 °C creates similar structural states in both quenched and deformed samples. Based on the obtained data, it can be concluded that heat treatment of the initially deformed Cu—1.5Pd—3Ag alloy for 1 h in the temperature range of 200—250 °C provides sufficiently high strength ($\sigma_{0.2} \approx$ 520 MPa) and ductility (δ = 8÷14 %). It is worth noting that the Cu—1.5Pd—3Ag alloy deformed by 90 % does not show the anomalous increase in strength after annealing in the 150—250 °C range that was observed in the mechanical tensile tests of the Cu—3Pd—3Ag alloy. In that case, we detected a 40 MPa increase in $\sigma_{0.2}$ after annealing the initially deformed alloy, and in cryodeformed alloy, the yield strength anomalously increased by ~100 MPa, reaching $\sigma_{0.2} \approx$ 720 MPa) [12].

We also noted that during the aging process, Cu—Ag alloys are typically cooled in air [17; 18]. To ensure a correct comparison with the literature data, subsequent experiments in our study were conducted using this cooling method. Fig. 2 shows the resistometry re-

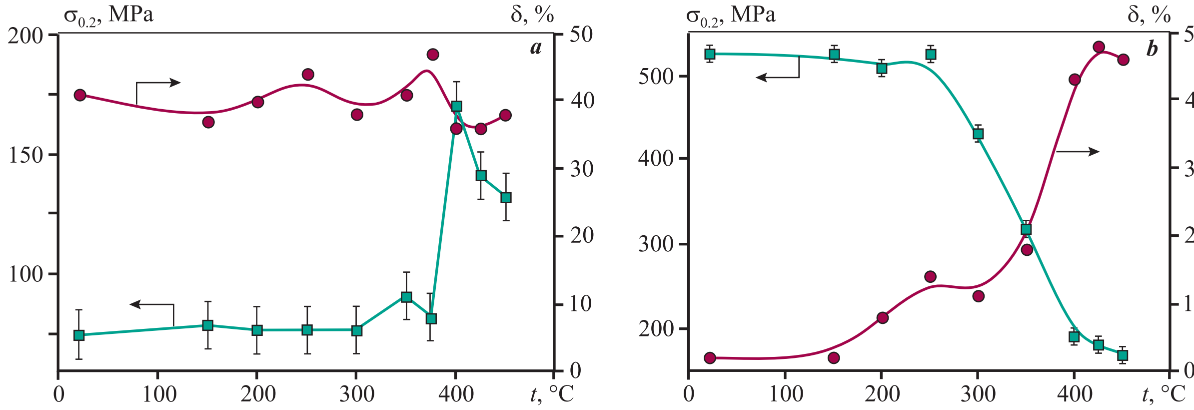

Fig. 1. Dependences of the yield strength ($\sigma_{0.2}$) and elongation to failure (δ) on annealing temperature of Cu–1.5Pd–3Ag alloy samples in the initially quenched (***a***) or pre-deformed (***b***) states

Holding time at each temperature – 1 h, cooling in water

Рис. 1. Зависимости предела текучести ($\sigma_{0,2}$) и удлинения до разрушения (δ) от температуры обработки образцов сплава Cu–1,5Pd–3Ag, находящихся в исходно закаленном (***a***) или предварительно деформированном (***b***) состояниях

Время выдержки при каждой температуре – 1 ч, охлаждение в воде sults for quenched and deformed wire samples of the Cu—1.5Pd—3Ag alloy after annealing in the temperature range of 150 to 450 °C. The holding time at each temperature ranged from 1 to 48 h.

Aging for 1 hour does not lead to significant changes in the specific electrical resistivity of the quenched alloy (Fig. 2, *a*); throughout the entire investigated temperature range, ρ remains at ~$3{,}55 \cdot 10^{-8}$ Ohm·m with a slight decrease at 450 °C. Extending the heat treatment duration (up to 48 h) results in an increase in the resistivity of the initially quenched samples, with a maximum observed in the 200—250 °C temperature range. The increase in resistivity during aging aligns well with the processes of decomposition in the alloy, as discussed above. As is known [19—21], fine second-phase particles act as scattering centers for charge carriers, leading to an increase in specific electrical resistivity. A precise solution to this problem is considered in quantum mechanics, specifically in the theory of single-channel particle scattering (see, for example, [22]). To simplify, the smaller the effective size of the interaction potential, the less it distorts the trajectory of passing charge carriers. Fewer charge carriers are affected, and distortion of their paths due to scattering processes is macroscopically observed as electrical resistivity (or its inverse, electrical conductivity). Individual atoms of alloying elements distort the trajectories of charge carriers far less than large dispersed particles, and therefore, they have a smaller impact on electrical conductivity. The increase in the size of precipitates at elevated processing temperatures leads to the disappearance of this effect's contribution to the material's overall resistivity. Indeed, after aging at 450 °C, the specific resistivity of the alloy samples does not exceed $\rho \sim 3.5 \cdot 10^{-8}$ Ohm·m.

In practice, electrical conductivity, measured according to the IACS (International Annealed Copper Standard), is increasingly used instead of the specific electrical resistivity of a conductor. According to this standard, the conductivity of any material is expressed as a percentage of the conductivity of pure copper. According to our data, the electrical conductivity of the Cu—1.5Pd—3Ag alloy is 49 % IACS. It is worth noting that the cathode copper used in this study has a lower conductivity than the standard, at 97 % IACS.

The high defect density in the structure of the initially deformed alloy slightly increases its resistivity compared to the quenched state: $\rho \sim 3.7 \cdot 10^{-8}$ Ohm·m. During annealing at temperatures up to 250 °C, regardless of the duration, there is a gradual decrease in the resistivity of the pre-deformed alloy (Fig. 2, *b*). Annealing above 250 °C causes a sharp drop in ρ, which is attributed to recovery/recrystallization processes. Extending the annealing duration increases the rate of resistivity reduction. After holding at 450 °C for 48 h, the resistivity of the alloy reaches $\rho \sim 3.25 \cdot 10^{-8}$ Ohm·m (53 % IACS). Thus, annealing the deformed alloy results in a reduction in its resistivity by approximately 12 %. As is known [16], a reduction in defect density during recrystallization leads to a 3—4 % decrease in

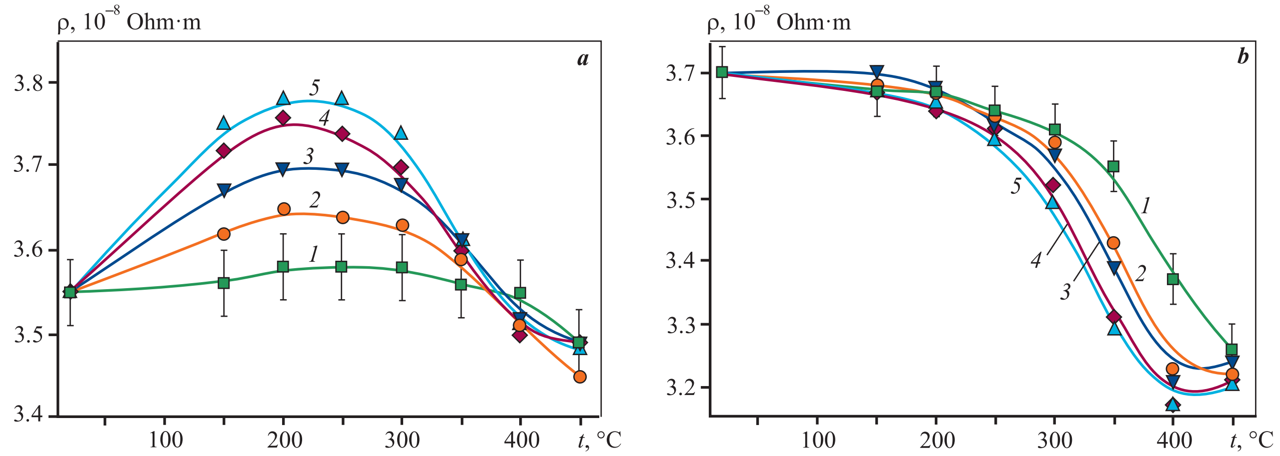

Fig. 2. Dependences of the electrical resistivity of Cu—1.5Pd—3Ag alloy samples quenched form 700 °C (***a***) and deformed by 90 % (***b***) on temperature (*t*) and heat treatment duration (τ)
τ, h: ***1*** – 1, ***2*** – 6, ***3*** – 12, ***4*** – 24, ***5*** – 48

Рис. 2. Зависимости удельного электросопротивления закаленных от 700 °С (***a***) и деформированных на 90 % (***b***) образцов сплава Cu–1,5Pd–3Ag от температуры (*t*) и продолжительности термообработки (τ)
τ, ч: ***1*** – 1, ***2*** – 6, ***3*** – 12, ***4*** – 24, ***5*** – 48

resistivity. Since in our case, annealing the deformed alloy reduces its resistivity by approximately 12 %, it is likely that structural changes related to the redistribution of silver in the material also contribute to the specific resistivity values. The obtained ρ values, alongside sufficient strength and ductility, may be of interest for using the alloy as an electrical signal conductor. It is well known that preliminary cryodeformation is an effective method for strengthening copper and copper alloys [18; 23; 24].

The change in microhardness after annealing in the temperature range of 150 to 450 °C for deformed Cu—1.5Pd—3Ag alloy samples is shown in Fig. 3. The microhardness of the samples after room and cryogenic deformation is 2000 and 2200 MPa, respectively (Fig. 3, *a*, *b*). The higher microhardness of the pre-cryodeformed alloy is observed across the entire annealing temperature range. It is worth noting that the microhardness of the cryodeformed sample increases particularly noticeably after annealing at 250 °C: a distinct "step" appears in the microhardness vs. temperature plot (Fig. 3, *b*).

Regardless of the temperature-time treatment conditions, all diffractograms of the Cu—1.5Pd—3Ag alloy (Fig. 4) show intense peaks from the matrix, which represents a face-centered cubic (FCC) solid solution of palladium in copper, along with much weaker reflections from an FCC phase enriched with silver. Notably, the (111) peak of this phase is already present in the alloy quenched from 700 °C (diffractogram *1* in Fig. 4, *a*). After cryodeformation, the peaks become less intense and broader (diffractogram *3* in Fig. 4, *a*), due to increased internal stresses and grain refinement [25].

As shown in the XRD data of the studied alloy (Fig. 4, *a*), the addition of palladium and silver increases the lattice parameter of both the quenched and deformed alloy across various temperatures to $a =$ $= 0.3644$ nm (compared to the lattice parameter of pure copper at $a = 0.3619$ nm). Heat treatments of the alloy samples (in all initial states) at 250 °C and 400 °C result in a reduction of the lattice parameter of the matrix (to 0.3639 nm and 0.3625 nm, respectively), causing the peaks to shift to the right (Fig. 4, *b*, *c*).

When heated to 700 °C, the formation of a silver-enriched phase begins, which is retained after subsequent quenching (diffractogram 1 in Fig. 4, *a*). Considering that the solubility of silver in copper is very low, it can be assumed that this phase consists of regions of pure or nearly pure silver. The most favorable regions for the precipitation of this phase are grain boundaries, dislocations, and other defects, as these areas have a lower concentration of solvent atoms. However, *X*-ray diffraction analysis, being an integral method, does not allow for precise determination of where the precipitates form. Deformation leads to the fragmentation and breakdown of the precipitated clusters, resulting in a more uniform distribution of silver in the matrix. During heat treatment at 250 °C, noticeable diffusion does not occur: the volume of the silver-enriched phase remains approximately the same as before the heat treatment (Fig. 4, *b*). The lattice parameter of the silver-based phase in the initially

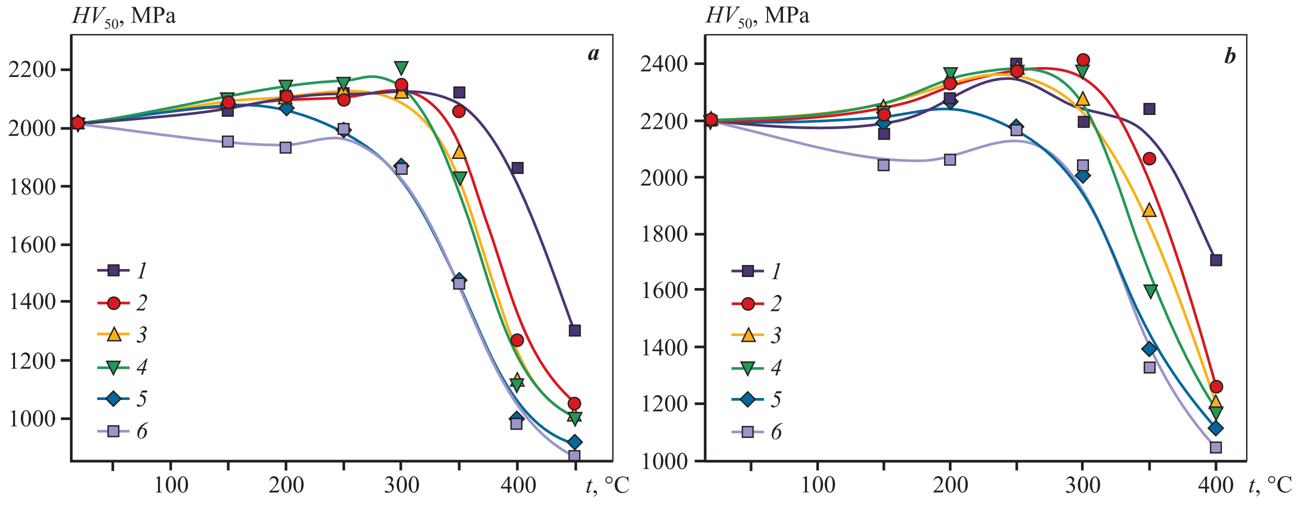

Fig. 3. Dependence of microhardness of Cu–1.5Pd–3Ag alloy samples on annealing temperature

a – 90 % deformation at room temperature, ***b*** – 90 % deformation at cryogenic temperature
τ, h: ***1*** – 1, ***2*** – 6, ***3*** – 12, ***4*** – 18, ***5*** – 24, ***6*** – 48

Рис. 3. Зависимости микротвердости образцов сплава Cu–1,5Pd–3Ag от температуры отжига

а – деформация на 90 % при комнатной температуре, ***b*** – деформация на 90 % при криогенной температуре
τ, ч: ***1*** – 1, ***2*** – 6, ***3*** – 12, ***4*** – 18, ***5*** – 24, ***6*** – 48

quenched alloy is 0.4027 nm, and after heat treatment at 250 °C, it remains nearly unchanged at 0.4023 nm.

After annealing at 400 °C, silver again forms clusters in the material initially deformed at various temperatures (diffractograms *2* and *3* in Fig. 4, *c*). Here, the splitting of weak peaks of the silver-enriched phase is observed. This may indicate that during annealing, silver segregation occurs, forming regions with different levels of palladium enrichment. Some regions may consist of clusters of nearly pure silver. Indeed, the lattice parameter of the silver-based phase (for the peaks on the left) after annealing at 400 °C (0.4080 nm) becomes close to that of pure silver (0.4077 nm).

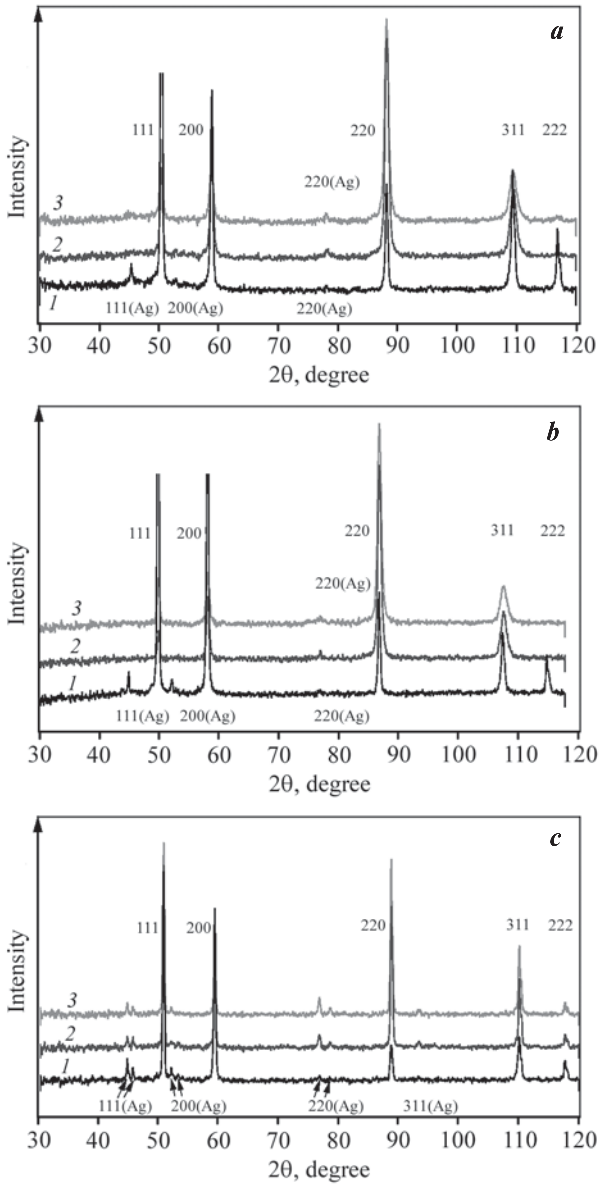

Fig. 4. *X*-ray diffraction patterns of Cu–1.5Pd–3Ag alloy samples

a – initial state: ***1*** – quenching from 700 °C, ***2*** – 90 % deformation at room temperature, ***3*** – 90 % deformation at cryogenic temperature;
b – initial state + 250 °C, 48 h, air cooling;
c – initial state + 400 °C, 48 h, air cooling

Рис. 4. Дифрактограммы образцов сплава Cu–1,5Pd–3Ag

a – исходное состояние: ***1*** – закалка от 700 °C, ***2*** – деформация на 90 % при комнатной температуре, ***3*** – деформация на 90 % при криогенной температуре;
b – исходное состояние + 250 °C, 48 ч, охлаждение на воздухе;
c – исходное состояние + 400 °C, 48 ч, охлаждение на воздухе

The lattice parameter of the second silver-based phase (for the peaks on the right) after annealing at 400 °C is 0.4007 nm. These regions may correspond to silver clusters that additionally contain dissolved palladium. For example, in study [26], field ion microscopy, which allows direct observation of atoms on the surface of solids, showed that during the early stages of decomposition in the Cu—50Pd—20Ag (at. %) alloy, the precipitate phase represents a solid solution of palladium in silver. However, this phase may also consist of small silver clusters within the original matrix that have not yet coalesced into larger formations. A definitive conclusion regarding the nature of this phase cannot be drawn based solely on *X*-ray diffraction analysis.

The diffractograms of the samples deformed at various temperatures, as well as after annealing at 250 °C, show a pronounced texture: the intensity of the (220) peak is an order of magnitude higher than the others (diffractograms *2* and *3* in Fig. 4, *a*, *b*). As is known, during cold rolling of face-centered cubic (FCC) alloys, the main rolling texture develops with the {110} plane parallel to the rolling plane and the <112> direction parallel to the rolling direction [27]. Additionally, even after prolonged annealing of the initially deformed samples at 250 °C, the width of the *X*-ray peaks does not decrease. This indicates that the recrystallization process is still far from complete at this stage of heat treatment. A similar conclusion was previously drawn from resistometry data and microhardness measurements.

Since the optimal set of functional characteristics (strength, ductility, and electrical conductivity) is observed after annealing at 250 °C, SEM analysis was performed on a sample annealed at this temperature.

Fig. 5 shows an SEM image of the microstructure of the Cu—1.5Pd—3Ag alloy after cryodeformation and annealing at 250 °C for 48 h. One of the detected precipitates is highlighted with an oval in Fig. 5, *a*. The particle of the new phase has an elongated “lens-like” shape, with a thickness of ~10 μm and a length of ~45 μm. The formation of such a large particle is caused by so-called overaging, where prolonged heat

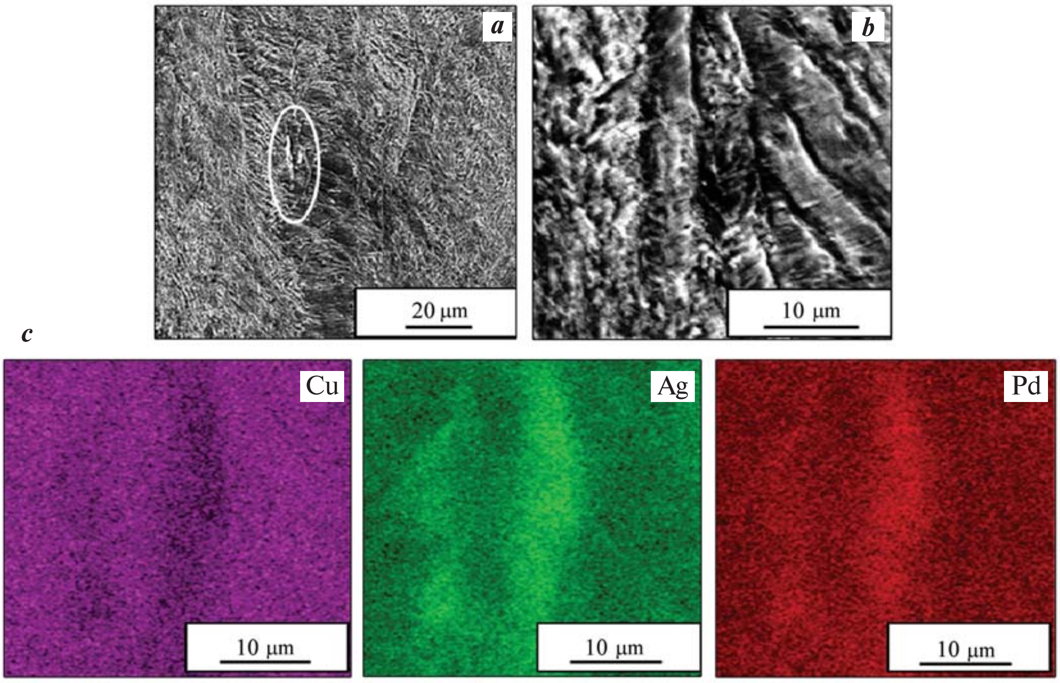

Fig. 5. Microstructure of the Cu–1.5Pd–3Ag alloy after annealing ($t = 250$ °C, $\tau = 48$ h) and air cooling after cryodeformation by 90 %

a – an elongated silver precipitation is shown by an oval; ***b*** – area from which distribution maps of chemical elements were obtained (***c***)

Рис. 5. Микроструктура сплава Cu–1,5Pd–3Ag после отжига ($t = 250$ °C, $\tau = 48$ ч) и охлаждения на воздухе после криодеформации на 90 %

a – участок, на котором овалом показано вытянутое выделение серебра
b – участок, с которого были получены карты распределения по химическим элементам (***c***)

treatment leads to the coalescence of small precipitates. It is well known that at this stage, the strength properties of aging alloys significantly decrease [28]. Indeed, as seen in the results in Fig. 3, *b*, the maximum microhardness values are observed after annealing at 250 °C for no more than 18 h.

The relatively large size of the precipitate allows for the determination of its elemental composition (Fig. 5, *b*, *c*). Energy-dispersive analysis performed using SEM revealed the following chemical composition of the particle (wt. %): 54.8 Cu, 1.2 Pd, and 44.0 Ag. The high copper content in the precipitated particle raises doubts and is more likely due to electrons reflected from the Cu matrix reaching the detector. Indeed, in a previous study [26] using field ion microscopy, it was established that in the Cu—50Pd—20Ag (at. %) alloy, Pd—Ag particles precipitate during the atomic ordering of the Cu—Pd matrix. Additionally, mathematical analysis of the *X*-ray peak shapes performed in [12] suggested that after cryodeformation and annealing at 250 °C in the Cu—3Pd—3Ag (at. %) alloy, two regions form: one enriched in silver and the other depleted.

Conclusions

1. Alloying copper with palladium (1.5 at. %) and silver (3 at. %) enhances the strength properties through the combination of two mechanisms: solid-solution strengthening and decomposition. Preliminary cryodeformation provides an additional strengthening effect of about 10 %.

2. Annealing the Cu—1.5Pd—3Ag alloy at temperatures below 450 °C leads to the precipitation of silver-based phase particles in the Cu matrix. The optimal combination of properties (high strength, adequate ductility, and electrical conductivity) is observed after annealing the preliminarily cryodeformed alloy at 250 °C for less than 18 hours. Prolonging the annealing time results in overaging.

3. In its optimal structural state, the Cu—1.5Pd—3Ag alloy exhibits a yield strength of ~500 MPa, a higher recrystallization temperature compared to copper (by ~100 °C), and electrical conductivity of 50 % IACS. The set of properties found in this alloy may be of interest for practical applications.

References

1. Osintsev O.E., Fedorov V.N. Copper and copper alloys. Domestic and foreign brands: Reference book. 2-nd ed., rev. and add. Moscow: Innovatsionnoe mashinostroenie, 2016. 360 p. (In Russ.).

   Осинцев О.Е., Федоров В.Н. Медь и медные сплавы. Отечественные и зарубежные марки: Справочник. 2-е изд., перераб. и доп. М.: Инновационное машиностроение, 2016. 360 с.

2. Valova-Zakharevskaya E.G., Deryagina I.L., Popova E.N., Khlebova N.E., Pantsyrnyi V.I. Special characteristics of the microstructure of high-strength multifiblamentary Cu—18Nb composites. *Diagnostics, Resource and Mechanics of materials and structures*. 2018;5:116—126. (In Russ.).
   https://doi.org/10.17804/2410-9908.2018.5.116-126

   Валова-Захаревская Е.Г., Дерягина И.Л., Попова Е.Н., Хлебова Н.Е., Панцырный В.И. Особенности микроструктуры высокопрочного многоволоконного композита Cu—18Nb. *Diagnostics, Resource and Mechanics of Materials and Structures*. 2018;5:116—126.
   https://doi.org/10.17804/2410-9908.2018.5.116-126

3. Chzhigan Ch., Tszyunvey L., Shitsyan L., Yanni S., Yuan M. Mechanisms of high-temperature deformation of the Cu–Be alloy in the high-elastic annealed state. *Fizika Metallov i Metallovedenie*. 2018;119(1):73—80. (In Russ.).
   https://doi.org/10.7868/S0015323018010096

   Чжиган Ч., Цзюньвэй Л., Шицянь Л., Янни С., Юань М. Механизмы высокотемпературной деформации сплава Cu—Be в высокоупругом отожженном состоянии. *Физика металлов и металловедение*. 2018;119(1):73—80.
   https://doi.org/10.7868/S0015323018010096

4. Loginov P.A., Vorotilo S., Sidorenko D.A., Lopatina Yu.V., Okubaev A., Shvyndina N.V., Levashov E.A. The effect of Ti and TiH_2 additives on structure and mechanical properties of copper alloys for diamond cutting tools. *Izvestiya. Non-Ferrous Metallurgy*. 2020;(3):51—58. (In Russ.). https://doi.org/10.17073/0021-3438-2020-3-51-58

   Логинов П.А., Воротыло С., Сидоренко Д.А., Лопатина Ю.В., Окубаев А.., Швындина Н.В., Левашов Е.А. Влияние добавок Ti и TiH_2 на структуру и свойства медных сплавов для алмазного режущего инструмента. *Известия вузов. Цветная металлургия*. 2020;(3):51—58.
   https://doi.org/10.17073/0021-3438-2020-3-51-58

5. Rajarshi Banerjee, Sangita Bose, Arda Genc, Pushan Ayyub. The microstructure and electrical transport properties of immiscible copper-niobium alloy thin films. *Journal of Applied Physics*. 2008;103(3):033511.
   https://doi.org/10.1063/1.2836970

6. Loginov Yu.N. Copper and deformable copper alloys: textbook. Ekaterinburg: UGTU–UPI, 2004. 136 p. (In Russ.).

   Логинов Ю.Н. Медь и деформируемые медные сплавы: Учеб. пос. Екатеринбург: УГТУ—УПИ, 2004. 136 с.

7. Volkov A.Yu., Novikova O.S., Kostina A.E., Antonov B.D. Effect of alloying with palladium on the electrical and mechanical properties of copper. *Physics of Metals and Metallography*. 2016;117(9):945—954.
   https://doi.org/10.1134/S0031918X16070176

   Волков А.Ю., Новикова О.С., Костина А.Е., Антонов Б.Д. Изменение электрических и механических свойств меди при легировании палладием. *Физика металлов и металловедение*. 2016;117(9):977—986.
   https://doi.org/10.7868/S0015323016070172

8. Maki K., Ito Yu., Matsunaga H., Mori H. Solid-solution copper alloys with high strength and high electrical conductivity. *Scripta Materialia*. 2013;68:778—780.
   https://doi.org/10.1016/j.scriptamat.2012.12.0217

9. Gorsee S., Ouvrard B., Goune M., Poulon-Quintin A. Microstructural design of new conductivity — high strength Cu-based alloy. *Journal of Alloys and Compounds*. 2015;633:42—47.
   https://doi.org/10.1016/j.jallcom.2015.01.234

10. Ohta M., Shiraishi T., Hisatsune K., Yamane M. Age-hardening of dental Ag—Pd—Cu—Au alloys. *Journal of Dental Research*. 1980;59(11):1966—71.
    https://doi.org/10.1177/00220345800590110701

11. Iwamoto C., Adachi N., Watanabe F., Koitabash R. Microstructure evolution in Cu—Pd—Ag alloy wires during heat treatment. *Metallurgical and Materials Transactions A*. 2018;49:4947—4955.
    https://doi.org/10.1007/s11661-018-4800-3

12. Novikova O.S., Kostina A.E., Salamatov Yu.A., Zgibnev D.A., Volkov A.Yu. The influence of deformation at cryogenic or room temperature followed by annealing on the structure and properties of copper and its Cu—3Pd and Cu—3Pd—3Ag (at. %) alloys. *Frontier Materials & Technologies*. 2023;(2):77—87. (In Russ.).
    https://doi.org/10.18323/2782-4039-2023-2-64-6

    Новикова О.С., Костина А.Е., Саламатов Ю.А., Згибнев Д.А., Волков А.Ю. Влияние деформации при криогенной или комнатной температуре с последующим отжигом на структуру и свойства меди и ее сплавов Cu—3Pd и Cu—3Pd—3Ag (at. %). *Frontier Materials & Technologies*. 2023;2:77—87.
    https://doi.org/10.18323/2782-4039-2023-2-64-6

13. Volkov A.Yu., Novikova O.S., Antonov B.D. The kinetics of ordering in an equiatomic CuPd alloy: A resistometric study. *Journal of Alloys and Compounds*. 2013;581:625—631.
    http://dx.doi.org/10.1016/j.jallcom.2013.07.132

14. Gong X., Wei B., Teng J., Wang Z., Li Yu.Regulating the oxidation resistance of Cu—5Ag alloy by heat treatment. *Corrosion Science*. 2021;190: 109686.
https://doi.org/10.1016/j.corsci.2021.109686
15. Straumal B.B., Kilmametov A.R., Baretzkyet B., Kogtenkova O.A., Straumal P.B., Litynska-Dobrzynska L., Chulist R., Korneva A., Zieva P. High pressure torsion of Cu—Ag and Cu—Sn alloys: Limits for solubility and dissolution. *Acta Materialia*. 2020;195:184—198.
https://doi.org/10.1016/j.actamat.2020.05.055
16. Freudenberger J., Kauffmann A., Klaub H., Marr T., Nenkov K., Subramanya S.V., Schultz L. Studies on recrystallization of single-phase copper alloys by resistance measurements. *Acta Materialia*. 2010;58:2324—2329.
https://doi.org/10.1016/j.actamat.2009.12.018
17. Shakhova I., Sakai Y., Belyakov A., Kaibyshev R. Microstructure evolution in a Cu—Ag alloy during large strain deformation and annealing. *Materials Science Forum*. 2011;667—669:493—498.
https://doi.org/10.4028/www.scientific.net/MSF.667-669.493
18. Kada S., Vadlamani S.S., Kauffmann A., Hegedus Z., Gubicza J., Lechner M., Freudenberger J., Wilde G. High strength and ductile ultra-grained Cu—Ag alloy through bimodal grain size, dislocation density and solute distribution. *Acta Materialia*. 2013;61:228—238.
https://doi.org/10.1016/j.actamat.2012.09.053
19. Wang H., Zhang Z., Zhang H., Hu Z., Li S., Cheng X. Novel synthesizing and characterization of copper matrix composites reinforced with carbon nanotubes. *Materials Science and Engineering A*. 2017;696:80—89.
https://doi.org/10.1016/j.msea.2017.04.055
20. Fine structure and properties of solid solutions: Collection of articles. Eds. V. Kester, I.Ya. Bokshitsky, Ya.P. Selissky. Moscow: Metallurgiya, 1968. 223 p. (In Russ.).
Тонкая структура и свойства твердых растворов: Сб. статей. Пер. с нем. под ред. В. Кестера, И.Я. Бокшицкий. Ред. Я.П. Селисский. М.: Металлургия, 1968. 223 с.
21. Islamgaliev R.K., Nesterov K.M., Valiev R.Z. Structure, strength, and electric conductivity of a Cu—Cr copper-based alloy subjected to severe plastic deformation. *Physics of Metals and Metallography*. 2015;116(2):209—218. https://doi.org/10.1134/S0031918X14090063
Исламгалиев Р.К., Нестеров К.М., Валиев Р.З. Структура, прочность и электропроводность медного сплава системы Cu—Cr, подвергнутого интенсивной пластической деформации. *Физика металлов и металловедение*. 2015;116(2):219—228.
https://doi.org/10.7868/S001532301409006X
22. Babikov V.V. Phase function method in quantum mechanics. 2-nd ed., rev. and add. Moscow: Nauka, 1976. 287 p. (In Russ.).
Бабиков В.В. Метод фазовых функций в квантовой механике. 2-е изд., испр. и доп. М.: Наука, 1976. 287 с.
23. Kon'kova T.N., Mironov S.Y., Danilenko V.N., Korznikov A.V. Effect of low-temperature rolling on the structure of copper. *Physics of Metals and Metallography*. 2010;110(4):318—330.
https://doi.org/10.1134/S0031918X10100029
Конькова Т.Н., Миронов С.Ю., Даниленко В.Н., Корзников А.В. Влияние низкотемпературной прокатки на структуру меди. *Физика металлов и металловедение*. 2010;110(4):336—348.
https://doi.org/10.1134/S0031918X10100029
24. Guo S., Liu S., Liu J., Gao Z., Liu Z. Investigation on strength, ductility and electrical conductivity of Cu—4Ag alloy prepared by cryorolling and subsequent annealing process. *Journal of Materials Engineering and Performance*. 2019;28:6809—6815.
https://doi.org/10.1007/s11665-019-04448-7
25. Umansky Ya.S., Skakov Yu.A., Ivanov A.N., Rastorguev L.N. Crystallography, *X*-ray diffraction and electron microscopy. Moscow: Metallurgiya, 1982. 632 p. (In Russ.).
Уманский Я.С., Скаков Ю.А., Иванов А.Н., Расторгуев Л.Н. Кристаллография, рентгенография и электронная микроскопия. М.: Металлургия, 1982. 632 с.
26. Syutkin N.N., Ivchenko V.A., Telegin A.B., Volkov A.Yu. Field emission microscopy of the early stages of ordering and decomposition of a palladium—copper—silver alloy. *Fizika Metallov i Metallovedenie*. 1986;62(5):965—969. (In Russ.).
Сюткин Н.Н., Ивченко В.А., Телегин А.Б., Волков А.Ю. Полевая эмиссионная микроскопия ранних стадий упорядочения и распада сплава палладий—медь—серебро. *Физика металлов и металловедение*. 1986;62(5):965—969.
27. Honeycomb R. Plastic deformation of metals. Moscow: Mir, 1972. 408 p. (In Russ.).
Хоникомб Р. Пластическая деформация металлов. М.: Мир, 1972. 408 с.
28. Toschi S., Balducci E., Ceschini L., Mørtsell E., Morri A., Di Sabatino M. Effect of Zr addition on overaging and tensile behavior of 2618 aluminum alloy. *Metals*. 2019;9:130.
https://doi.org/10.3390/met9020130

Information about the authors

Oksana S. Novikova – Cand. Sci. (Phys.-Math.), Senior Research Scientist, M.N. Mikheev Institute of Metal Physics of Ural Branch of the Russian Academy of Sciences (IMP UB RAS).
https://orcid.org/0000-0003-0474-8991
E-mail: novikova@imp.uran.ru

Yuriy A. Salamatov – Cand. Sci. (Phys.-Math.), Senior Research Scientist, IMP UB RAS.
https://orcid.org/0000-0002-3857-2392
E-mail: salamatov@imp.uran.ru

Alina E. Kostina – Postgraduate Student, Junior Research Scientist, IMP UB RAS.
E-mail: alina_30_93@mail.ru

Aleksey Yu. Volkov – Dr. Sci. (Eng.), Head of the laboratory, IMP UB RAS.
https://orcid.org/0000-0002-0636-6623
E-mail: volkov@imp.uran.ru

Информация об авторах

Оксана Сергеевна Новикова – к.ф.-м.н., ст. науч. сотрудник Института физики металлов им. М.Н. Михеева (ИФМ) УрО РАН.
https://orcid.org/0000-0003-0474-8991
E-mail: novikova@imp.uran.ru

Юрий Александрович Саламатов – к.ф.-м.н., ст. науч. сотрудник ИФМ УрО РАН.
https://orcid.org/0000-0002-3857-2392
E-mail: salamatov@imp.uran.ru

Алина Евгеньевна Костина – аспирант, мл. науч. сотрудник ИФМ УрО РАН.
E-mail: alina_30_93@mail.ru

Алексей Юрьевич Волков – д.т.н., заведующий лабораторией ИФМ УрО РАН.
https://orcid.org/0000-0002-0636-6623
E-mail: volkov@imp.uran.ru

Contribution of the authors

O.S. Novikova – conceptualization, methodology, participation in SEM studies, resistometry, manuscript writing.

Yu.A. Salamatov – processing of *X*-ray diffraction data, discussion of results.

A.E. Kostina – sample preparation, microhardness measurements, mechanical tensile testing, discussion of results.

A.Yu. Volkov – supervision, validation, review, and editing of the manuscript.

Вклад авторов

О.С. Новикова – концептуализация, методология, участие в СЭМ-исследовании, резистометрия, написание статьи.

Ю.А. Саламатов – обработка данных рентгеноструктурного анализа, обсуждение результатов

А.Е. Костина – подготовка образцов, измерение микротвердости, проведение механических испытаний на растяжение, обсуждение результатов.

А.Ю. Волков – курирование, проверка, анализ и редактирование статьи.

The article was submitted 25.12.2023, revised 22.03.2024, accepted for publication 25.03.2024

Статья поступила в редакцию 25.12.2023, доработана 22.03.2024, подписана в печать 25.03.2024